



## This is to certify that the

### dissertation entitled

Synthesis and Characterization of Substituted Polyphenylene Oligomers

presented by

Susan T. Pasco

has been accepted towards fulfillment of the requirements for

Ph.D. degree in Chemistry

Major professor

Date 12/11/97

MSU is an Affirmative Action/Equal Opportunity Institution

0-12771

LIBRARY
Michigan State
University

# PLACE IN RETURN BOX to remove this checkout from your record. TO AVOID FINES return on or before date due.

ļ	DATE DUE	DATE DUE	DATE DUE
	<del>JUN 2 3 200</del> 3.		
	NOW & 12 25 0 0 3		

1/98 c:/CIRC/DateDue.p65-p.14

# SYNTHESIS AND CHARATERIZATION OF SUBSTITUTED POLYPHENYLENE OLIGOMERS

Ву

Susan T. Pasco

## A DISSERTATION

Submitted to
Michigan State University
in partial fulfillment of the requirements
for the degree of

**DOCTOR OF PHILOSOPHY** 

Department of Chemistry

1997

#### **ABSTRACT**

## SYNTHESIS AND CHARATERIZATION OF SUBSTITUTED POLYPHENYLENE OLIGOMERS

By

#### Susan T. Pasco

Due to their high thermal stability, conductivity in the doped state and large band gaps, polyphenylenes are desirable materials for electronic applications but they are often insoluble, intractable and cannot be synthesized reproducibly. Long alkyl side chains on the monomer units impart solubility and processibility to the polymers, however, the exact effect of the side chains on the solubility, crystallinity and optical properties of polyphenylenes is poorly understood. We synthesized a series of 2,5-dialkyl substituted exact-length polyphenylene oligomers to study the effect of side chains and oligomer length on the properties of the oligomers and how these effects can be extrapolated to the parent polymer. We synthesized oligomers of chain lengths ranging from 2 to 7 phenyl rings with methyl, ethyl or hexyl side chains using the Suzuki coupling reaction in an iterative scheme. The oligomers were characterized by Variable Temperature Nuclear Magnetic Resonance (VTNMR), UV absorbance and fluorescence emission spectroscopies, thermal analysis and optical microscopy. The VTNMR experiments showed that the barrier to rotation around phenyl-phenyl bonds is 18.5 kcal/mol for the methyl-substituted oligomers and ~20.5 kcal/mol for the ethyl- and hexyl-substituted oligomers. The oligomer length had no effect on the rotational barrier. The optical spectroscopy showed that the conjugation length for substituted polyphenylenes reached a limiting value at less than 5 phenyl rings.

We also examined the solid state properties of the oligomers. The methyl-substituted oligomers crystallize readily while the ethyl-substituted oligomers crystallize slowly, over a period of 2-3 days. Solid state fluorescence of an ethyl-substituted glassy oligomer shows a 2 band spectrum. After the oligomer crystallizes, the low energy band decreases in intensity and the high energy band increases in intensity. We attribute the two bands to fluorescence from the amorphous and crystalline forms of the oligomer. In conjunction with optical microscopy and thermal analysis measurements, these fluorescence experiments allowed us to propose a crystalline packing structure for ethyl-substituted polyphenyls.

To my parents

#### **ACKNOWLEDGMENTS**

First, I would like to thank my advisor, Professor Greg Baker, for his guidance and for always showing me a "real world" view of chemistry. Thanks also go to my committee members: Professors Gary Blanchard, Ned Jackson, Jeff Ledford and Simon Garrett. Thanks especially to Professor Garrett for serving on very short notice. I would also like to thank the past and present members of the Baker group: Jun Hou, Jun Qiao, Jingpin, Yiyan, Micah, Chun, Cory, J. B., Tara, Mao, Gao and Tianqi, for always providing a fun and interesting work environment – Go To Polybeers!!

I would also like to thank Professor Matt Platz, without whom this degree would not have been possible. He gave me the confidence and support I needed to come to MSU and succeed. This degree also would not have been possible without the awesome work of the Glass, Electronic and Machine shops — thanks for always knowing what I needed, even if I didn't. I also must acknowledge Long Le and Kermit Johnson for all their help on the NMRs. Thanks also to Lisa Dillingham, not only for all her hard work in the Graduate Office but also for her friendship and for getting through orientation '96 together.

On a more personal level, there are many people I have met here who have made Lansing feel like home to me and helped make graduate school a little easier. The "Cheeters": Craig, Dave, Mike, Micah, Bill, Aimee, Rod, Danielle, Patti, and Suzanne,

thanks for cheering even after my 3<sup>rd</sup> strikeout of the game and for all the fun times on and off the softball field. Rod and Danielle, my homebrew-drinking, sushi-eating buddies- I can't wait for England and Scotland (Traquair House)! Shannon, whose daily emails make Wyoming seem not so far away. Thanks for always being a great friend. Per, for his constant friendship and support, especially during these last few months. Thanksgiving next year? Micah, for all the hours gabbing in the lab when we should have been working. Joy and Gary, for all the new recipes and fun conversations over the past 4 ½ years.

Matt, my friend and partner. Thanks for always being on my team. We've been through a lot together and I can't wait for the adventures to come.

Finally, I want to thank my family: Mom, Dad and Bill for their love and support throughout my academic career.

## **TABLE OF CONTENTS**

I. INTRODUCTION	1
A. Aryl Couplings and Polymerizations	4
1. Early Methods	4
2. Modern Aryl Coupling Methods	8
B. Exact Length Conjugated Oligomers	17
C. Optical Properties of PPPs and PPP Oligomers	19
D. Rotational Barriers in Polyphenylenes	28
E. Side Chains	32
II. RESULTS	37
A. Synthesis	38
B. Rotational Barriers	46
C. Optical Properties	57
1. UV-vis Absorbance	57
2. Fluorescence Emission	68
3. Solid State Spectra	72

D. Thermal Properties	75
E. Self-Assembled Monolayers	89
III. DISCUSSION	96
A. Electronic Properties of Poly(p-phenylene)s	96
B. Band Gap Engineering	97
C. Solubility and Crystallinity	102
1. Increased Ring Twist	103
2. Rotational Barriers	105
3. Increased Entropy of Oligomers	111
4. Steric Blocking	113
D. Effect of Side Chains on Morphology	114
E. Design Rules	117
F. Suggestions for Future Work	118
1. Synthetic Methodology	118
2. Self-Assembled Monolayers	119
3. Crystallinity and Thermal Transitions	125
E. Summary	126
IV. EXPERIMENTAL	128
APPENDIX I: <sup>1</sup> H NMR spectra of selected compounds	154
APPENDIX II: Numbering of compounds	165
BIBLIOGRAPHY	167

## **LIST OF TABLES**

Table		Page
Table 1.	Nomenclature of unsubstituted oligophenyls	2
Table 2.	Melting points of PPP oligomers	33
Table 3.	Abbreviations of oligomers used in the text	37
Table 4.	Microsoft Excel macro for computing barriers with HyperChem	49
Table 5.	Rotational barriers for alkyl-substituted terphenyls	50
Table 6.	Rotational barriers for methyl-substituted oligomers	52
Table 7.	UV-vis absorbance edge values for PPP oligomers	66
Table 8.	Fluorescence $\lambda_{max}$ values for PPP oligomers	68
Table 9.	Melting points of PPP oligomers	81
Table 10.	Solubilities and melting points for substituted PPP oligomers	99
Table 11.	Solubility in toluene of substituted quinquephenyls	105

## **LIST OF FIGURES**

Figure		Page
Figure 1.	Poly(para-phenylene)	1
Figure 2.	Numbering system in polyphenyls	2
Figure 3.	A "hairy rod"	3
Figure 4.	Oxidative-cationic polymerization of benzene	4
Figure 5.	Fittig Reaction	5
Figure 6.	Wirth's Ullmann coupling of substituted iodoaryls	6
Figure 7.	Diels Alder polymerization.	7
Figure 8.	Tour's synthesis of soluble PPP	7
Figure 9.	Proposed mechanism for Yamamoto coupling	10
Figure 10.	Stille coupling reaction	12
Figure 11.	Suzuki coupling reaction	12
Figure 12.	Catalytic cycle of Pd(0) mediated Suzuki coupling	13
Figure 13.	Proposed mechanism for self-coupling of boronic acids	15
Figure 14.	Synthesis of aryl boronic acids	16
Figure 15.	Accelerated Suzuki coupling reaction	17
Figure 16.	Linear conjugated oligomers for use as molecular wires	18
Figure 17.	Poly(p-phenylenevinylene)	19

Figure 18.	Schematic energy level diagram	20
Figure 19.	Morse potential energy curves demonstrating the Franck-	
	Condon Principle	22
Figure 20.	Decrease in band gap for conjugated molecules	23
Figure 21.	Excited state structures of polyphenylene and	
	polyacetylene	24
Figure 22.	Absorption spectra of PPP oligomers in chloroform	26
Figure 23.	Twisted biphenyl	27
Figure 24.	Coalescing peaks in an NMR spectrum	29
Figure 25.	Heitz's methyl-substituted sexiphenyl	34
Figure 26.	Traditional and accelerated Suzuki coupling reactions	38
Figure 27.	Synthesis of the first oligomers	39
Figure 28.	Synthesis of TMS-functionalized materials	40
Figure 29.	Bromination and iodination of 4,4'-bis(TMS)-TMB	41
Figure 30.	Incomplete reaction in accelerated Suzuki coupling	42
Figure 31.	Synthesis of ethyl-substituted starting materials	43
Figure 32.	Synthesis of hexyl-substituted oligomers	45
Figure 33.	The two diastereomeric rotational states of HMT	46
Figure 34.	Dihedral angles for substituted terphenyls	47
Figure 35.	HyperChem calculation of rotational barriers for	
	substituted terphenyls	48
Figure 36.	Variable temperature NMR spectra of HMT	51
Figure 37.	Variable temperature NMR spectra of HET in the methyl	

	region	53
Figure 38.	Actual and Simulated VTNMR spectra of HET	55
Figure 39.	Plot of T <sub>1</sub> versus temperature for HET	56
Figure 40.	UV-Vis absorbance spectra of methyl-substituted	
	oligomers	59
Figure 41.	UV absorbance spectra of ethyl-substituted oligomers	61
Figure 42.	UV absorbance spectra of hexyl-substituted oligomers	62
Figure 43.	UV absorbance spectra of substituted terphenyls	63
Figure 44.	Plot of energy vs. oligomer length	67
Figure 45.	Fluorescence spectra of methyl-substituted oligomers	69
Figure 46.	Fluorescence spectra of ethyl-substituted oligomers	70
Figure 47.	Fluorescence spectra of hexyl-substituted oligomers	71
Figure 48.	Solid state UV absorbance spectra of ethyl-substituted	
	oligomers	<b>7</b> 3
Figure 49.	Solid state fluorescence emission of ethyl-substituted	
	oligomers	74
Figure 50.	DSC plot of HMT	76
Figure 51.	DSC plot of OMQ	77
Figure 52.	DSC plot of OEQ	78
Figure 53.	DSC plot of DHQ	79
Figure 54.	DSC plot of THS	80
Figure 55.	DMA plot of OEQ	84
Figure 56.	Solid state fluorescence of OEQ	85

Figure 57	Variable temperature fluorescence spectra of OEQ	87
Figure 58.	Plot of emission intensity vs. temperature for VT	
	fluorescence of OEQ	88
Figure 59.	Structure of a self-assembled monolayer	90
Figure 60.	Synthetic scheme for SAMs	91
Figure 61.	FT-IR spectra of SAMs on A200 fumed silica	93
Figure 62.	TGA plots of SAMs on silica	94
Figure 63.	Grubbs's synthesis of soluble polyacetylene	99
Figure 64.	UV absorbance spectra of Rehahn's copolymers	100
Figure 65.	Soluble ladder polymers	101
Figure 66.	Comparison of a random coil polymer with a rigid-rod	
	polymer	103
Figure 67.	Side view of PPPs with different dihedral angles	104
Figure 68.	Rotational barriers of substituted PPPs	106
Figure 69.	Measurement of crystallization rate of OEQ	107
Figure 70.	Photograph of crystalline HET under crossed polarizers	109
Figure 71.	Photograph of crystalline OEQ under crossed	110
	polarizers	
Figure 72.	Schematic energy diagram for dissolution of PPPs	112
Figure 73.	DSC curves of substituted PPP derivatives	112
Figure 74.	Polyacetylenes solubilized by terminal t-butyl groups	113
Figure 75.	Sandwich type morphology of 2,5-didodecyl PPP	114
Figure 76.	HyperChem depiction of proposed packing structure for	116

	OEQ	
Figure 77.	Proposed NLO chromophore	120
Figure 78.	Proposed synthetic route to NLO chromophore	121
Figure 79.	PPP oligomer functionalized with a cross-linking group	122
Figure 80.	Thermal cross-linking of PPP oligomers	124
Figure 81.	Chemical cross-linking of PPP oligomers	124
Figure 82.	<sup>1</sup> H NMR spectrum of TMB	154
Figure 83.	<sup>1</sup> H NMR spectrum of HMT	155
Figure 84.	<sup>1</sup> H NMR spectrum of OMQ	156
Figure 85.	<sup>1</sup> H NMR spectrum of DMQ	157
Figure 86.	<sup>1</sup> H NMR spectrum of TEB	158
Figure 87.	<sup>1</sup> H NMR spectrum of HET	159
Figure 88.	<sup>1</sup> H NMR spectrum of OEQ	160
Figure 89.	<sup>1</sup> H NMR spectrum of DEQ	161
Figure 90.	<sup>1</sup> H NMR spectrum of HHT	162
Figure 91.	<sup>1</sup> H NMR spectrum of DHQ	163
Figure 92.	<sup>1</sup> H NMR spectrum of THS	164

## I. INTRODUCTION

Polyphenylenes are a series of benzene rings connected by single bonds (Figure 1) in an *ortho, meta,* or *para* fashion, or any combination of the three. The most commonly studied phenylene is poly(*para*-phenylene) (PPP), since its large degree of conjugation and rigid-rod structure make it a good candidate for many electronic, photonic and structural applications.

Figure 1: Poly(para-phenylene)

PPP is thermally stable to 400 °C in air and only 7% of the mass is lost after heating to 900 °C under nitrogen. When doped with AsF<sub>5</sub>, its conductivity is 500 S/cm, approaching that of polyacetylene. Because of its high thermal and oxidative stability, high mechanical strength<sup>1</sup> and conductivity in the doped state,<sup>2</sup> PPP has been explored for use in light emitting diodes, as insulators for semiconductors and for metal catalyst supports. Despite these desirable properties, PPP is an intractable, insoluble, highly crystalline material that is difficult to synthesize reproducibly.

2

The established nomenclature for polyphenylenes is summarized in a review article by Speight, Kovacic and Koch.<sup>3</sup> The terms polyphenyl, poly(phenylene), oligophenyl, and oligophenylene have all been used to describe the structure in Figure 1. The term polyphenyl is usually reserved for molecules with a well-defined number of phenyl rings, either substituted or unsubstituted, with the neighboring phenyl rings joined in an *ortho*, *meta* or *para* arrangement. The most common unsubstituted para-linked oligomers are

Table 1: Nomenclature of unsubstituted oligophenyls

n = 2	biphenyl
n = 3	<i>p</i> -terphenyl
n = 4	<i>p</i> -quaterphenyl
n = 5	<i>p</i> -quinquephenyl
n = 6	p-sexiphenyl

Figure 2: Numbering system in polyphenyls. 2, 2', 2'', 5'', 5'', 5''' octamethylquaterphenyl

listed in Table 1. As shown in Figure 2, the numbering of the aromatic carbons of polyphenylene begins at the carbon atom that links the first ring to an adjacent ring, and each ring in turn is numbered from the preceding ring. Sites in each successive ring are denoted by primes following the carbon number.

One difficulty in working with PPP is the inability to synthesize a soluble structurally regular polymer of high molecular weight.<sup>4</sup> An important aspect of PPP is its rigid rod structure, which imparts many of its desirable properties but also leads to poor solubility. The rigidity is caused by the *para* linkages, so it is imperative to find polymerization or coupling reactions that ensure all *para* products. Several methods such as synthesizing a soluble precursor<sup>5,6</sup> or placing long alkyl side chains on the polymer have been devised to overcome the synthetic difficulties in preparing PPP. The use of large alkyl side chains to impart solubility on polyphenylenes has been widely investigated. Rehahn, *et al.*<sup>7,8</sup> first employed this strategy in the synthesis of the first example of structurally regular, soluble, high molecular weight polyphenylenes. (Figure

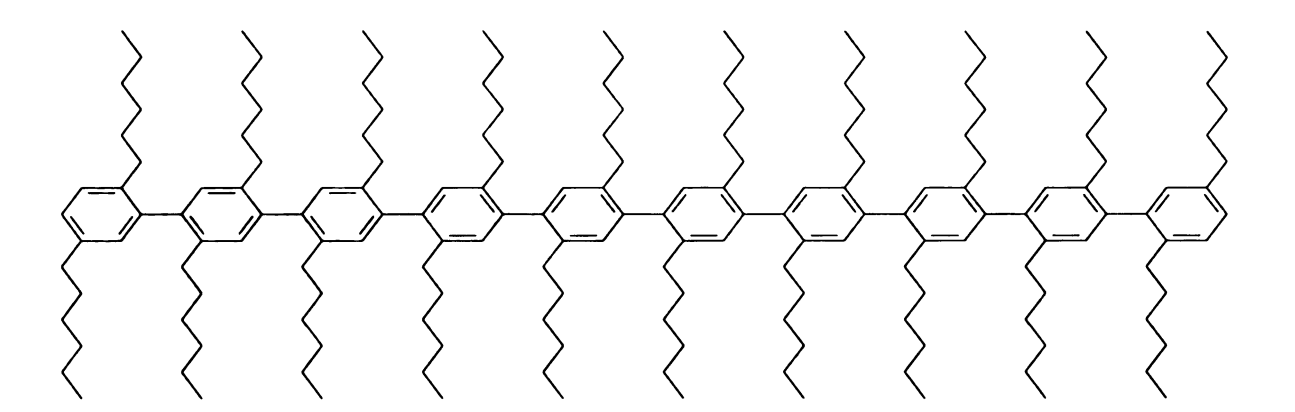


Figure 3: A "hairy rod"

Figure 4: Oxidative-cationic polymerization of benzene

3) Since the report of these "hairy rods", the addition of side chains to polyphenylenes has become a common route to soluble PPPs. While it is obvious that the side chains impart solubility to PPP, the details of how solubility is achieved are poorly understood. The goal of this research is to conduct a detailed study of exact length substituted poly(*p*-phenylene) oligomers in order to define the side chain-solubility relationships. We chose a series of 2,5-disubstituted, exact-length poly(*p*-phenylene) oligomers and systematically investigated the effect these side chains have on the rotational barriers, optical properties, thermal properties and solubility of the polymer. These oligomers were synthesized using an iterative approach, so that coupling reactions can be used to assemble a series of oligomers of increasing length from a library of common intermediates. The remainder of this introduction summarizes the synthetic methods used for aryl couplings, including polymerizations, as well as a background of the basic optical and structural analysis tools used, and how these methods apply in this work.

## A. Aryl couplings and polymerizations

## 1. Early Methods

Numerous reviews have been published on the synthesis and properties of polyphenylenes.<sup>3,9,10</sup> Until the late 1980's, the most common method for synthesizing polyphenylenes was oxidative-cationic polymerization.

Oxidative-cationic polymerizations of benzene to yield polyphenylenes (Figure 4)

were discovered and developed by Kovacic and the products are frequently referred to as "Kovacic PPP" in the current literature. To be effective, the catalyst system should be a good Friedel-Crafts catalyst and it must also be a good oxidizing agent. Other systems that were effective in this polymerization were AlCl<sub>3</sub> in combination with MnO<sub>2</sub>, PbO<sub>2</sub>, NO<sub>2</sub>, benzoquinone, air or chloranil, but the reactions produced variable yields and irregular structures. Interestingly, while benzene gave a polymeric product, biphenyl and terphenyl yielded only sexiphenyls except upon heating, from which a polymer with *meta* and *para* linkages resulted. Alkylated benzenes were poor substrates and gave a complex mixture of low molecular weight *ortho*-linked molecules.

Another route to polyphenylenes is the coupling of halogenated aromatic compounds. The Fittig reaction (Figure 5) has been known for over 100 years, but is not commonly used for polymerizations because the anionic nature of the reaction results in a large number of side products. However, it can be used to synthesize a symmetric biaryl in reasonable yield. There are a few reports of the preparation of *para*-linked polymers using the Fittig reaction, but since the melting points of the polymers are lower than that of *p*-quaterphenyl, these are probably either branched polymers or very small oligomers.

Figure 5: Fittig Reaction

a. 2 H 
$$\xrightarrow{CH_3}$$
  $\xrightarrow{CH_3}$   $\xrightarrow{CH_3}$   $\xrightarrow{CH_3}$   $\xrightarrow{CH_3}$   $\xrightarrow{H_3C}$   $\xrightarrow{H_3C}$   $\xrightarrow{H_3C}$   $\xrightarrow{H_3C}$ 

b. 
$$H \xrightarrow{CH_3} CH_3$$
 $CH_3$ 
 $C$ 

Figure 6: Wirth's Ullmann coupling of substituted iodoaryls. a. even oligomers. b. odd oligomers

For synthesizing oligomers such as biphenyl or quaterphenyl, a more useful coupling reaction is the Ullmann reaction. 11-13 This reaction is commonly used for synthesizing symmetrical biphenyls, but it has been used in the synthesis of asymmetric oligophenyls. Cross-coupling reactions usually yield a statistical mixture of symmetric and asymmetric coupling products, but often these mixtures can be easily separated. A templating scheme can also be used 14 to facilitate cross-coupling reactions. Wirth *et al* 15 used this method in the first reported synthesis of exact length substituted polyphenylene oligomers. They synthesized 2,5-dimethyl-substituted polyphenyls from biphenyl to quinquephenyl by coupling iodoaryls (Figure 6).

The Diels-Alder reaction of bis-tetraphenylcyclopentadienones and bis-diacetylenes has also been used to synthesize polyphenylenes. (Figure 7) This polymerization yielded white amorphous polymers of molecular weights from 20,000 to 100,000. The Diels-Alder reaction is not regiospecific, and thus some *meta* linkages are found in the polymer backbone. These kinks, in addition to the aromatic rings attached to the phenylene

Figure 7: Diels Alder polymerization

backbone, contribute to the high solubility of the polymers.

Aryl lithium reagents have also been coupled to form polyphenylenes. Early attempts to synthesize a polymer from phenyllithium in the presence of oxygen resulted in a good yield (>65%) of biphenyl. However, oxygenated products are also often found in this reaction. More recently, Tour and his group 16-18 synthesized a soluble polyphenylene from 1-bromo-4-lithiobenzene (Figure 8). This instantaneous polymerization is facilitated by the addition of HMPA to the lithiated bromobenzene solution. The polymer is soluble because of several defects present in the polymer,

Figure 8: Tour's synthesis of soluble PPP

namely phenylated rings capped with halogens. A mechanistic study <sup>18</sup> suggests that ortho-benzyne intermediates are responsible for the defects.

## 2. Modern Aryl Coupling Methods

Organometallic reagents have been widely used for aryl couplings. The first attempt to use a Grignard-type reagent was by Ullmann, who tried to use magnesium instead of copper to couple halobenzenes. This attempt was unsuccessful, but biaryls have been successfully synthesized using metal halides such as CuCl<sub>2</sub>, AgBr, MoCl<sub>5</sub>, CoCl<sub>2</sub>, CrCl<sub>3</sub> and FeCl<sub>3</sub> which oxidize the aryl Grignard, and form an intermediate (possibly radical?) which couples to form the biaryl. Another early success was the coupling of aryl halides with zero-valent nickel compounds such as Ni(COD)<sub>2</sub> (COD = cyclooctadiene) to yield biaryls.<sup>19</sup> Yamamoto expanded on this work by studying several transition metal catalysts for the catalytic coupling of Grignard reagents prepared from dihalobenzenes.<sup>20</sup> For the polymerization of p-dibromobenzene, NiCl<sub>2</sub>(bpy) and PdCl<sub>2</sub>(bpy) were the most effective catalysts, giving a 95% yield of PPP. The polymers were light yellow in color and decomposed in air at 550 °C. Their thermal stability is comparable to that of a polymer synthesized by the Kovacic method, but the color is considerably lighter, indicating that there are fewer impurities in the polymer from halogens, traces of the catalyst, or oxidizing agent. The Yamamoto PPPs show a high degree of crystallinity by X-ray diffraction, indicating that the reaction is highly selective for coupling in a parafashion. The coupling mechanism proposed by Yamamoto is shown in Figure 9. The first step involves formation of NiR<sub>2</sub>L<sub>2</sub> followed by R<sub>2</sub> loss and reaction of the resulting unsaturated complex with R'-X to yield NiR'(X)L<sub>2</sub>, which is the active catalytic species

in the coupling. This species is alkylated with R-MgX and the resulting nickel compound reductively eliminates R-R' to regenerate  $NiR'(X)L_2$ .

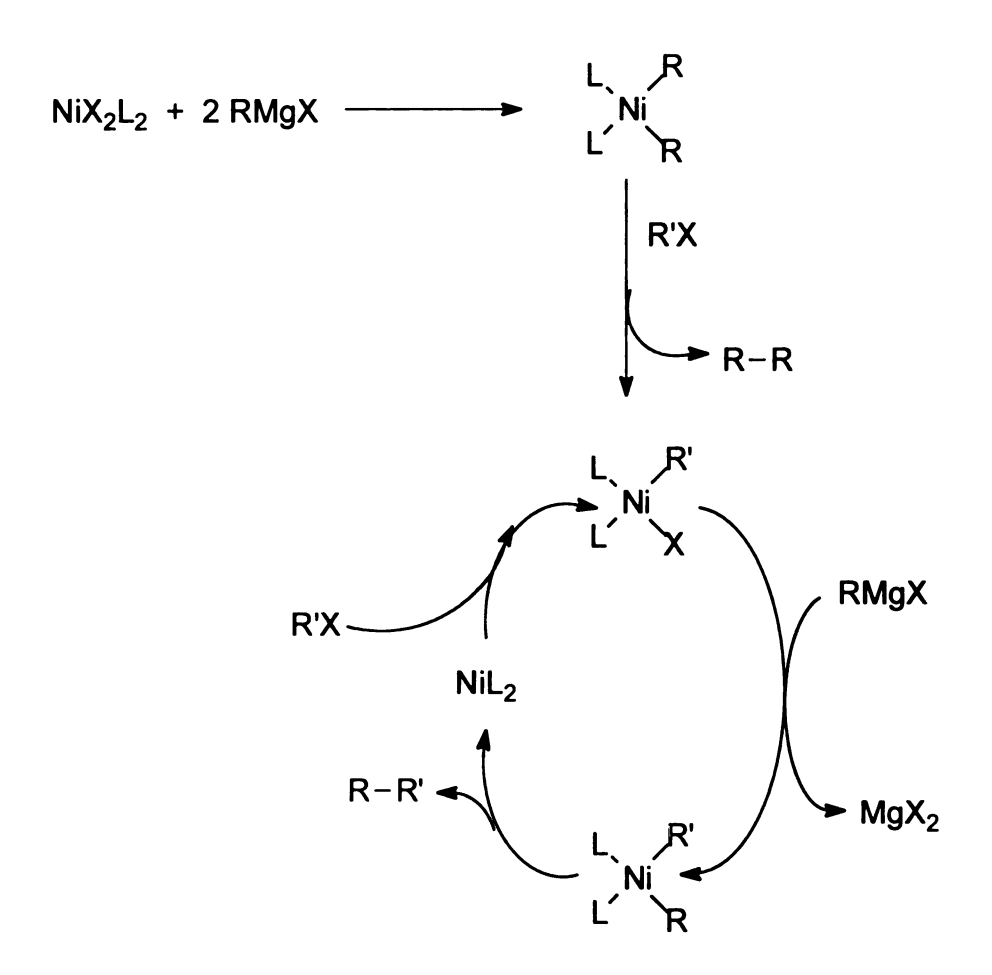


Figure 9: Proposed mechanism for Yamamoto coupling

The Yamamoto reaction was the first catalytic reaction to show the specificity needed to synthesize the exact length, *para* linked PPP oligomers that is the focus of our work. As we will see throughout this Introduction, even one *meta* or *ortho* linkage can greatly change the thermal stability, solubility and optical properties of PPP polymers or oligomers. Although the Yamamoto coupling was a breakthrough for the polymerization of bromobenzenes to polyphenylene, the reactivity of the Grignard reagent leads to modest molecular weights. The polymerization of hexyl-substituted dibromobenzenes by Rehahn<sup>7</sup> resulted in a degree of polymerization of only 13. Newer coupling methods including the Stille coupling and the Suzuki coupling, follow similar mechanisms but use other organometallic reagents as different transmetallation agents. As we will see, the judicious choice of a transmetallation agent can allow for several options in a coupling scheme, and the scientist can choose based on the requirements of the reaction in question.

Several investigators have used transition metal couplings involving zinc as the transmetallation agent. Rieke<sup>21,22</sup> used an activated zinc powder formed from ZnCl<sub>2</sub> and lithium naphthalide to selectively form a variety of organic halozinc compounds. Aryl bromides gave the corresponding aryl zinc compounds in 90-100% yield, which could then be polymerized with a Pd(0) catalyst. Jutand<sup>23</sup> used activated zinc (formed from zinc powder and acetic acid) as a reducing agent for the coupling of aryl halides. Iyoda<sup>24</sup> used zinc in the presence of tetraethylammonium iodide and a nickel catalyst to couple substituted aryl halides. This combination of reagents presumably forms a more active catalyst species, but the authors did not complete a detailed mechanistic study to prove this theory.

The Stille coupling<sup>25</sup> (Figure 10) is a palladium catalyzed coupling of aryl triflates with organostannanes. This reaction is widely used,<sup>26-32</sup> but a sometimes fails for halobenzenes with electron-donating groups. This reaction is still tolerant of many functional groups and is frequently used for coupling vinyl stannanes. The Stille coupling has been conducted under microwave irradiation,<sup>33</sup> improving the rate of the reaction, and in the solid phase<sup>34</sup> using an amide resin to produce biaryls in slightly lower yields than the analogous solution phase syntheses.

Probably the most commonly used coupling method is the Suzuki reaction (Figure

Figure 10: Stille coupling reaction

Figure 11: Suzuki coupling reaction

11), which involves the palladium catalyzed coupling of an aryl halide with an aryl boronic acid. 35,36 The stability and low toxicity of boronic acids give the Suzuki

coupling distinct advantages compared to other coupling schemes. Both the highly reactive Grignard reagent of the Yamamoto coupling and the toxic organotin species of the Stille coupling are avoided. The stability of boronic acids allows Suzuki couplings to be run under a variety of reaction conditions. As for all Pd(0) catalyzed reactions, the most reactive halide is the aryl iodide followed by the bromide, and the chloride does not couple.<sup>37</sup>

Steric hindrance can be a factor in the Suzuki coupling, but generally this reaction is compatible with a wide range of functional groups. This coupling does not proceed without the use of a base<sup>38</sup>, which is thought to aid the transmetallation of the boronic acid moiety. Figure 12 demonstrates that a crucial difference between the catalytic cycle for Suzuki coupling and those of most Pd-catalyzed reactions is that the oxidative addition step is followed by a displacement of the halide ion from the Ar-Pd-X complex

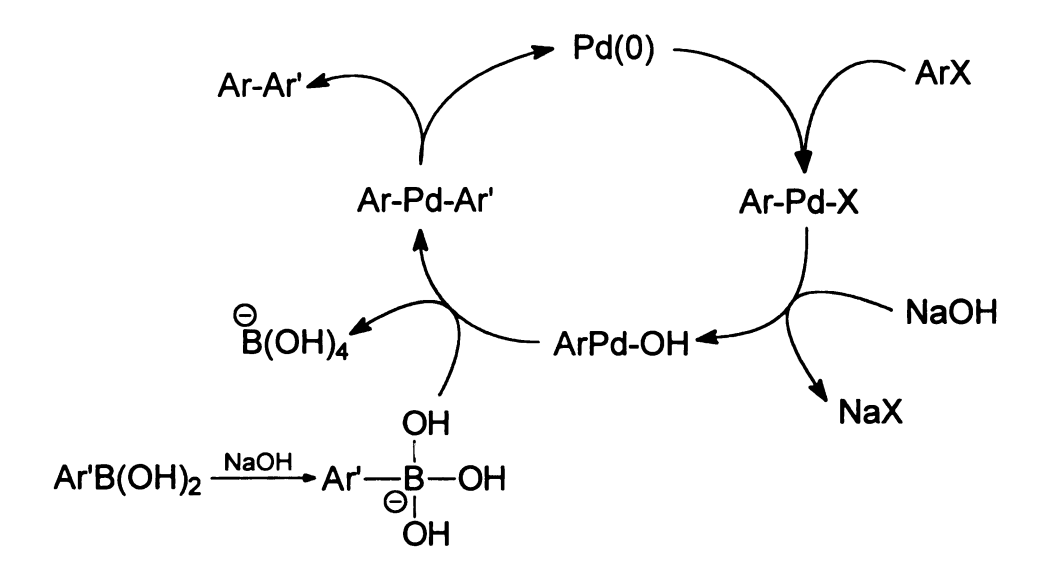


Figure 12: Catalytic cycle of Pd(0) mediated Suzuki coupling

by a base. In Figure 12, the organo-palladium hydroxide is more reactive than the organo-palladium halide since the Pd-O bond is more polar than the Pd-Br bond. As a result, the organo-palladium hydroxide species is much more electrophilic and therefore facilitates the transmetallation step.

Although the Suzuki coupling is an excellent method for carbon-carbon bond formation in aryl species, there are several limitations to this reaction. hindered boronic acids, especially those substituted in the ortho position, undergo coupling much slower than less hindered boronic acids.<sup>39,40</sup> A common side reaction in the traditional Suzuki coupling is homocoupling of the aryl boronic acid. Homocoupling is undesirable because it leads to lower yields, and the disruption of stoichiometry results in low molecular weight products in polymerization reactions. In a mechanism proposed by Moreno-Mañas and coworkers<sup>41</sup>, oxidative addition of the aryl-boron bond is followed by a hybrid oxidative addition-transmetallation step to yield two aryl groups and two boronic acid moieties bound to the palladium atom (Figure 13). The authors claim that the metaboric acid O=B-OH is converted to borate under the aqueous alkaline conditions usually present in the Suzuki coupling reaction. However, they reported no evidence for this product in the mechanism, only for the intermediates formed, so it is not certain that this pathway is correct. For slow coupling reactions, this self-coupling side reaction can be significant.

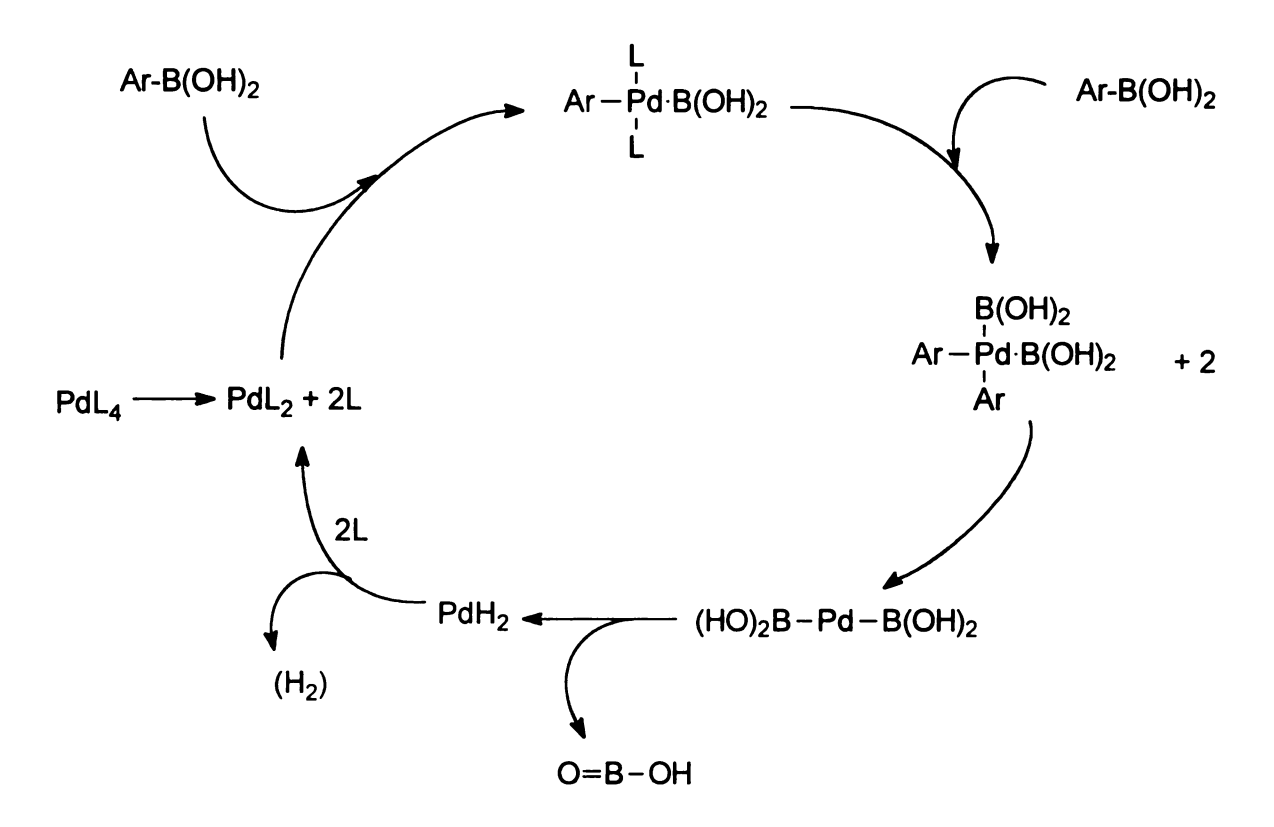


Figure 13: Proposed mechanism for self-coupling of boronic acids

A large body of work targeted improved syntheses of sterically hindered biaryls from boronic acid substrates. Boronic acids are typically synthesized from organolithium or organo-magnesium reagents and a borate ester (Figure 14).42-47 The most common side products from a boronic acid synthesis are borinic acids, which are molecules in which two aryl groups add to one borate ester and triphenyl borate Neither couple under the usual reaction conditions. Thompson and derivatives. Gaudino<sup>40</sup>, in their synthesis of 5-arylnicotinates, reported that these side products can be minimized by using a large excess of a bulky borate such as triisopropyl borate, and by extremely slow addition of the organometallic reagent to a concentrated borate solution at cold temperatures. Electron withdrawing groups on aryl boronic acids cause hydrolytic deboronylation that competes with coupling and decreases product yield. 39,48,49 Suzuki expanded on his original work by developing new conditions to help eliminate these limitations. By using the esters of boronic acids and anhydrous reaction conditions, they were able to couple aryl halides with a mesitylboronic acid, an o-methoxyphenyl boronic acid and an o-benzaldehyde boronic acid in good yield, usually about 80 %.

Recently, Novak, et al.50 developed an accelerated Suzuki coupling method

Figure 14: Synthesis of aryl boronic acids

Figure 15: Accelerated Suzuki coupling reaction

(Figure 15) which uses a phosphine-free palladium source. The reaction only takes 1 to 2 hours to complete as opposed to 24 hours for traditional Suzuki couplings. The advantage of a phosphine-free catalyst is that it eliminates a side reaction, the transfer of a phenyl group from the triphenyl phosphine ligand to the aryl halide. Novak's method works well for aryl iodides, but is very sensitive to steric hindrance in aryl bromide substrates.

## **B. Exact Length Conjugated Oligomers**

It is important to understand the optical properties of PPPs, since devices based on conjugated organic molecules, particularly oligomers, have been the focus of much interest recently.<sup>51</sup> Examples of these molecules are phenylene-ethynylene oligomers<sup>52</sup>, oligothiophenes<sup>53</sup>, poly(phenylacetylene) oligomers<sup>54,55</sup>, poly(phenylenevinylene)<sup>56</sup> and polyphenylenes.<sup>57</sup> Exact length conjugated oligomers have found applications as molecular wires<sup>58</sup>, thin film transistors<sup>59</sup>, and electroluminescent devices<sup>60</sup>. Exact length oligomers serve as models for the intractable PPP,<sup>61-65</sup> materials for second order nonlinear optical applications, or to alter surfaces as self-assembled monolayers.

Tour, et. al. 54,55 synthesized a 128Å linear conjugated oligomer of poly(p-phenylacetylene) that has been touted as a molecular wire (Figure 16). The synthesis permits selective functionalization of the ends of the oligomer. These oligomer ends can

be converted to "molecular alligator clips" by attaching thiol acetates that can be hydrolyzed to thiols. Upon exposure to gold surfaces gold thiolates are formed, creating the link between two metal probes. With ethyl side groups, the chains are only soluble up to the octamer, but by using a 3-ethylheptyl substituent the 16-mer is soluble. This side chain introduces a stereogenic center, which affords many diastereomers. Tour reports that racemization of the alkyl side chains provides solubility of the longer oligomer by retarding crystallization, but the solubility may also be imparted by the steric bulk of the branched chain.

Poly(p-phenylenevinylene) (PPV) oligomers (Figure 17) have also been studied

$$\mathsf{Et_2N_3} - \mathsf{SiMe_3}$$

Figure 16: Linear conjugated oligomers for use as molecular wires

as model compounds for the polymer<sup>61</sup>. Since poly(*p*-phenylenevinylene) becomes insoluble with increasing chain length, these well-defined oligomers can be used to gain insight into the structural and physical properties of the polymers such as the number of accessible oxidation states. Well-defined short conjugated oligothiophenes were also investigated as the active materials in organic field effect transistors and in light emitting diodes (LEDs).<sup>62-65</sup> Polyphenylene oligomers, which have been investigated as blue LEDs, are good candidates for electronic materials because of their high thermal and oxidative stability.

Figure 17: Poly(p-phenylenevinylene)

The precise length of these oligomers makes them especially attractive for electronic applications. There is a narrow distribution of conjugation lengths, which results in molecule-specific properties rather than averaged properties resulting from the molecular weight distribution in polymers.

## C. Optical Properties of PPPs and PPP Oligomers

The attractive electronic properties of exact length oligomers can be understood by considering the basic principles of electronic spectroscopy (Figure 18).66,67 When a molecule absorbs a photon at a certain wavelength, an electron is promoted from the ground state (S<sub>0</sub>) to one of a number of higher level excited states (S<sub>1</sub>, S<sub>2</sub>, S<sub>3</sub>, S<sub>4</sub>). The molecule can then lose the energy either radiatively or nonradiatively. In Figure 18, the curvy arrows indicate nonradiative processes, involving heat transfer, while the straight arrows denote radiative processes, involving transfer of photons. If the molecule loses the energy radiatively, fluorescence or phosphorescence occurs. Fluorescence is defined as the radiative transition between two states of the same multiplicity and phosphorescence is defined as the radiative transition between two states of different multiplicities, caused by an intersystem crossing from an excited singlet state to an excited triplet state followed by emission from the excited triplet state to the singlet ground state.

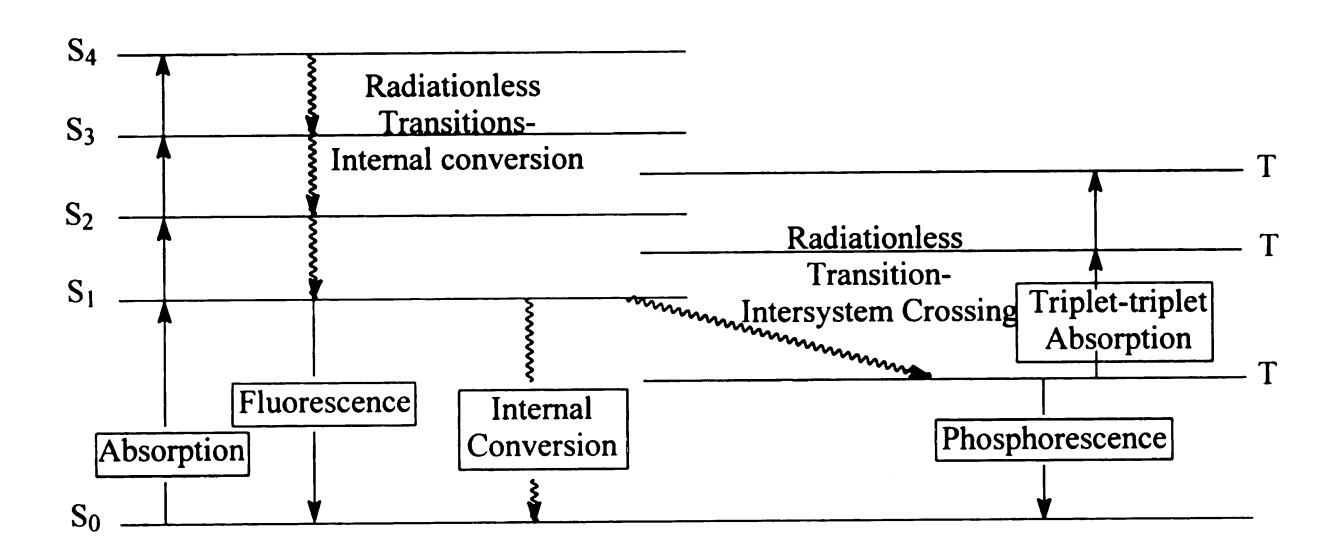


Figure 18: Schematic energy level diagram

Fluorescence spectra are seen at lower energy than absorbance spectra because the transition is from the lowest vibrational level of the electronic excited state to the ground state. The lowest energy absorption and the highest energy emission are often due to the same transition, namely the 0-0 transition and thus the low energy edge of the absorption band is usually structurally similar to the fluorescence spectrum, often in a mirror-like pattern if the vibrational structures of the singlet ground and excited states are similar. The displacement between these two bands is referred to as the "Stokes shift". Similar ground and excited state geometries lead to small Stokes shifts, while significant changes in geometry following excitation lead to large Stokes shifts. The Franck-Condon principle states that electronic transition are vertical and between levels on the Morse potential energy curves. If the minima in the Morse potential energy curves are not at the same coordinates, the minimum energy for absorption will be larger than the difference in energy between the lowest energy excited states and the ground state. When an excited molecule relaxes through the vibrational states and fluoresces from the S<sub>1</sub> state, a lower energy transition results, and the difference in energy for the absorption and emission is the Stokes shift.

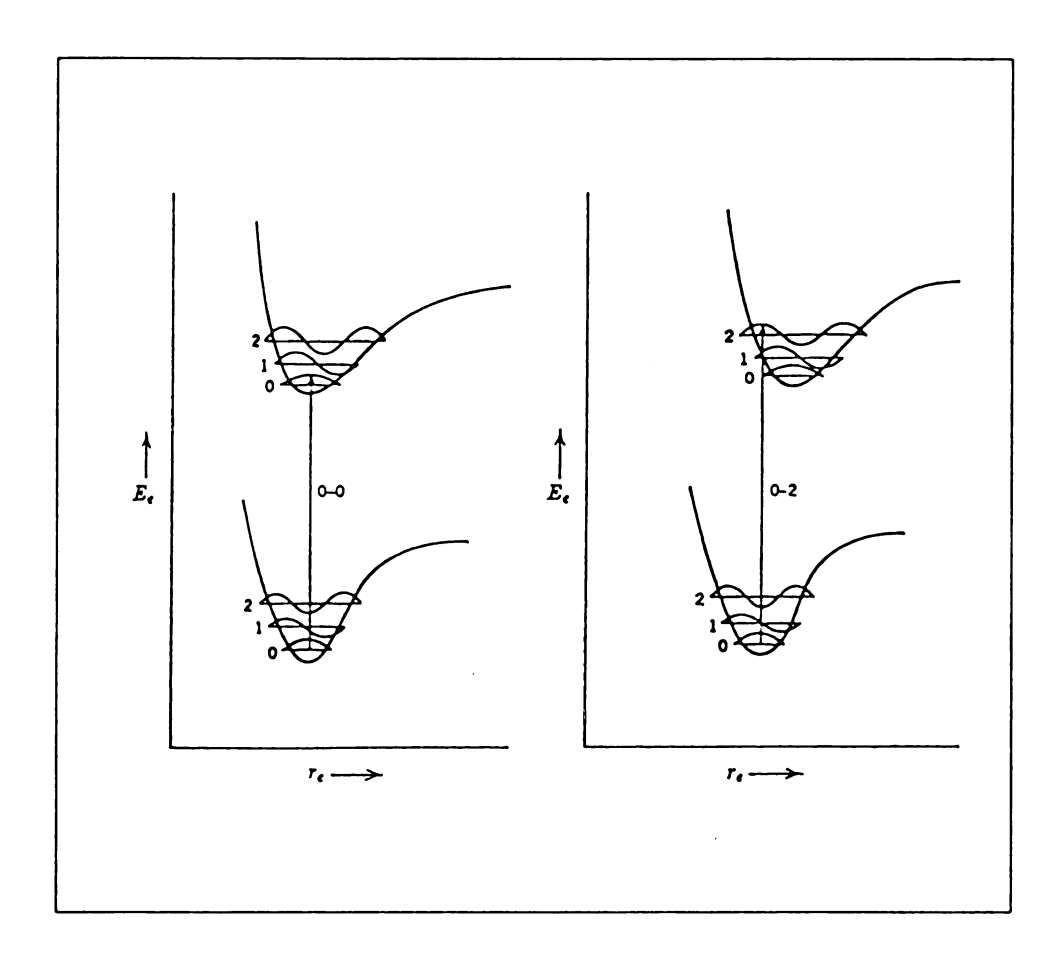


Figure 19: Morse potential energy curves demonstrating the Franck-Condon  ${\bf Principle}^{66}$ 

The length of the phenylene chain has an important effect on the optical spectra. Theoretically, the longer the chain is, the smaller the band gap should become. Figure 20 shows how the gap between the  $\pi$  and  $\pi^*$  orbitals (called the band gap) decreases as more p orbitals are in conjugation. The band gap is defined as the energy gap between the HOMO and LUMO (or conduction band and valence band) in a molecular orbital diagram. This gap can be measured by absorption spectroscopy by observing the optical absorption edge. The band gap of PPP is about 2.7 eV, 68 polyacetylene (PA) is about 1.4 eV and a conducting metal has a band gap approaching zero. However, the band gaps of most conjugated polymers are finite. The band gap energy (Eg) is inversely proportional to the number of conjugated units in the polymer. This number, called the "effective conjugation length", corresponds to the size of the lowest energy excitation, meaning the distance over which the excited state is delocalized. The conjugation length is an effect of the amount of double bond character between  $\pi$ -electron-containing units

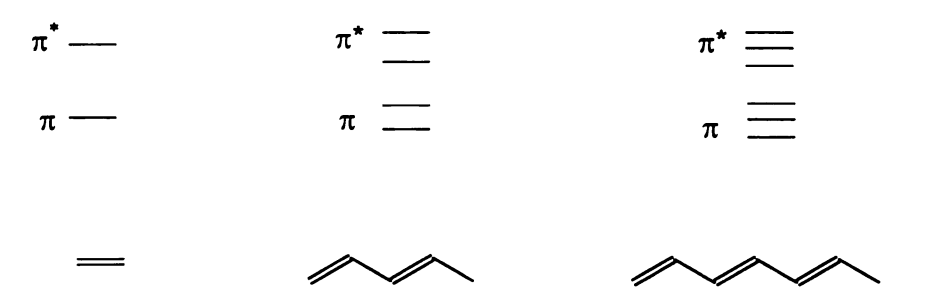


Figure 20: Decrease in band gap for conjugated molecules

so a molecule with an infinite effective conjugation length would have all its bonds exactly the same length. The effective conjugation length for polyphenylene is not equal

to the length of the polymer because the steric interactions of the protons *ortho* to ring junctions cause the rings to twist slightly out of alignment to a dihedral angle of about 23°.<sup>2</sup> This twisting results in a decrease on the p-orbital alignment, causing decreased overlap. Alkyl groups cause a twist of about 45° between the rings. Thus, oligomers that are longer than the effective conjugation length have the same properties as PPP, allowing the use of a processible oligomer in place of an intractable polymer in electronic applications.

Figure 20 is adequate for describing the electronic structure of simple polyenes, but is perhaps too simple for PPPs. We must consider aromaticity in polyphenyls to describe the electronic structure of PPPs. The conjugation between each ring is decreased relative to PA because the aromaticity of the individual phenyl rings prevents electron delocalization along the polymer chain. Calculating the band gap for polyphenylenes is actually quite complicated and has been studied extensively 69-73, but a complete explanation of these studies is not necessary to understand our work. We will use a more simple model, treating the phenyl rings as individual conjugated units and examine how connected the units are to each other and how substituents affect that connection. The excited state structures of a simple polyene and a polyphenylene are

Figure 21: Excited state structures of polyphenylene and polyacetylene

represented in Figure 21. This diagram shows how the singlet excited state structure of a PPP destroys the aromaticity and therefore  $\pi$  electron delocalization is not spread over a large number of units.

The spectra of PPP oligomers contain two main bands, the K band and the B band. The B band is attributed to the excitation of individual benzene rings, and is affected by changes in substitution but not by differences in chain length. In benzene, this band is found at 256 nm (hexane), but substituting the ring with methyl groups shifts the B band to 261 nm for toluene, 266 for mesitylene and 272 for hexamethylbenzene. The K band is polarized along the backbone of PPPs and is sensitive to changes in the conjugation of the benzene ring. In benzene, the K band is found at 204 nm and in biphenyl it shifts to 252 nm, obscuring the B band. Figure 22 illustrates the bathochromic shift of the K band with increasing oligomer length. To

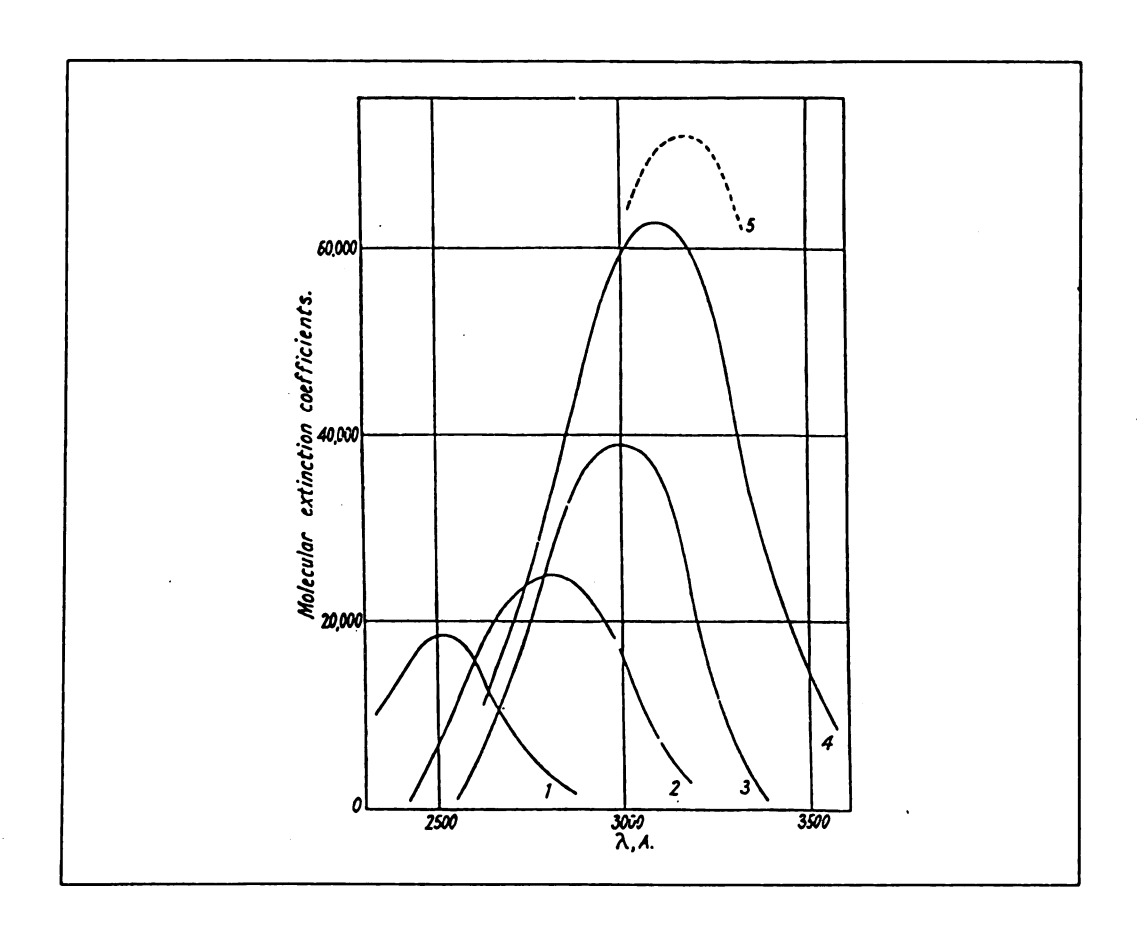


Figure 21: Absorption spectra of PPP oligomers in chloroform.. 1. biphenyl 2. terphenyl 3. quaterphenyl 4. quinquephenyl 5. sexiphenyl (qualitative only)

Grem and Leising<sup>76</sup> investigated the tunability or "band-gap engineering" of LEDs designed from polyphenylenes. The band gap in conjugated polymers can be tuned by introducing alkyl side chains on the rings, increasing the degree of twisting due to *ortho* interactions. The band gap is directly related to the degree of  $\pi$ -overlap along the polymer chain, and by increasing the twist angle, the  $\pi$ -overlap is decreased. (Figure 23).

The effect of alkyl chains can be observed in the UV absorption spectra. In 2,5-dihexyl-substituted PPP,  $\lambda_{max} = 318$  nm.<sup>77,78</sup> The calculated  $\lambda_{max}$  is ~344 nm for unsubstituted PPP, but thin film samples exhibit  $\lambda_{max}$  at 379 nm.<sup>79</sup> Both the calculated and measured values of  $\lambda_{max}$  are at longer wavelengths, reflecting the better  $\pi$  overlap for polyphenyls without *ortho* substituents.

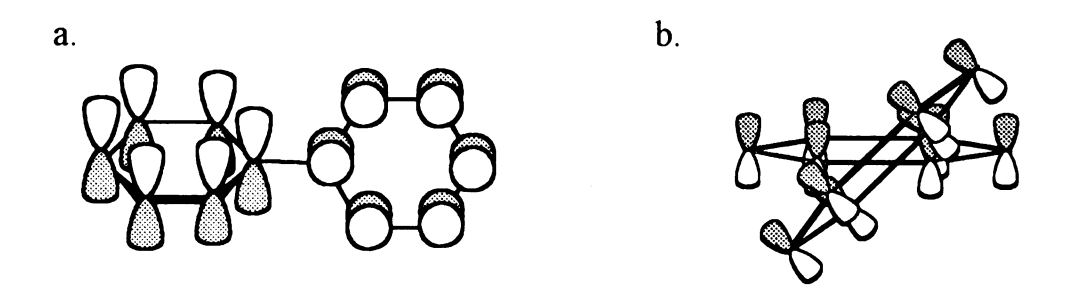


Figure 23: Twisted biphenyl. a. side view, b. end-on view

## D. Rotational Barriers In Polyphenylenes

One particularly interesting aspect of polyphenylenes is that by placing a substituent on the main chain, the barrier to rotation around the phenyl-phenyl bond is significantly increased. Barriers can often be characterized by Nuclear Magnetic Resonance (NMR). Dynamic NMR is useful in determining rotational barriers if the two rotamers are nonequivalent, meaning that distinct peaks will be present in the NMR spectrum for a each rotamer as long as the rotation is slow on the NMR time scale. This phenomenon can be caused by a steric effect, in which a bulky group prevents easy rotation around a bond, or an electronic effect where conjugation makes free rotation energetically unfavorable. A classic example is N,N-Dimethylformamide (DMF), which typically shows two peaks for the two methyl groups at room temperature due to the considerable double bond character of the C-N bond, but as the sample is heated, the two peaks coalesce into one peak. A typical set of coalescing peaks is shown in Figure 24.

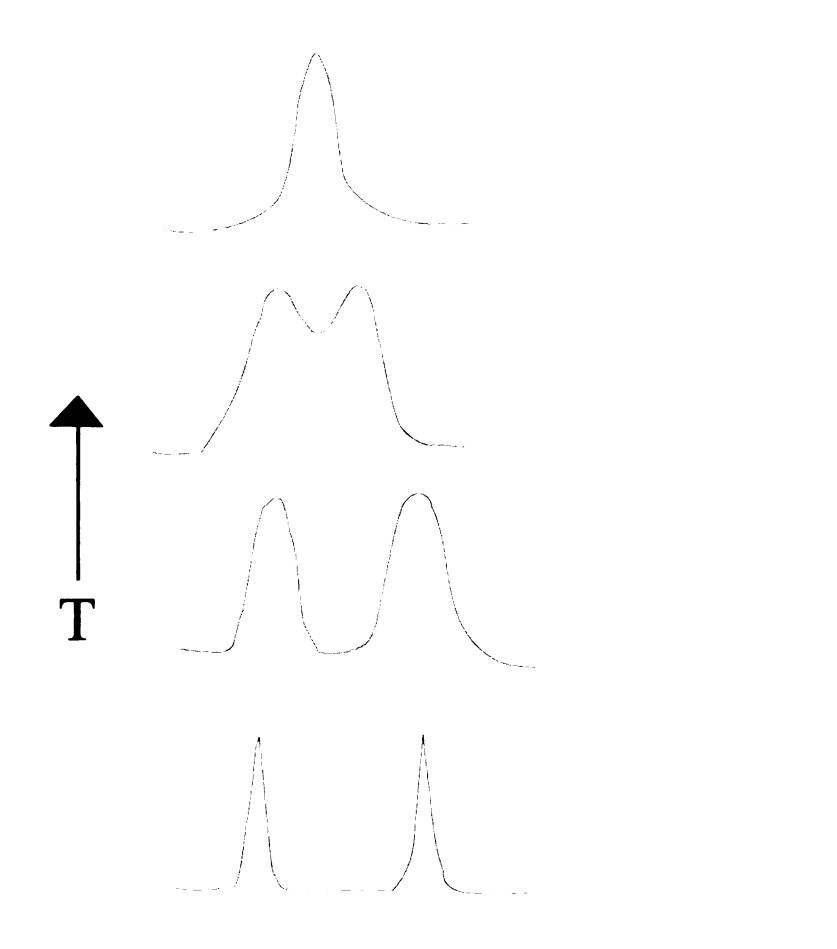


Figure 24: Coalescing peaks in an NMR spectrum

By measuring the spectrum at several temperatures and observing the temperature where the signals for the two states coalesce, one can derive the rate constants and the energy needed to cause the bond in question to rotate freely on the NMR time scale. The Gutowsky-Holm approximation<sup>80,81</sup> is probably the most commonly equation used to determine rotational barriers from NMR data. In practice, the coalescence point is determined by gradually increasing the temperature of the NMR sample until the small valley between the two coalescing peaks just disappears. The value of  $\delta v$  varies with the solvent used, but this variability is inconsequential, since the coalescence temperature varies as well. Outlined below is a brief derivation of the Gutowsky-Holm approximation for calculating rotational barriers.

The absolute rate theory developed by Eyring based on statistical thermodynamics

$$k = \kappa \frac{k_B T}{h} e^{-\Delta G^{\ddagger}/RT}$$

where k is the first order rate constant,  $k_B$  is the Boltzmann constant,  $\kappa$  is the transmission coefficient (the fraction of all molecules reaching the transition state that proceed forward to product molecules), h is Planck's constant and T is temperature. If k and T are known, and we assume that  $\kappa$  is unity, one can obtain the equation for  $\Delta G^{\ddagger}$ .

$$\Delta G^{\ddagger} = aT[10.319 + \log(T/k)]$$

$$a = 1.914 \times 10^{-2} \text{ for } \Delta G^{\ddagger} \text{ in kJ mol}^{-1}$$

$$a = 4.575 \times 10^{-3} \text{ for } \Delta G^{\ddagger} \text{ in kcal mol}^{-1}$$

To determine the barrier to rotation from the coalescence temperature, k is replaced by  $\pi \delta \upsilon / \sqrt{2}$ , where  $\delta \upsilon$  is the frequency difference in Hertz between the two peaks at the slow exchange limit, and the Gutowsky-Holm equation is obtained.

$$\Delta G_c^{\ddagger} = aT[9.972 + \log(T/\delta v)]$$

The equation is only slightly sensitive to error in measurement; an error of  $\pm$  2 °C in determining  $T_c$  results in an error of 0.12 kcal mol<sup>-1</sup>.

The barriers to rotation around the phenyl-phenyl bond of many biphenyl derivatives have been studied by VTNMR and by computational methods. The first application of this technique to biphenyls, reported by Mever and Mever<sup>82</sup>, examined the energy barrier to inversion of 2,2'-bis(acetoxymethyl)biphenyl. The methylene protons showed an AB quartet signal at room temperature which coalesced to a singlet at 94 °C in CS<sub>2</sub>, indicating a rotational energy barrier of 13 kcal/mol. Oki and Yamamoto<sup>83</sup> determined that the barrier for 2.2'-diisopropylbiphenyl was greater than 27 kcal/mol, at which point the NMR signals showed no broadening or coalescence. Bott, et al.84 studied the steric effects on the rotational barriers of 2,2'-disubstituted biphenyls by introducing a prochiral group that can be monitored by NMR. The prochiral group is necessary if the molecule is symmetric in either rotational state. They found that the rotational barrier showed the expected linear increase with increasing van der Waals radii of the substituents. More recently, the rotational barrier for oligothiophenes has been studied.85-87 which is much lower than for phenylenes, because the ring angles are smaller in thiophenes, so there is less steric interaction between adjacent rings.

Hindered rotation in aryl systems has been investigated due to its effect in biologically active compounds<sup>88</sup> and as potential models and/or building blocks for devices.<sup>89</sup> Charlton, *et al.*<sup>90</sup> studied hindered rotation in arylnaphthalene lignans by dynamic NMR and found that the barriers to rotation ranged from 16.9 to 21.5 kcal/mol for the compounds they studied. This hindered rotation produces optically active compounds due to the possibility of 2 or more possible rotational states. 1,1'-Binaphthyl has a computed<sup>91</sup> (PM3) barrier of 23.1 kcal/mol which is almost in exact agreement with the experimentally determined<sup>92,93</sup> barrier of 22.5 kcal/mol. This feature has been recently examined in liquid crystals<sup>94</sup> and optically active polymers.<sup>95,96</sup>

NMR relaxation studies can also provide important information the amount of motional freedom of a molecule. There are two mechanisms by which the nucleus can relax, denoted by the time constants  $T_1$  and  $T_2$ .  $T_1$ , also called the spin-lattice relaxation time, involves transfer of energy from the nucleus to the surroundings, or "lattice". The longer the  $T_1$  time, the less efficient the relaxation. A very constrained molecule (by steric effects or covalent bonding) will have a much longer  $T_1$  than a molecule which has many motional degrees of freedom.  $T_2$ , or spin-spin relaxation time, is the time constant that represents the loss of energy from one nucleus to another.

### E. Side Chains

Side chains are commonly placed on many types of molecules to increase their solubility. Examples include phenacenes<sup>97</sup>, polyphenylene vinylene, polythiophenes, polyacetylenes, polyphenylenes. Wirth reported that the solubilities of several polyphenylene oligomers in toluene correlated with their melting points; the more

soluble a compound, the lower its melting point. These results inspired some of the research done for this thesis, which contains a full analysis of the exact effects of side chains of differing lengths on oligomers of various lengths.

One significant effect of adding side chains is a change in melting point. Heitz<sup>98</sup> synthesized a series of mono-methyl substituted poly(*p*-phenylene) oligomers and showed that the addition of the methyl groups decreased the melting point. Wirth<sup>15</sup> reported a similar melting point decrease for 2,5-dimethyl substituted oligomers. (Table 2) Interestingly, the melting points for the tetramethyl-substituted oligomers were higher than those for the dimethyl-substituted oligomers, demonstrating that perhaps symmetry

Table 2: Melting points of PPP oligomers 15

n	2	3	4	5
-{\bigs_n}_n	71 °C	215 °C	320 °C	395 °C
CH <sub>3</sub>	54	183	266	309
H <sub>3</sub> C CH <sub>3</sub>	137	272	272	N/A

plays a role in the melting point.

A number of polymers have been studied to determine the effect of the degree of polymerization and/or side chain substitution on the thermal transitions of the polymer. Heitz characterized a series of 2- and 3-methyl substituted, exact-length oligomers, (Figure 25) and found that the Differential Scanning Calorimetry (DSC) plots of oligomers containing up to 6 rings showed only one transition, a crystalline-isotropic transition. However, when the number of phenyl rings was increased from 6 to 8, simple melting at 142 °C was replaced by a smectic liquid crystal (L.C.) phase between 273 and 311 °C. Increasing the chain to 10 rings resulted in a smectic phase from 242 to 260 °C and a nematic phase at temperatures greater than 260 °C with no isotropic phase reported. Finally, when the number of rings was increased to 12, the oligomer showed only one transition to a nematic phase at 298 °C. Heitz also examined oligomers with one or two

Figure 25: Heitz's methyl-substituted sexiphenyl

meta linkages, and these compounds did not show any ordered phases. This work suggests that for an ordered phase to occur, a polyphenyl must be at least 8 rings in length and be completely linear.

McCarthy, et al<sup>99</sup> synthesized didodecyl-substituted PPPs with molecular weights ranging from 8000 amu to 137,000 amu as determined by gel permeation chromatography (polystyrene standards). Using DSC, they showed that polymers with

molecular weights less than 44,000 amu showed only one transition, polymers with molecular weights from 44,000 to 73,000 showed two transitions, and the 137,000 amu polymer showed only one. By comparing their DSC results to polarized optical microscopy, these investigators showed that the lower molecular weight polymers did not show any liquid crystallinity, the middle polymers showed an L.C. phase and an isotropic phase, and the highest molecular weight polymer showed only a transition to a liquid crystalline phase. These studies showed that liquid crystal phases formed at length: width ratios (axial ratio) of 6 or greater. They assigned the geometry of the lower molecular weight polymers to be "starlike" and the longer polymers to be of the "hairy-rod" type. The difference in geometry for these two polymer types was also shown in a viscosity study. For the longer hairy rods, the steady shear viscosity drops upon formation of the mesophase while the viscosity of the shorter polymers remains constant. This shear thinning effect is well known for liquid crystalline polymers.

Rehahn, Schlüter and Wegner<sup>77</sup> used Suzuki coupling to synthesize 2,5-disubstituted polyphenylenes with side chains ranging from one to 16 carbons. The polymers having at least a six-carbon side chain were completely soluble in hot toluene. When examined by DSC, these polymers showed two transitions, which the authors named T<sub>1</sub> (lower temperature) and T<sub>2</sub> (higher temperature). The T<sub>1</sub> transitions ranged from 60 °C for the longest chain to 80 °C for the shortest chain, while the T<sub>2</sub> transitions ranged from 160 °C to 280 °C. The authors attributed the T<sub>1</sub> transition to side chain melting, while T<sub>2</sub> corresponded to the transition to the isotropic melt (as seen by polarized optical microscopy). A small change in T<sub>1</sub> with increasing side chain length and a large change in T<sub>2</sub> indicates that the nature of the side chains has a significant effect

on the polymer properties. In this paper, the authors were not able to determine the nature of these transitions, or identify the phases between  $T_1$  and  $T_2$ .

# II. RESULTS

Throughout the Results and Discussion sections, the following abbreviations for oligomers are used. (Table 3)

Table 3: Abbreviations of oligomers used in the text

$$H \xrightarrow{R} H$$

Compound	Side Chain (R)	Number of rings (n)	Abbreviation
9a	-CH <sub>3</sub>	2	TMB
10a	-CH <sub>3</sub>	3	HMT
15a	-CH <sub>3</sub>	4	OMQ
16a	-CH <sub>3</sub>	5	DMQ
9b	-CH <sub>2</sub> CH <sub>3</sub>	2	TEB
10b	-CH <sub>2</sub> CH <sub>3</sub>	3	HET
15b	-CH <sub>2</sub> CH <sub>3</sub>	4	OEQ
16b	-CH <sub>2</sub> CH <sub>3</sub>	5	DEQ
10c	-C <sub>6</sub> H <sub>13</sub>	3	ННТ
16c	-C <sub>6</sub> H <sub>13</sub>	5	DHQ
17c	-C <sub>6</sub> H <sub>13</sub>	7	THS

## A. Synthesis

All oligomers in this project were synthesized by a combination of accelerated and traditional Suzuki coupling reactions. (Figure 26) As stated in the introduction, these reactions were chosen for their general applicability to a wide variety of coupling

Figure 26: Traditional and accelerated Suzuki coupling reactions

reactions, and their proven reliability in the synthesis of polyphenylenes. We devised an iterative scheme in which, once a library of starting materials was synthesized, the oligomers could be pieced together rather quickly. A similar scheme has been recently reported by Liess, *et al.* <sup>100</sup> Figure 27 shows the synthesis of the first methyl-substituted oligomers.

The boronic acid synthesis was optimized by using a Grignard reagent as the aryl nucleophile and triisopropyl borate as the borate ester. When an aryllithium reagent was used, residual alkyl groups were often seen in the <sup>1</sup>H NMR spectrum. One possible source of these peaks is a butyl benzene derivative, caused by nucleophilic attack on butyl bromide that was formed after the lithium-halogen exchange reaction. When the

Figure 27: Synthesis of the first oligomers

Grignard reagent was used, these impurities disappeared. By using triisopropyl borate, we reduced the amount of borinic acid in the product and achieved a purer crude product.

Oligomers 9a and 10a were quickly synthesized and the problem of obtaining the quaterphenyl and quinquephenyl oligomers was approached. Shorter oligomers need to be halogenated so that they can be coupled with aryl boronic acids to make longer oligomers. We initially attempted the direct solid state bromination of TMB and HMT, 101 but this reaction resulted in an inseparable mixture of products, including those resulting from benzylic bromination. We developed a new scheme in which the trimethylsilyl (TMS) group serves as a masked halogen. Figure 28 outlines the synthesis

Figure 28: Synthesis of TMS-functionalized materials

of these new TMS-functionalized starting materials. The TMS group does not interfere with Suzuki couplings, and the bis(TMS)-oligophenyl products can be transformed into dibromo- or diiodooligophenyls by reaction with bromine 102 or iodine monochloride/AgBF<sub>4</sub>, 103 respectively. (Figure 29) It is common practice to quench bromination or iodination reactions with Na<sub>2</sub>S<sub>2</sub>O<sub>3</sub>, but residual thiosulfate in the recrystallized product repeatedly deactivated the Pd catalyst used for coupling. Stannous chloride or an aqueous potassium hydroxide solution gave satisfactory results.

$$CH_3$$
 $CH_3$ 
 $CH_3$ 

Figure 29: Bromination and iodination of 4,4'-bis(TMS)-TMB

Once this problem was solved, we attempted to couple 8a and 4.4'-dibromo-2,2',5,5'-tetramethylbiphenyl **(A** in **Figure** 30) synthesize bis-(TMS)to octamethylquaterphenyl using the traditional Suzuki coupling, and obtained a mixture of at least seven products, with the major fraction (~20%) being the product of coupling at one ring of the dibromobiphenyl (Product B in Figure 30). All components were in solution after the 24 hour reaction time, so solubility is not a problem with this particular reaction. Longer reaction times and higher temperatures did not result in appreciable formation of product. We then synthesized 13a and attempted the coupling reaction again, since aryl iodides are more reactive than aryl bromides in the Suzuki coupling reaction. We again obtained a similar mixture of many products. It is unclear what caused this reaction to fail, considering that the steric requirements are the same for all of the couplings with methyl-substituted phenyl rings.

We finally synthesized OMQ using Novak's accelerated Suzuki coupling reaction using Pd(OAc)<sub>2</sub> as the catalyst.<sup>50</sup> As a test reaction, we attempted to synthesize **9a** by this method from the aryl bromide but found that this reaction can only be used with aryl iodides since the bromides are more sensitive to steric hindrance causing a slower

$$X \longrightarrow H_3C$$
 $H_3C$ 
 $H_3C$ 

Figure 30: Incomplete reaction in accelerated Suzuki coupling

oxidative addition step in the catalytic cycle. Novak recommends acetone as the solvent of choice due to its polarity and miscibility with water. In a reaction of 13a and 7a, the almost exclusive product was that from the first coupling reaction (Figure 30). This intermediate is insoluble in acetone and accounts for failure of the reaction. The catalyst was not soluble in toluene, but when we used tetrahydrofuran as the solvent, the reaction yielded almost exclusively OMQ. We also synthesized DMQ by this method. Both OMQ and DMQ precipitated from solution as they were formed, so these longer oligomers could not be prepared by this method. These oligomers could not be purified by recrystallization, distillation or conventional column chromatography; instead they were purified in small amounts using preparatory thin layer chromatography (TLC). We found that it is imperative that the starting materials are of the highest possible purity, as any impurities were very difficult to remove, even using prep TLC plate.

After we established the synthetic methodology for the exact length methyl-substituted oligomers, we moved to the ethyl-substituted oligomers. Unfortunately, 2,5-dibromo-1,4-diethylbenzene is not commercially available for a reasonable price, so we synthesized the ethyl-substituted starting materials from ethyl benzene (Figure 31). This synthesis proceeds in about 63% overall yield for 3b, with the Clemmenson reduction being the yield limiting step. However, the starting materials are relatively inexpensive

Figure 31: Synthesis of ethyl-substituted starting materials

and the reactions are easy to run on a large scale. From these starting materials, the ethyl-substituted oligomers were synthesized in the same manner as the methyl-substituted compounds, except that the shorter oligomers (TEB and HET) could not be synthesized directly by coupling **6b** and **7b**. Instead, they were first synthesized and purified as the bis(TMS) compounds, and then the TMS groups were removed with trifluoroacetic acid. <sup>104</sup> We did not investigate why the coupling failed, but it is likely due to impure starting materials.

The hexyl-substituted bromobenzenes were synthesized using literature procedures 105. We chose the hexyl side chain because a hexyl substituent is the smallest one that will make a PPP completely soluble in toluene. We synthesized 2-bromo-1,4-di-n-hexylbenzene (6c) in the same manner as 6a and 6b. However 1,4-di-n-hexyl-5-trimethylsilyl-2-phenylboronic acid (8c), was much more difficult to synthesize and purify than 8a and 8b. When we used the usual procedure, the yield of boronic acid was very low. The main side product was 2-trimethylsilyl-1,4-dihexylbenzene, suggesting

that the Grignard reagent was formed and then quenched by a proton source at some point in the reaction. We did not conduct any deuterium studies to determine if the quenching occurred during the Grignard formation or during the boronic acid addition, but since the use of a less bulky borate increased the yield of boronic acid, the borate addition step seemed the likely culprit. Even ensuring that the Grignard step went to completion and by using trimethylborate instead of triisopropyl borate, the highest yield of boronic acid we obtained was ~60%. This product was purified by column chromatography using toluene to elute the side products followed by diethylether to elute the boronic acid. We also found that it was very important to work up the reaction promptly after hydrolyzing the borate ester since the boronic acid moiety partially hydrolyzed to a phenol after prolonged stirring in water.

We chose only to synthesize the odd-numbered oligomers so we could work up to a long chain length quickly. We were able to synthesize iodinated hexylbenzenes with a mixture of I<sub>2</sub> and H<sub>5</sub>IO<sub>6</sub> in acetic acid. We found that the best method to make the long hexyl oligomers was to add biphenyl boronic acid units instead of phenyl boronic acids. This eases the separation of incomplete oligomers from the desired product because the longer the oligomers are, the more similar their properties are, making them more difficult to separate. Figure 32 shows the synthetic scheme for these oligomers.

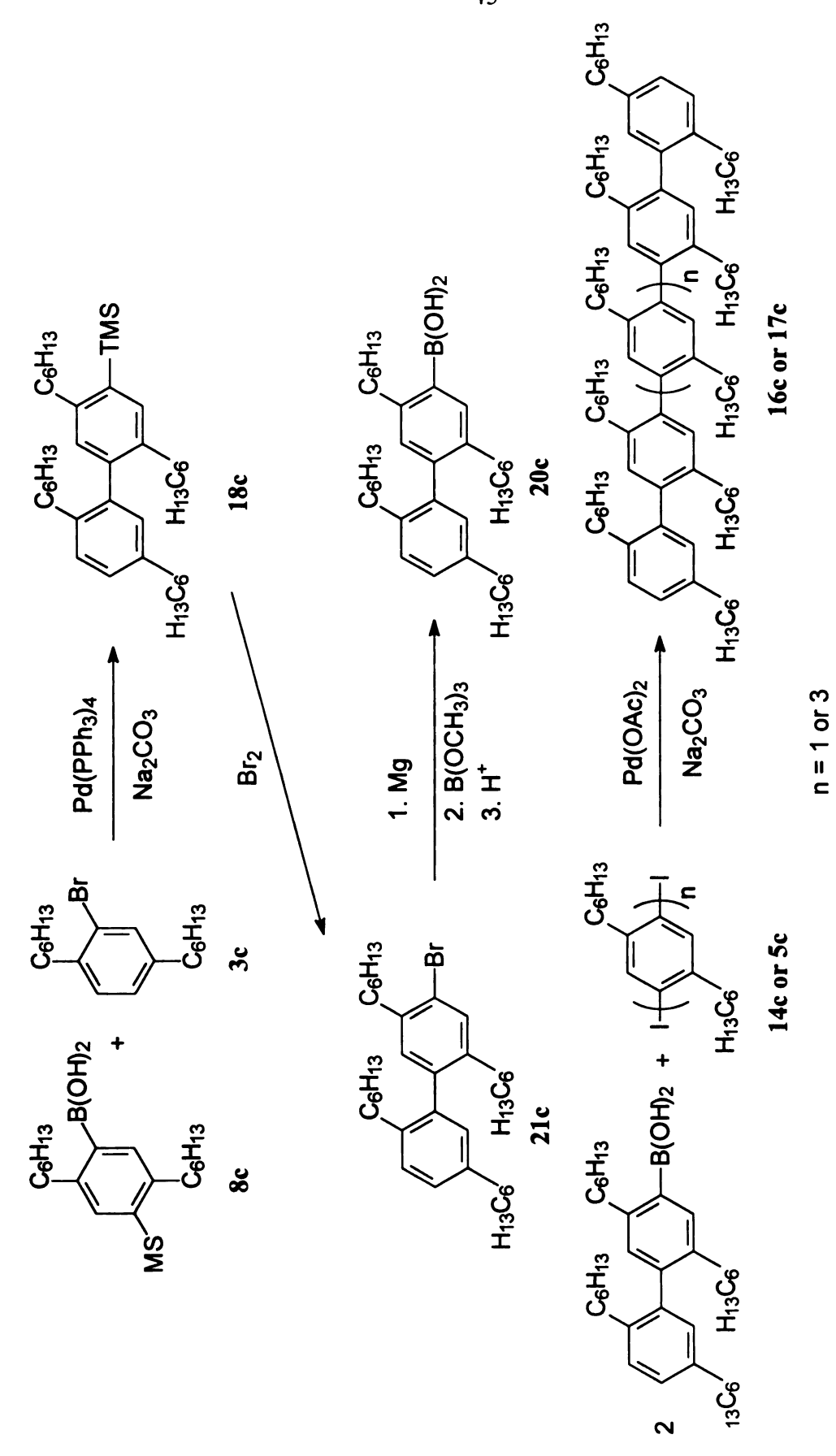


Figure 32: Synthesis of hexyl-substituted oligomers

### **B.** Rotational Barriers

As mentioned in the introduction, the two rotational isomers of HMT (Figure 33) are diastereomers, and therefore show different NMR spectra. Knowing the magnitude of the barriers to rotation might be important for understanding why some substituted polyphenylenes are soluble and some are not.



Figure 33: The two diastereomeric rotational states of HMT

We measured the barriers to rotation around the bonds connecting phenyl rings in a series of oligomers that have side chains of different lengths. We also measured the rotational barriers for oligomers with the same side chain length but differing in the number of rings in the oligomer to see if increased conjugation affects the barrier. To examine whether it was feasible to determine the barriers experimentally, we calculated the barriers by using the program *HyperChem* in conjunction with *Microsoft Excel*. (Figure 35) Table 3 outlines the macro used to run *HyperChem* through *Excel*.

We calculated the barriers by first defining the dihedral angle  $\Theta$  (Figure 34) between the two rings. While fixing the 4 carbons that define the angle, the geometry of the rest of the molecule was optimized by a molecular mechanics algorithm (using MM+ force field) followed by a molecular dynamics scheme. The total energy of the molecule was calculated, then the angle was reset and the steps are repeated. We ran the entire cycle twice for each computation, once "forward" (from -180° to +180°) and once

"backward" (from +180° to -180°) because the calculated geometries just past the barrier maximum were not fully relaxed. Although the angle we defined requires that the phenyl rings be perfectly planar and this is not necessarily true, this calculation provided us with a good first approximation of what the rotational barriers looked like. The *HyperChem* calculation is intended as a rough indicator of the barriers to rotation, and does not take

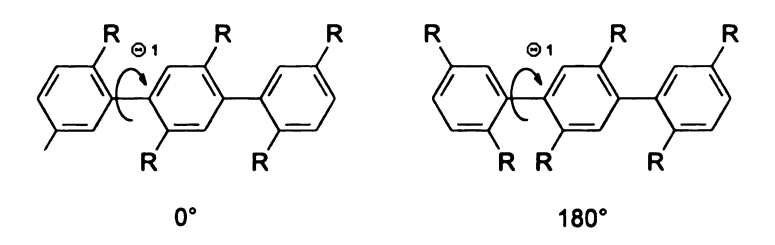


Figure 34: Dihedral angles for substituted terphenyls

into consideration all the factors necessary to do a complete computational assessment of the compounds. The curve for HHT should not be asymmetrical, but due to the large number of conformations available to a molecule with large alkyl side groups, the program is not capable of producing completely reproducible results. We chose to calculate the barriers for terphenyls, since we experimentally determined the barriers for the same compounds. The plots for biphenyls produce artificially low barriers, since the steric barrier can be significantly decreased by the alkyl groups moving away from the other phenyl ring. Terphenyl does still not provide an entirely accurate picture, but it provides a reasonable result in a short period of time.

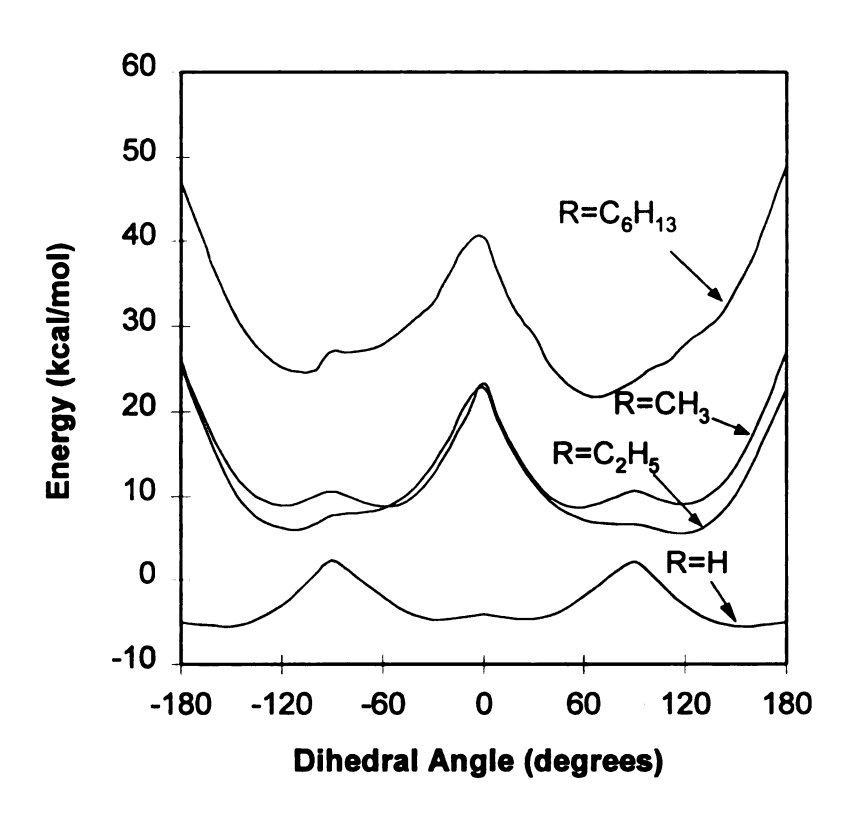


Figure 35: HyperChem calculation of rotational barriers for substituted terphenyls

Table 4: Microsoft Excel macro for computing barriers with HyperChem

Control-R	Compute.Results
Channel	=OpenFile()
	=IF(ISERROR(Channel))
	= RETURN()
	=END.IF()
Command	=EXECUTE(Channel, "[select-none]")
	=WHILE(NOT(ISBLANK(SELECTION())))
	=EXECUTE(Channel,"[query-response-has-tag(no)]")
	=EXECUTE(Channel, "[selection-target atoms]")
	=EXECUTE(Channel, "[select-atom 3 1]")
	=EXECUTE(Channel, "[select-atom 4 1]")
<u> </u>	=EXECUTE(Channel, "[select-atom 7 1]")
	=EXECUTE(Channel, "[select-atom 8 1]")
	=EXECUTE(Channel, "[set-bond-torsion("&SELECTION()&")]")
NewChan	=EXECUTE(Channel, "[menu-select-select-all]")
	=EXECUTE(Channel,"[un-select-atom 3 1]")
	=EXECUTE(Channel, "[un-select-atom 4 1]")
	=EXECUTE(Channel,"[un-select-atom 7 1]")
	=EXECUTE(Channel, "[un-select-atom 8 1]")
	=EXECUTE(Channel, "[calculation-method molecular-
	mechanics]")
	=EXECUTE(Channel, "[dynamics-run-time 0.5]")
	=EXECUTE(Channel, "[dynamics-time-step 0.001]")
	=EXECUTE(Channel, "[do-molecular-dynamics]")
	=EXECUTE(Channel, "[optim-algorithm fletcherreeves]")
	=EXECUTE(Channel, "[periodic-boundaries(no)]")
	=EXECUTE(Channel,"[screen-refresh-period 1]")
	=EXECUTE(Channel,"[optim-max-cycles 500]")
	=EXECUTE(Channel, "[do-optimization]")
	=FORMULA.ARRAY(REQUEST(Channel, "total-energy"), "rc[1]")
	=SELECT("r[1]c")
	=EXECUTE(Channel,"[select-none]")
	=NEXT()
	=TERMINATE(Channel)
	=RETURN()
	OpenFile
	=INITIATE("HyperChem","System")
	=IF(ISERROR(NewChan))
	= IF(ISERROR(EXEC("c:\chem\ship\chem",1)))
	= RETURN(NewChan)
	= END.IF()
	= RETURN(INITIATE("HyperChem", "System"))
	=END.IF()
	=RETURN(NewChan)

The results of the preliminary calculations indicate that in all of the substituted terphenyls, both steric barriers (where the rings are coplanar and the two alkyl groups must pass by each other) are greater than the electronic barrier (where the rings are orthogonal and the conjugation between the two rings is completely broken). However, for terphenyl, the electronic barrier is greater than the steric barrier, since only two hydrogen atoms have to pass by each other. Table 5 shows the calculated and experimental values obtained for the series of terphenyls.

Table 5: Rotational barriers for alkyl-substituted terphenyls

Compound	NMR (kcal/mol)	HyperChem (kcal/mol)
terphenyl	not measured	6.9 <sup>a</sup>
HMT	18.5	14.7 <sup>b</sup>
HET	20.8	16.0 <sup>b</sup>
HHT	21.4	18.7 <sup>b</sup>

a.  $\Theta = 90^{\circ}$ 

b. 
$$\Theta = 0^{\circ}$$

The calculated data show a big jump in the rotational barrier between the unsubstituted and substituted terphenyls, but the effects of increasing the side chain length were minor. To determine the values experimentally, we used a Varian VXR-500 spectrometer at 500 MHz to measure the coalescence temperature for the methyl resonances by taking <sup>1</sup>H NMR spectra at several temperatures. To ensure the reliability of the data, the samples were equilibrated for 10 minutes at each temperature and the spectrometer was shimmed and tuned before each spectrum was taken. Figure 36 shows spectra of HMT in the

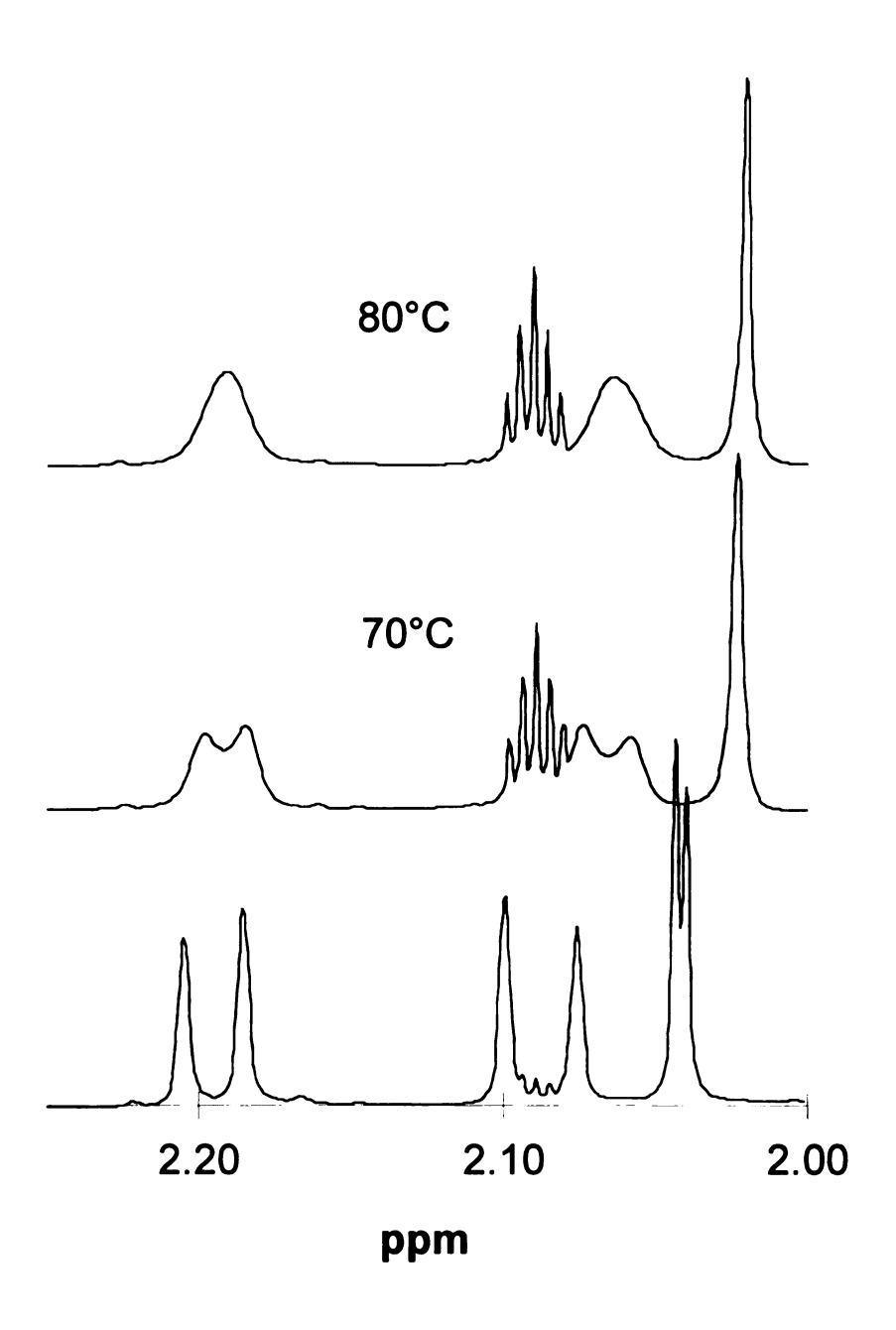


Figure 36: Variable temperature NMR spectra of HMT

methyl region at various temperatures. The chemical shift associated with temperature may be due to a change in the solvent density. The spectra shown in Figure 36 were taken in toluene- $d_8$  and the quintet at 2.09 ppm from residual toluene was used as a reference peak. The coalescence temperature for HMT was 80 °C, which corresponds to a rotational barrier of 18.5 kcal mol<sup>-1</sup>.

To determine if the barrier depended on chain length, we measured the barriers for the entire series of methyl-substituted oligomers (Table 6). The barrier for TMB cannot be measured because this molecule is symmetric and therefore the methyl groups are magnetically equivalent. Bott measured the barrier for TMB using line shape analysis at different temperatures of a biphenyl, using a prochiral group to monitor the bands.

Table 6: Rotational barriers for methyl-substituted oligomers

Compound	Number of rings	Rotational Barrier (kcal/mol)
TMB	2	19.484
HMT	3	18.5
OMQ	4	18.6
DMQ	5	18.3

It is fortunate that within experimental error (~0.3 kcal mol<sup>-1</sup>) the rotational barriers we measured for all of the methyl-substituted oligomers are the same, and thus a given oligomer in a series should be representative for all oligomers and polymers in that series. We chose to examine the terphenyl oligomer from each series, since its spectrum is the least complex and the chance for error is minimized. However, determining the rotational barrier for an ethyl-substituted oligomer such as HET is not as simple as for

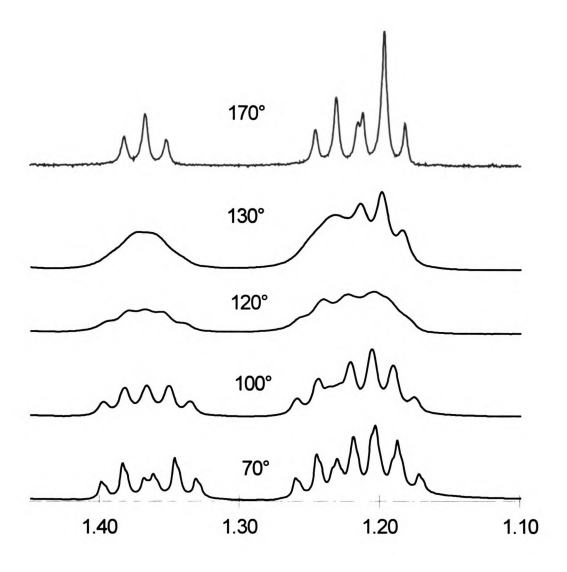


Figure 37: Variable temperature NMR spectra of HET in the methyl region

HMT. First, there are two alkyl sites that could be monitored, the methyl and the methylene moieties, and secondly, the spectra are much more complicated due to the coupling of these two groups. Figure 37 shows the variable temperature NMR spectra of HET in the methyl region. It is difficult to determine the coalescence point visually, since the coalescing peaks are triplets rather than singlets, and to our knowledge there are no literature precedents for monitoring the coalescence of triplets. To simplify the measurements, we employed a decoupling scheme in which the methylene protons were irradiated so that the methyl protons appeared as singlets instead of triplets. We thus determined that the coalescence temperature for HET is 130 °C in o-dichlorobenzene-d<sub>4</sub>. To help confirm this result, we simulated the decoupled spectra using *Microsoft Excel*. By using the center frequencies of the coalescing triplets and adjusting the line widths at different temperatures, we achieved simulated spectra that closely approximate the actual decoupled spectra. (Figure 38) Although we are confident that this method is valid for measuring the rotational barrier of coupled systems, we further confirmed our result by using an established method. A plot of the  $T_1$  spin-lattice relaxation time for an aromatic proton against the temperature should change in slope at the point where the rings can rotate freely. For the T<sub>1</sub> measurements, the samples were deoxygenated by bubbling dry nitrogen through the solution for at least 10 minutes immediately before the tube was placed in the spectrometer. The samples were allowed to equilibrate for 10 minutes and the spectrometer was shimmed and tuned as in the previous experiments. experiment was repeated several times, since there are many sources for error in a T<sub>1</sub> measurement.

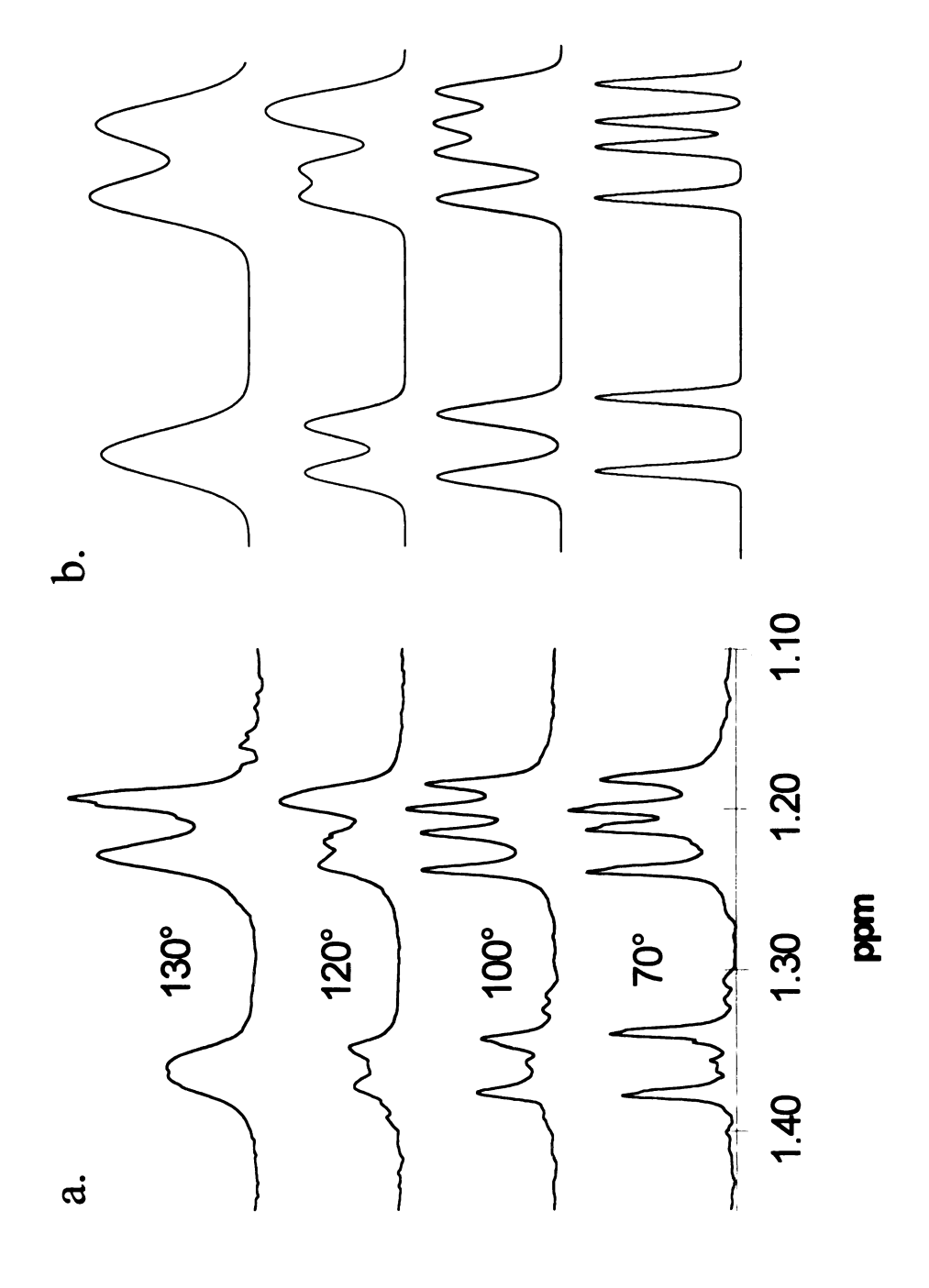


Figure 38: Actual and Simulated VTNMR spectra of HET

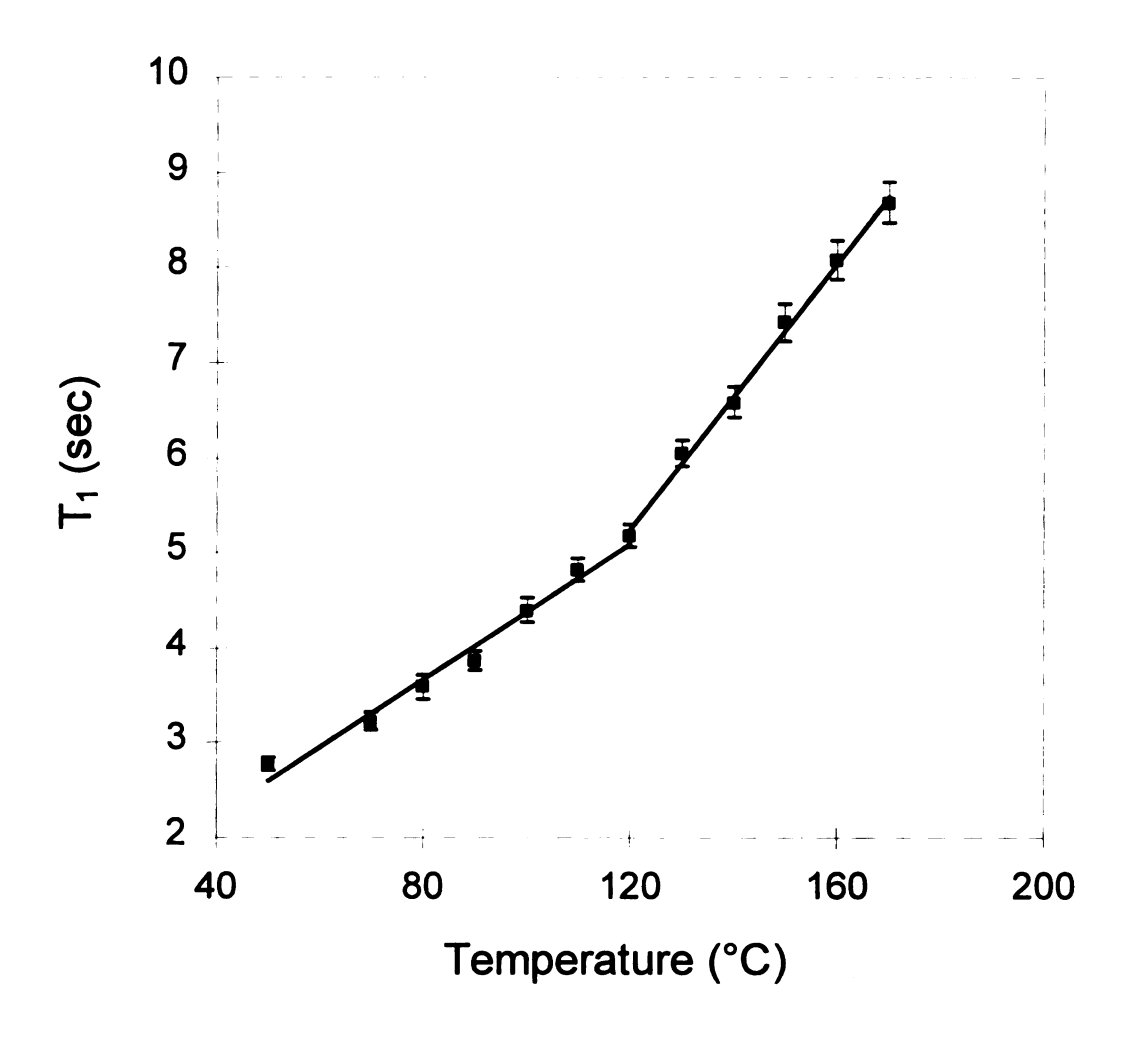


Figure 39: Plot of T<sub>1</sub> versus temperature for HET

Figure 39 shows the plot of T<sub>1</sub> versus temperature. The trend lines are guides for the eye. The slope changes at 120 °C, which is in good agreement with the results of the coalescence experiment. Coalescence at 120 °C corresponds to a rotational barrier of 20.3 kcal mol<sup>-1</sup>, while coalescence at 130 °C in *o*-dichlorobenzene, corresponds to a 20.8 kcal mol<sup>-1</sup> barrier to rotation for HET. The rotational barrier for HHT, determined using the same method, was 21.4 kcal mol<sup>-1</sup>, nearly the same as that of HET. Since an ethylsubstituted PPP is only partially soluble in hot toluene, but a hexyl-substituted PPP is completely soluble, we can conclude that rotational barriers do not significantly influence the solubility of a substituted polymer. This topic of solubility will be discussed in further detail in the discussion section.

## C. Optical Properties

PPPs are often examined for use in optical devices such as Light Emitting Diodes (LEDs) so it is important to understand how making these polymers soluble and processible can affect the optical properties. We examined the solution and solid state absorbance and fluorescence emission spectra of all oligomers synthesized. It is important to note that the solutions used for all absorption spectra were 1 x 10<sup>-4</sup> M solutions in cyclohexane. However, for clarity, the intensities of some fluorescence spectra were normalized to account for the large differences in quantum yield.

#### 1. UV-Vis Absorbance

Figure 40 illustrates the UV absorbance spectra for the methyl substituted oligomers. These data show an approximately linear relationship between the number of

phenyl rings and the integrated intensity of the absorbance peak for the oligomer. DMQ shows a slightly lower absorbance intensity due to the insolubility of the compound. By examining the absorbance spectra, we can extract information about the order in the system, which may be observed as line broadening or as a loss of structure in the spectra. One possible source of disorder is the number of rotational isomers. The number of rotational isomers possible increases geometrically with the number of phenyl rings in the chain. Each phenyl ring can rotate in a positive or negative sense relative to an adjacent ring, and since the calculated potential wells are symmetrical about  $\Theta = 0$ , this rotation is

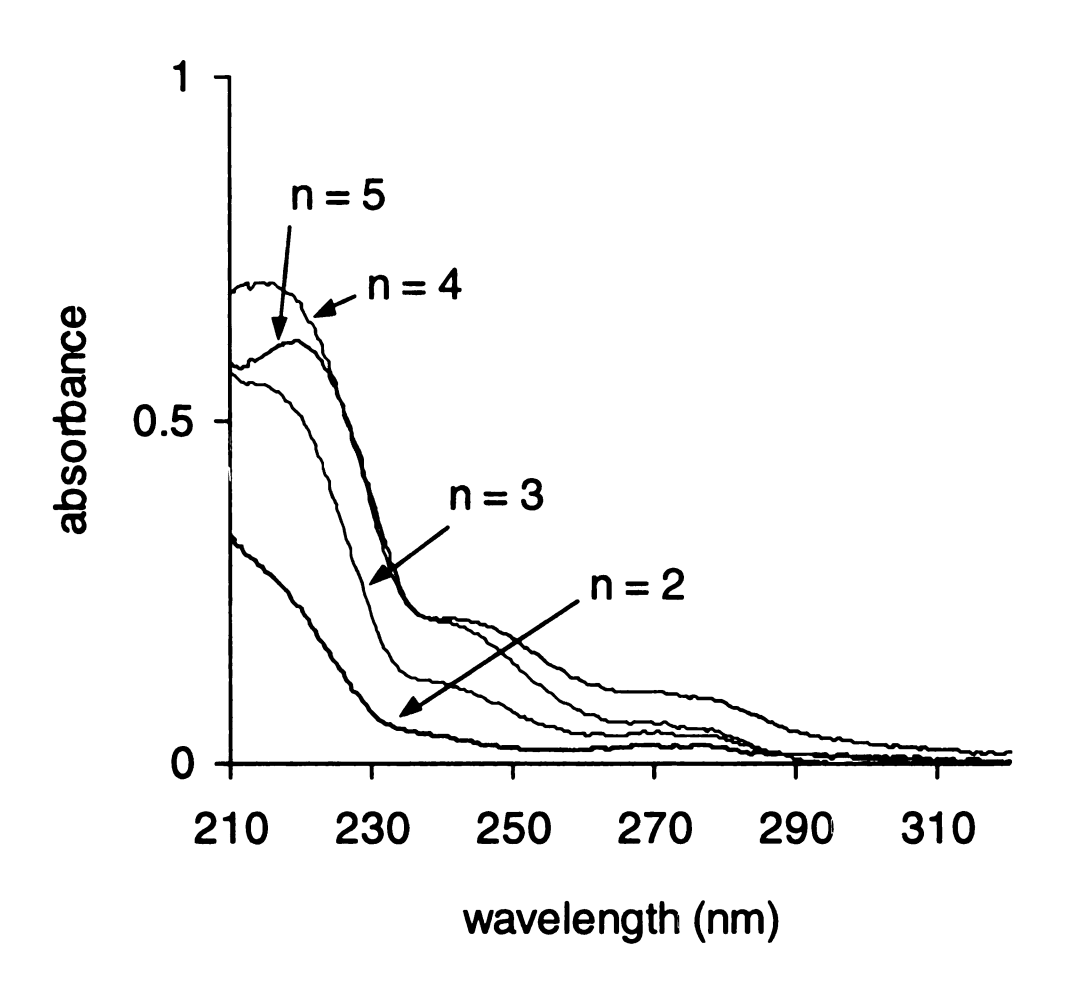


Figure 40: UV-Vis absorbance spectra of methyl-substituted oligomers

entirely random. Since these spectra behave as expected, showing an increase in the absorbance and in  $\lambda_{max}$ , we can conclude that the rotational isomers do not have a significant affect on the order in the system.

The spectra of the ethyl-substituted oligomers also show an expected increase in abosorbance intensity with an increasing number of phenyl rings (Figure 41). As the number of rings increases, the structure of the absorbance bands becomes less distinct. This could be caused by either the K band beginning to overtake the B band, or it could be an effect of the increased disorder. Although the B band is not affected by increases in conjugation and will not shift to lower energies with increasing oligomer length, it is possible that the loss of structure is due to an increased disorder in the overall system, so the band represents a combination of many differently configured benzene rings. By comparing the spectra of the ethyl-substituted oligomers with those of the methyl-substituted oligomers, the changes in the features are consistent with this hypothesis.

Figure 42 illustrates the spectra of the hexyl-substituted oligomers synthesized in this study. These spectra cannot be directly compared to those of the ethyl- and methyl-substituted oligomers, since the oligomer lengths are different, but the general trends can be compared. The absorbance increases as expected with increasing oligomer length, and

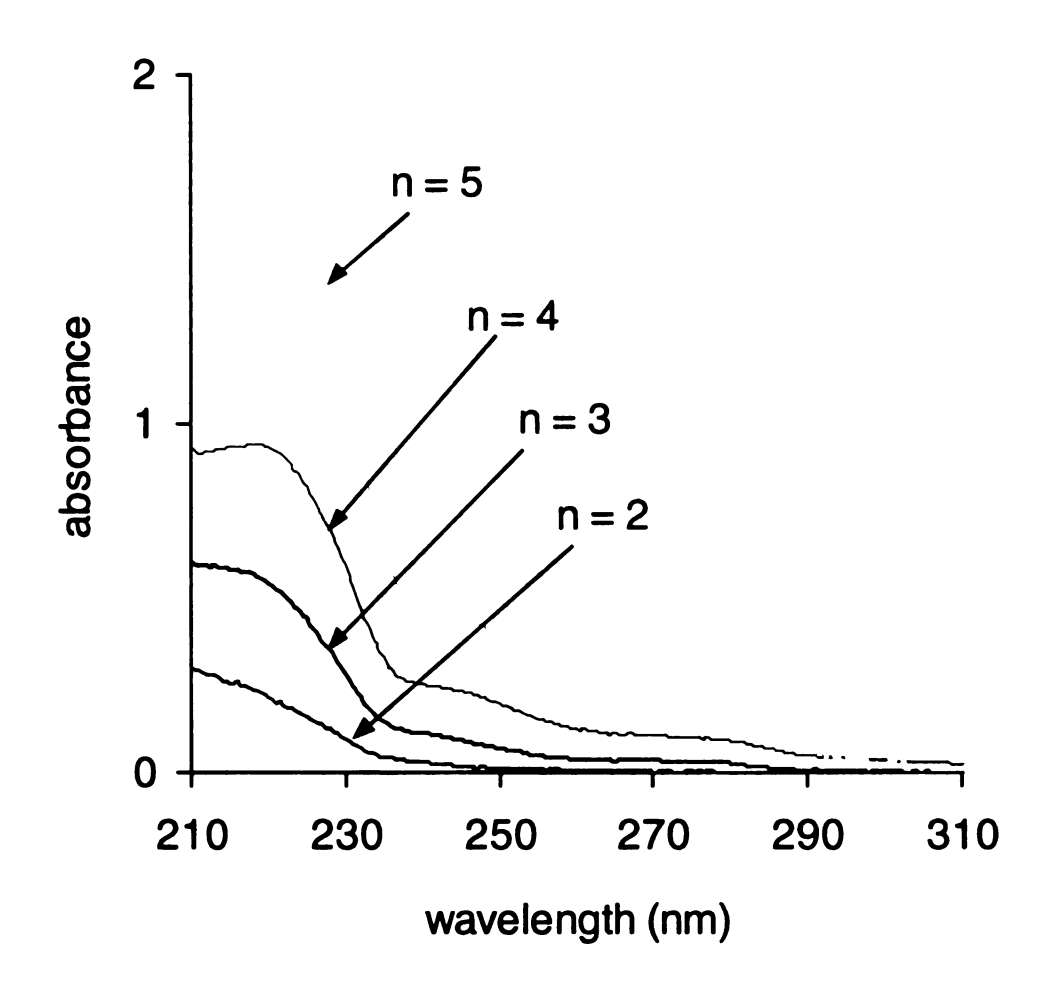


Figure 41: UV absorbance spectra of ethyl-substituted oligomers

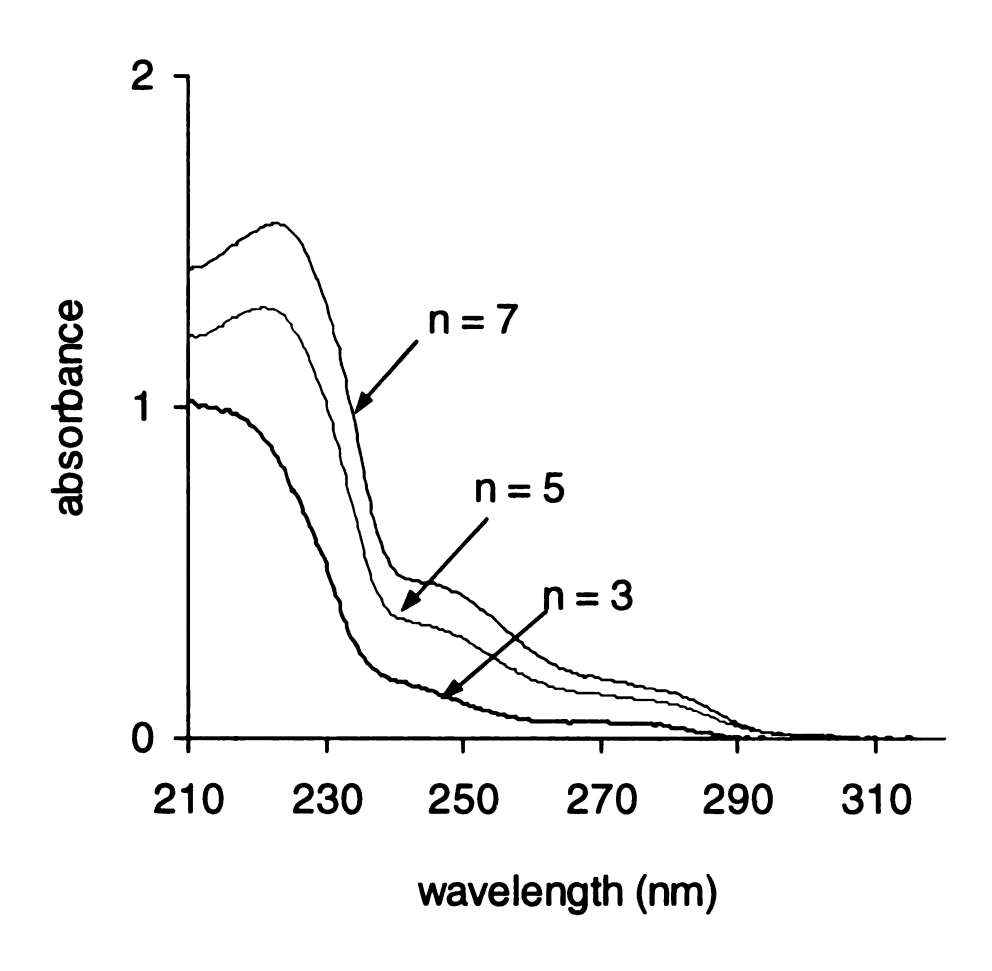


Figure 42: UV absorbance spectra of hexyl-substituted oligomers

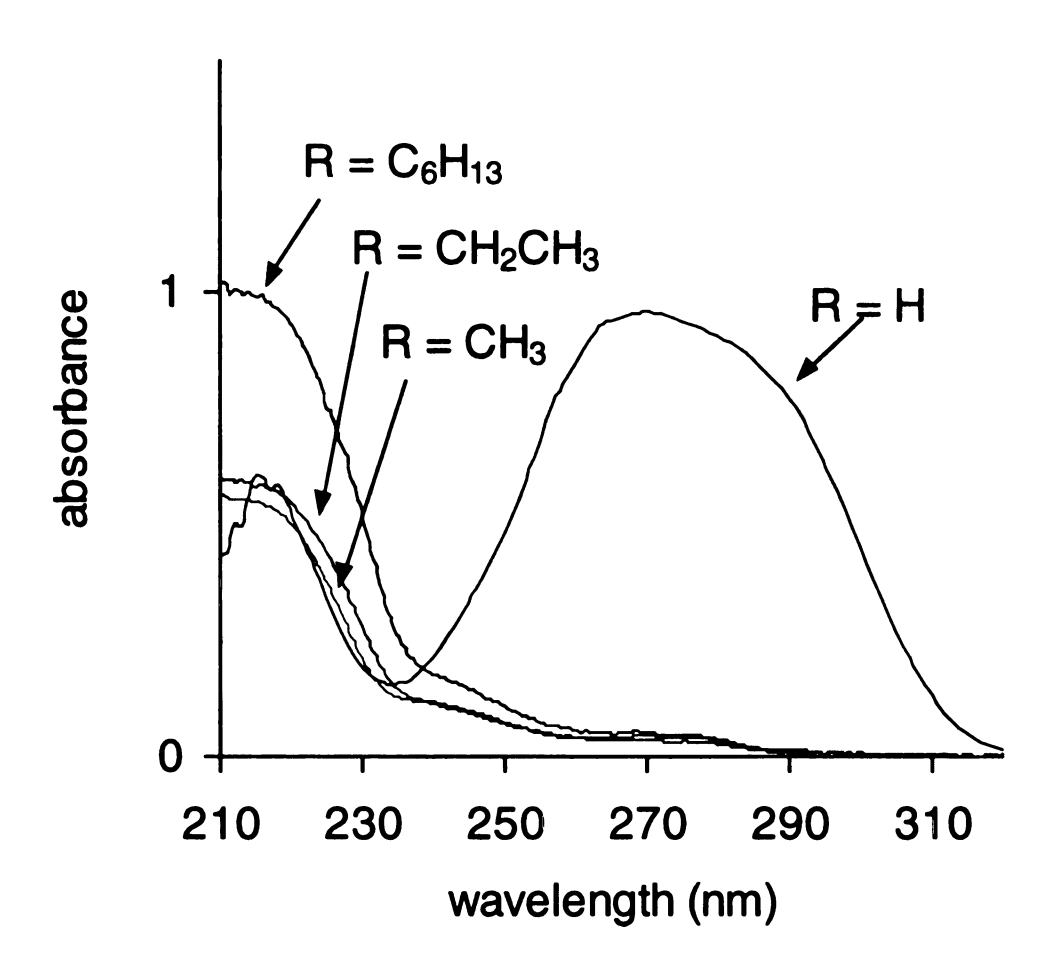


Figure 43: UV absorbance spectra of substituted terphenyls

the structure of the bands becomes less defined as there are more configurations available to the molecule.

We also examined spectra that compare the different length side chains. (Figure 43) The spectrum of the unsubstituted terphenyl is obviously much different from that of the substituted terphenyls. The K band completely obscures the B band, which can still be seen in all the substituted terphenyl spectra. The K band is red-shifted because the lack of *ortho* interactions allows the adjacent phenyl rings to be more nearly coplanar, so that the degree of conjugation is greater than for the substituted terphenyls. By extrapolating the absorption edge of the K band for each terphenyl, we can see more clearly how the substitution affects the absorbance spectra. The absorption edges for HMT, HET and HHT are ~270 nm, indicating that the alkyl substituent does not have a significant impact on the conjugation of an oligomer.

Another important piece of information we can extract from the absorbance spectra is an idea of the effective conjugation length of a substituted PPP. The reported  $\lambda_{max}$  of a dihexyl-substituted polymer is 318 nm. By plotting the energy of the absorption edge versus 1/n, where n is the number of phenyl rings, we can determine either the effective conjugation length of a polymer, or predict the wavelength of the absorbance of an unknown polymer. Table 7 lists the absorption edge values of the oligomers synthesized and Figure 44 is a plot of their energy vs. 1/n. All the spectra taken in this work are  $10^{-5}$  M in cyclohexane, and the values ( $\lambda_{max}$ ) for the unsubstituted oligomers were taken from the literature, 106 which did not specify a solvent but the values seem to be in accordance with our results.

Figure 44 provides information on how additional rings and different substituents affect the spectra. The slope of the line indicates how each additional ring affects the band gap of the oligomer, which reflects the amount of conjugation coplanarity of adjacent groups. The y-intercept is the band gap for an infinite length oligomer. The slope for PPP is steeper than those for the methyl, ethyl and hexyl derivatives, which all have similar slopes. This is expected since the degree of conjugation is greater for an unsubstituted PPP because of the smaller twist angle. The intercept for PPP is much lower than for the substituted polyphenyls, as expected. The methyl-, ethyl- and hexylsubstituted polyphenyls have similar plots. An increase in electron donation should result in a decrease in band gap, or y-intercept. Therefore, we expect hexyl-substituted PPP to have the lowest intercept, followed by the ethyl- and methyl-substituted PPPs. The similarity between the three side chains indicates that inductive effects play a small role in the band gap energy of polyphenyls. The diamond-shaped point on the y-axis represents the reported value for 2,5-di-n-hexyl-PPP. This point does not correspond to our data since Eg for this point is much lower than that predicted by Figure 44 for a 2,5di-n-hexyl substituted oligomer of infinite length. This reported value was probably taken from a spectrum of a film of the polymer and thus cannot be compared with our solution spectra.

Table 7: UV-vis absorption edge values for PPP oligomers

oligomer	$\lambda_{max}$			
Terphenyl	279 (λ <sub>max</sub> )			
Quaterphenyl	292 (λ <sub>max</sub> )			
Quinquephenyl	299 (λ <sub>max</sub> )			
Sexiphenyl	308 (λ <sub>max</sub> )			
TMB	260.5			
HMT	265.5			
OMQ	267			
DMQ	277.5			
TEB	271			
HET	270			
OEQ	275.5			
DEQ	276			
HHT	268			
DHQ	274.5			
THS	276			

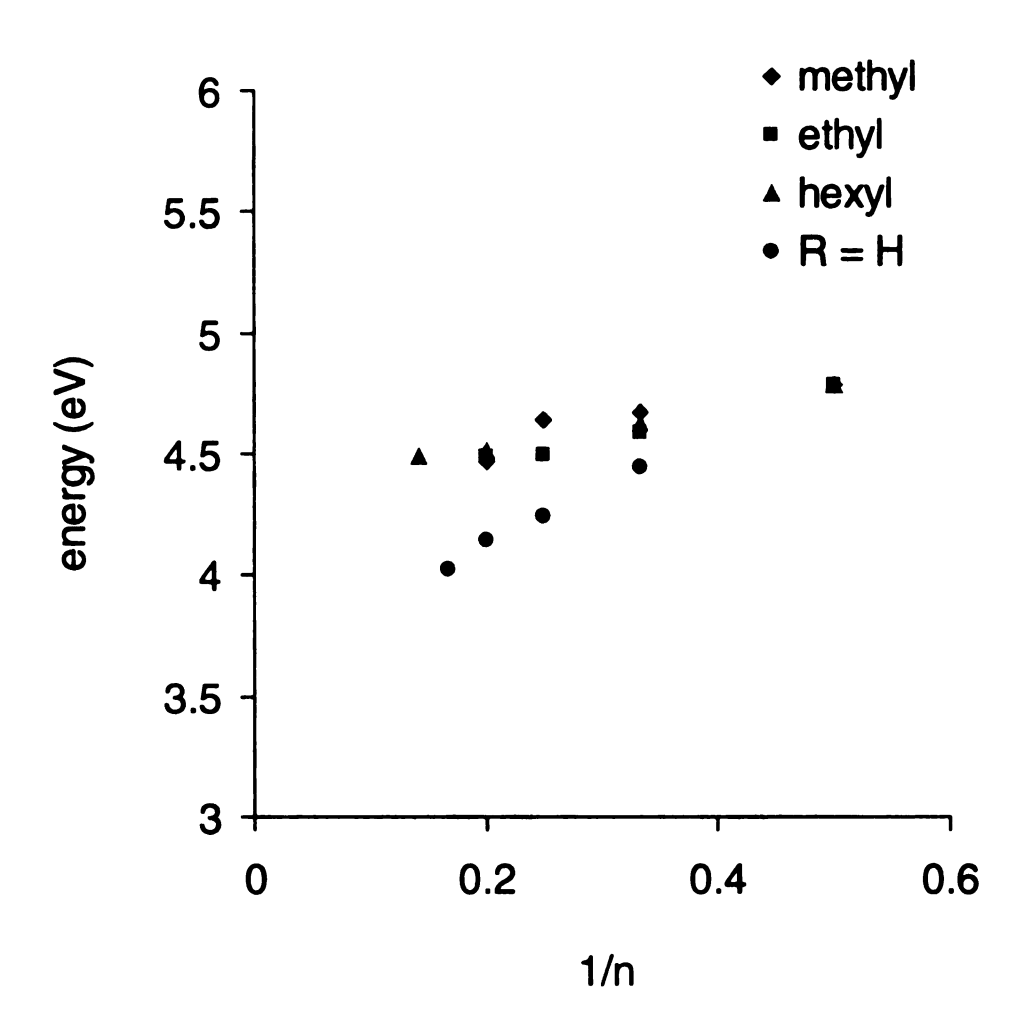


Figure 44: Plot of energy vs. oligomer length

#### 2. Fluorescence emission

The emission spectra of the series of methyl-, ethyl-, and hexyl-substituted oligomers are shown in Figures 45, 46 and 47. The spectra for the three sets of oligomers follow the same trend, with the  $\lambda_{max}$  values converging to their limiting values at 4-5 rings (Table 8). It is known that the fluorescence emission spectra of unsubstituted PPP oligomers show a well-defined vibrational structure,  $^{107}$  presumably due to the quinoid structure of the excited state.  $^{108}$  The study also showed that the emission bands shift to longer wavelengths and show less structure with increasing chain length. Khanna's data suggest that the excited states of longer oligomers may be less planar in comparison to smaller oligomers. The structureless shape of the emission bands shows that the structure of the excited state of the molecule is not exactly planar, and this deviation from planarity is probably caused by interaction of the side groups with each other. We did not attempt to calculate any quantum yields for PPP oligomers.

Table 8: Fluorescence  $\lambda_{max}$  values for PPP oligomers

Oligomer	$\lambda_{max}$		
TMB	303		
HMT	316		
OMQ	327		
DMQ	329		
TEB	302		
HET	315		
OEQ	330		
DEQ	332		
DHB	289		
ННТ	322		
DHQ	333		
THS	336		

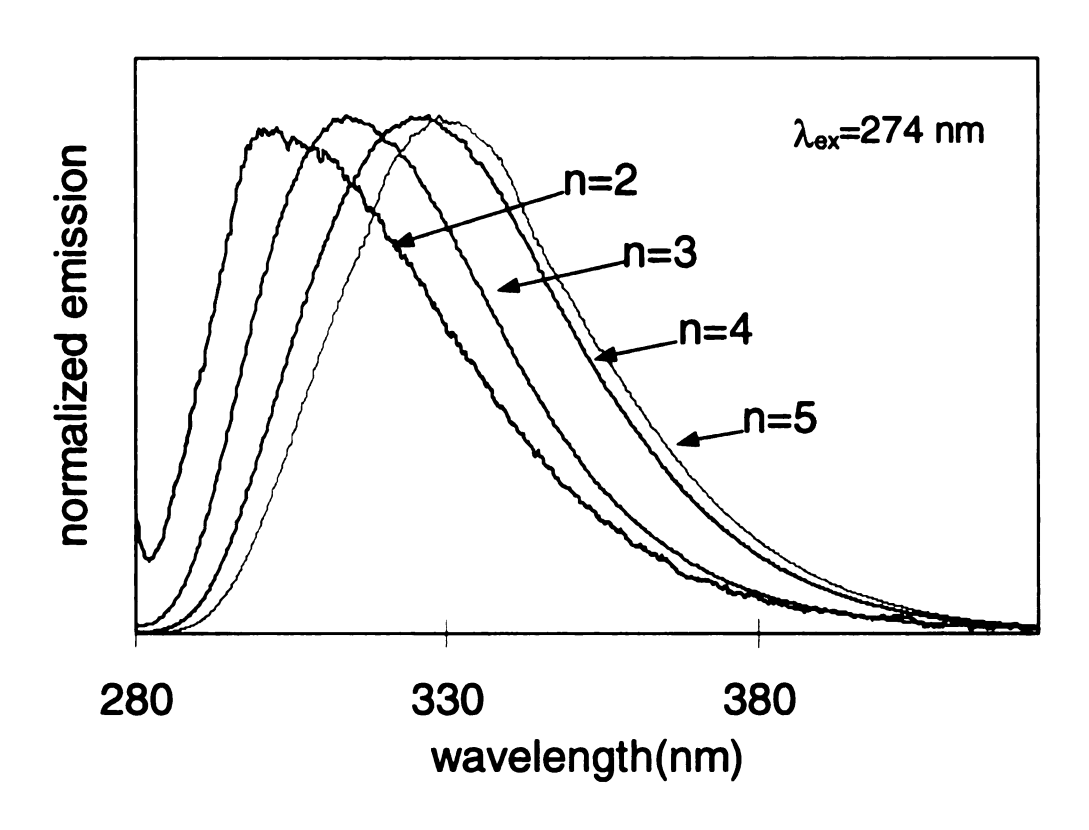


Figure 45: Fluorescence spectra of methyl-substituted oligomers

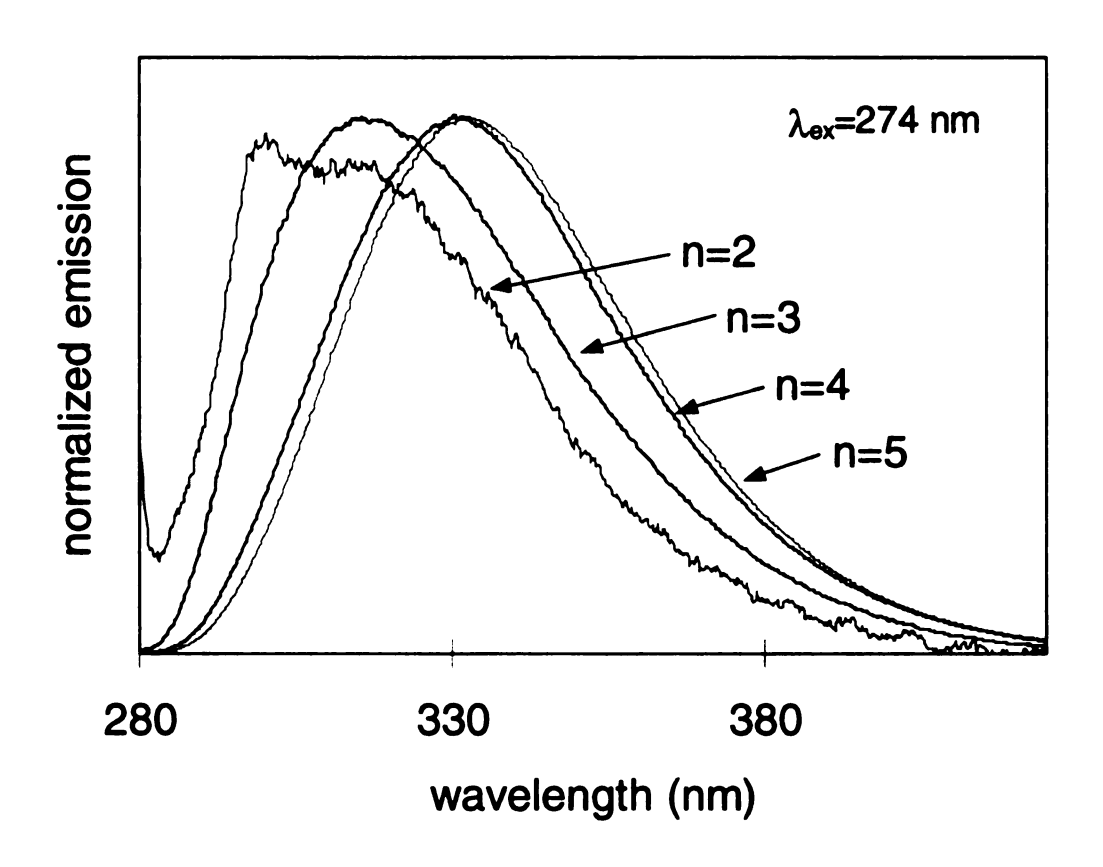


Figure 46: Fluorescence spectra of ethyl-substituted oligomers

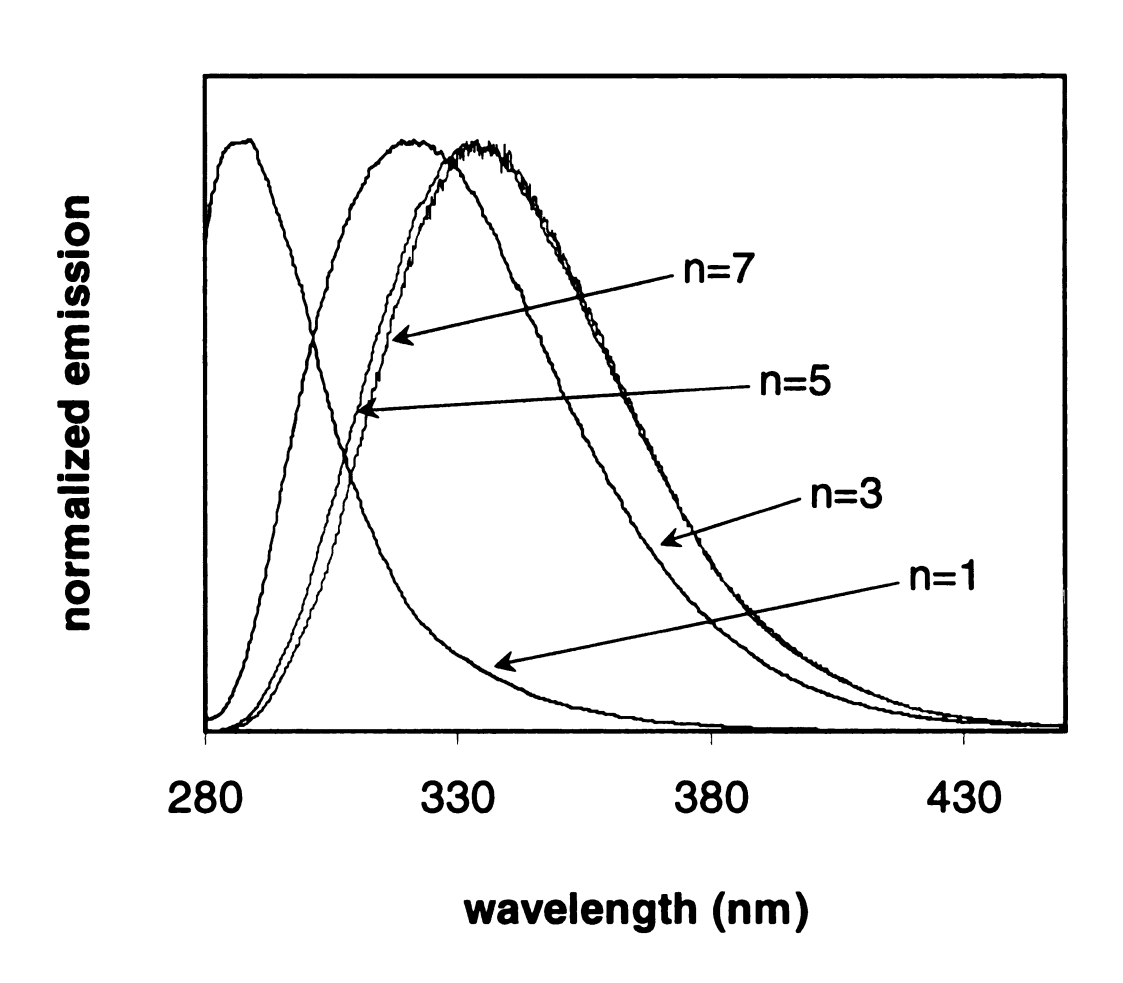


Figure 47: Fluorescence spectra of hexyl-substituted oligomers

# 3. Solid state spectra

The solid state UV absorbance and fluorescence emission spectra of the ethyl-substituted oligomers are shown in Figures 47 and 48. These films were created either from the melt or from a solution cast from toluene, and the film thicknesses were not measured. The same spectrum resulted regardless of film preparation method. Because of the imprecise methods used to create the films, all the spectra are normalized. We did not examine the methyl-substituted oligomers because all the films we created were too crystalline to obtain a reasonable spectrum. Aside from OEQ, all the spectra look very similar to the solution state spectra, indicating that the conformations in the solid state and in solution are similar. These results will be analyzed in further detail in the discussion section.

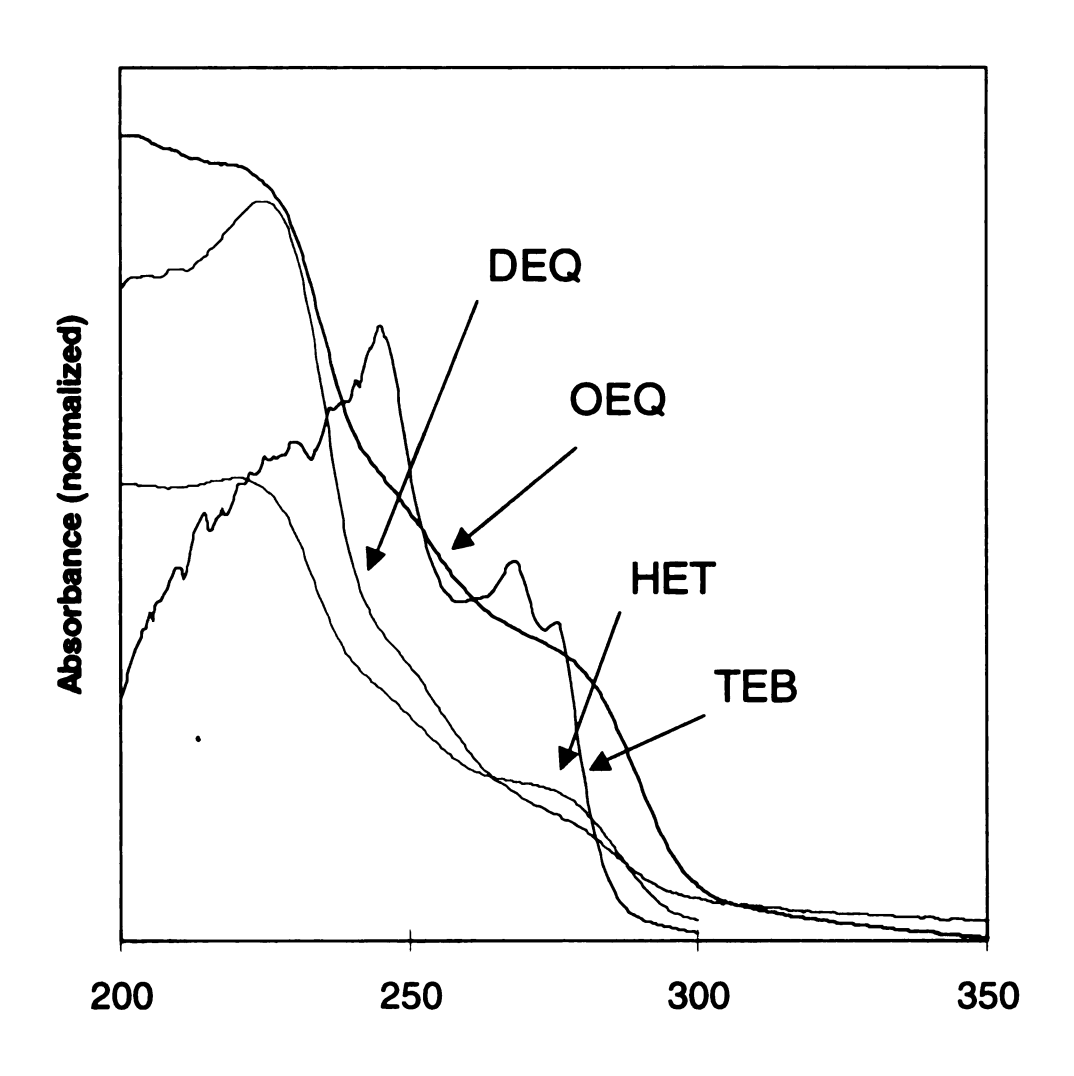


Figure 48: Solid state UV absorbance spectra of ethyl-substituted oligomers

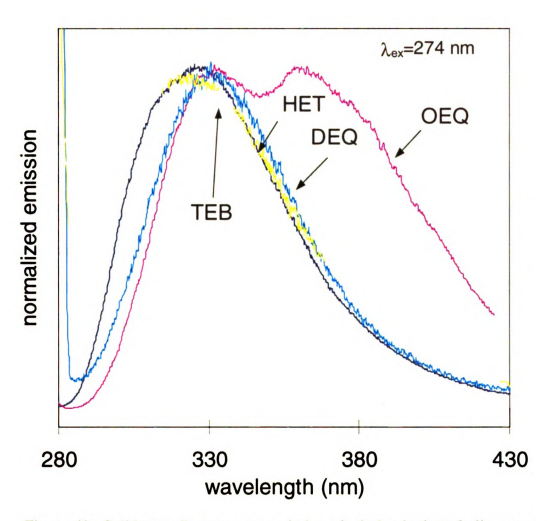


Figure 49: Solid state fluorescence emission of ethyl-substituted oligomers

# D. Thermal Properties

As described in the introduction for alkyl-substituted PPPs, DSC and polarized optical microscopy are useful tools for characterization of the solid state properties of materials. Shown in Figures 50-54 are the DSC results for HMT, OMQ, OEQ, DHQ and THS. Positive deflections from the baseline (endothermic) correspond to melting temperatures, while negative deflections (exothermic) indicate crystallization or similar disorder-order transitions. For all compounds studied, the phase transitions detected by DSC were simple melting or crystallization events. Parallel observations using optical microscopy confirmed the assignments and also showed that none of the compounds formed thermotropic liquid crystalline phases.

We determined that all of the methyl-substituted oligomers are crystalline compounds. The DSC plot of HMT is typical, showing a melting peak on the heating curve at ~185 °C, and crystallization on cooling at ~90 °C. Note that there is a large hysteresis, which is characteristic of simple melting and crystallization. In contrast, liquid crystalline transitions generally show small degrees of supercooling. We confirmed these transitions by optical microscopy under crossed polarizers.

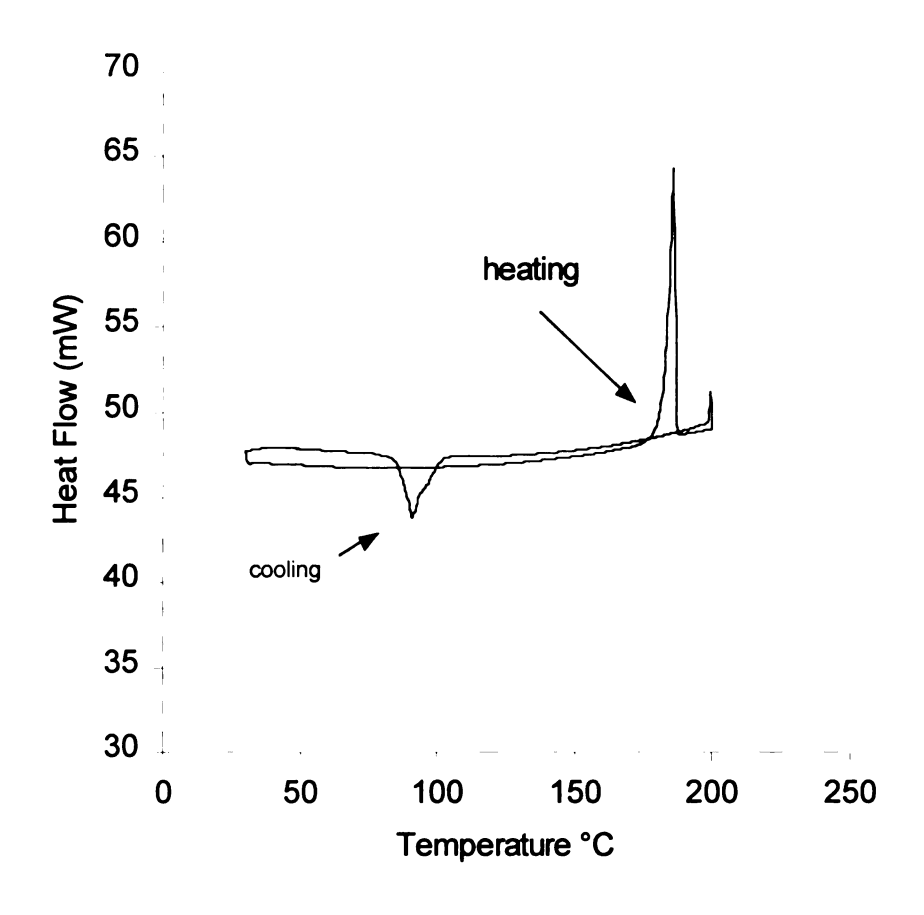


Figure 50: DSC plot of HMT

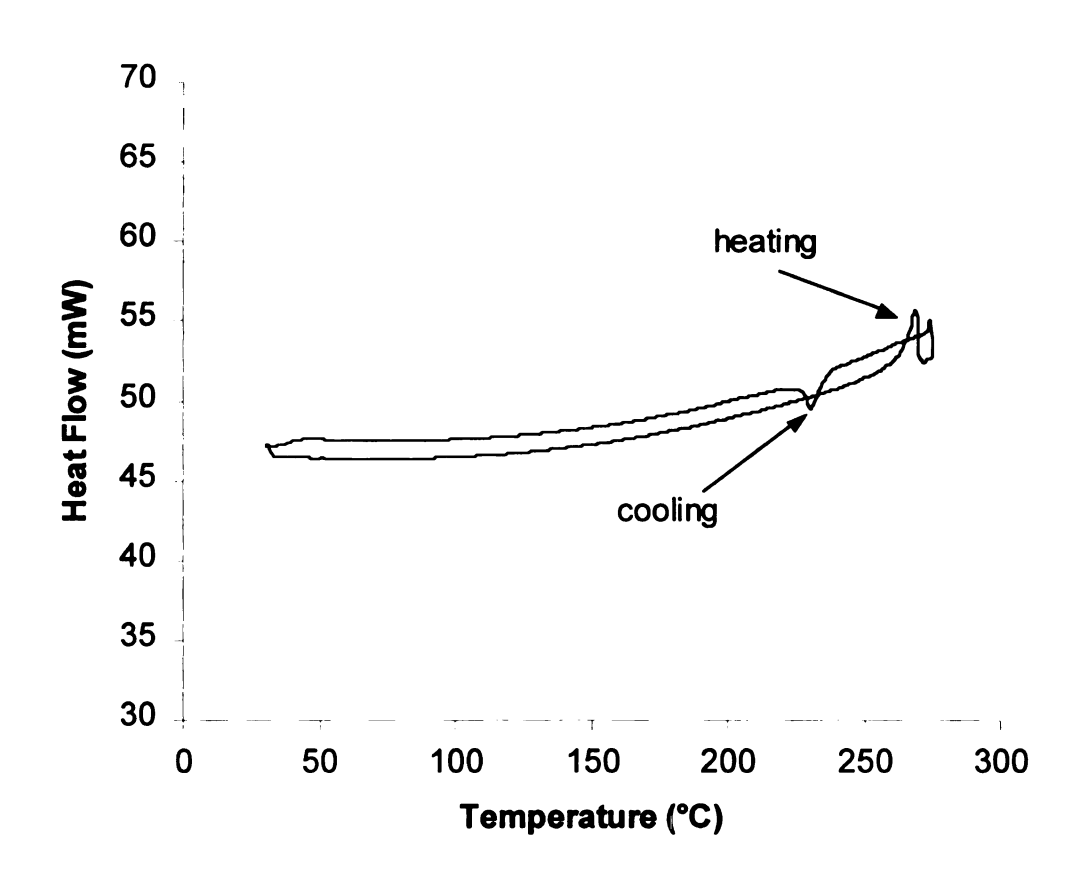


Figure 51: DSC plot of OMQ

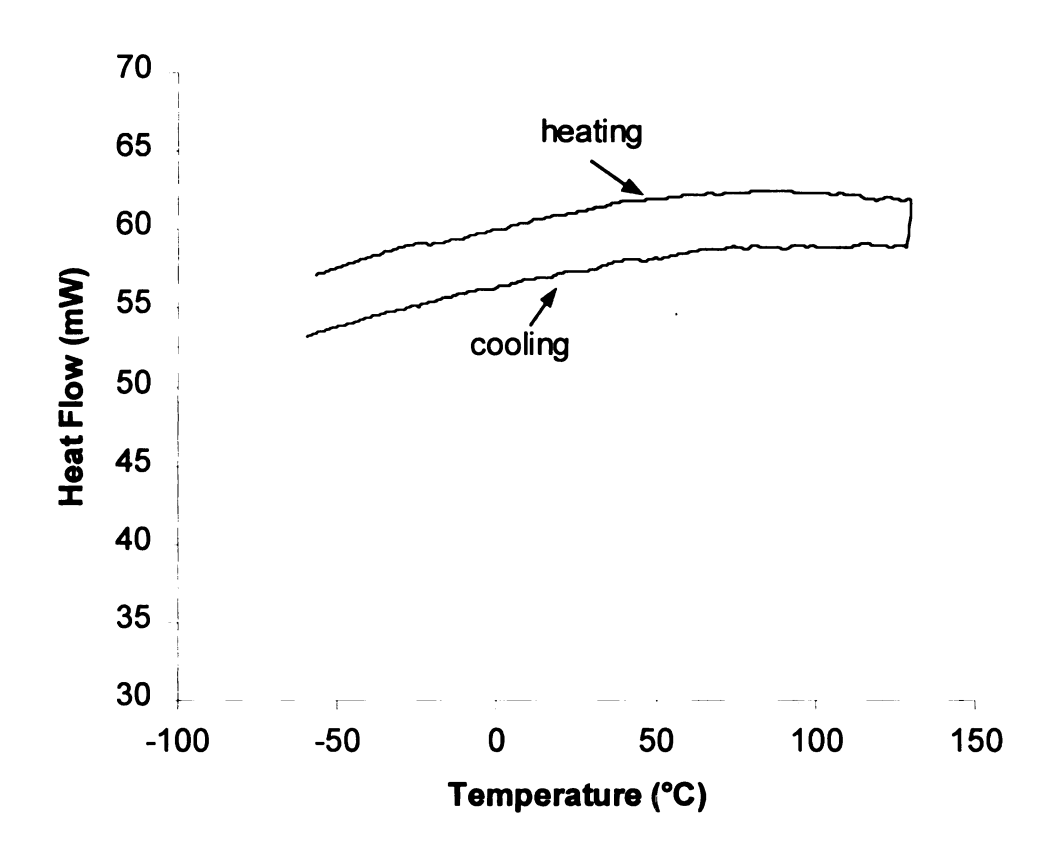


Figure 52: DSC plot of second heating and cooling scans of OEQ

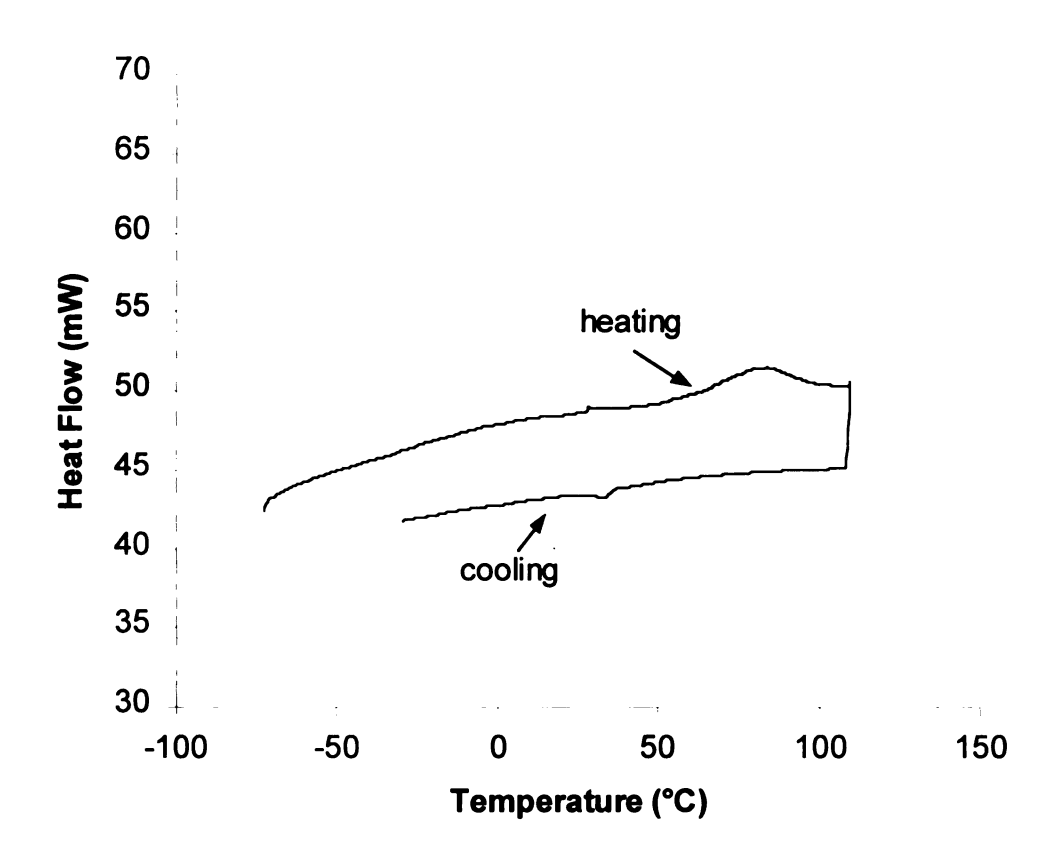


Figure 53: DSC plot of second heating and cooling scans of DHQ

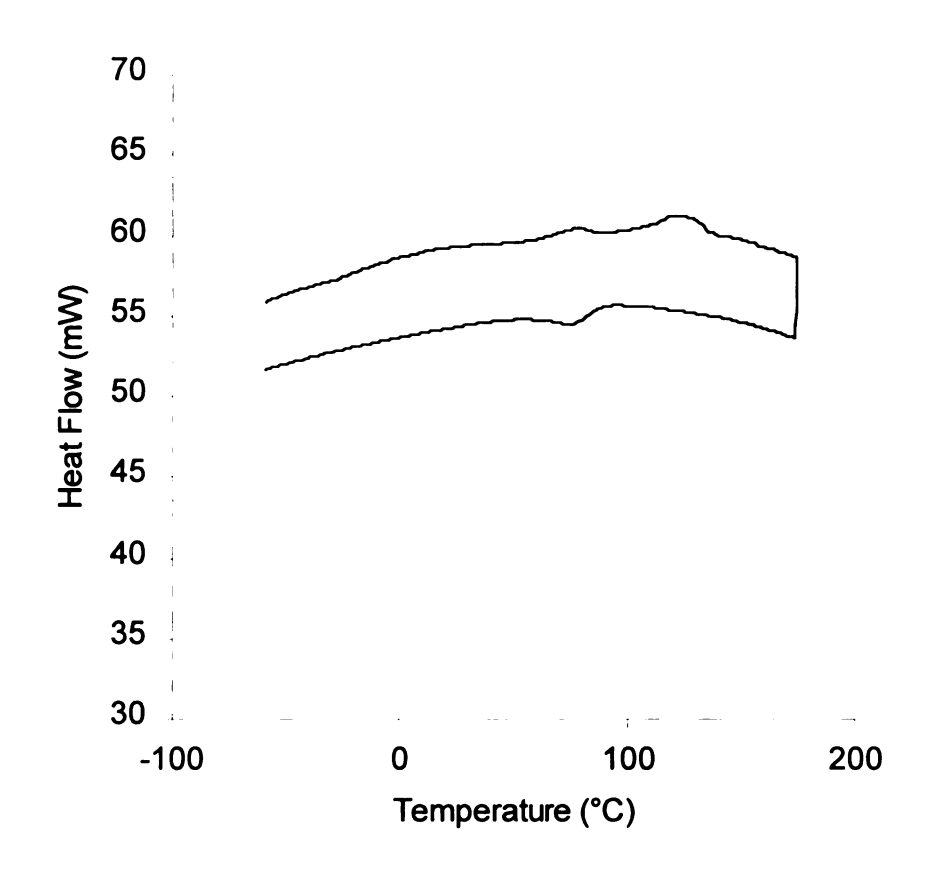


Figure 54: DSC plot of the second heating and cooling scans of THS

The DSC results show systematic trends in the melting point behavior. As shown in Table 9, adding side groups of increasing length leads to progressively lower melting points. The effect is dramatic. For example, adding hexyl groups to quinquephenyl lowers the melting from 395 to 97. Within a series with identical side chains, the melting point increases with the number of rings, as expected. TEB and HET were isolated as oils and HET crystallized over the course of several months. DEQ decomposes at 235 °C before melting. All of the members of this series show weak transitions in DSC measurements. OEQ has particularly interesting thermal properties. OEQ forms a clear glass that is stable for days. DSC scans of the OEQ glass show no first order thermal transitions.

Table 9: Melting points of PPP oligomers

R\n	2	3	4	5	7
Н	71 °C	215 °C	320 °C	395 °C	
CH <sub>3</sub>	54	183	266	309	
C <sub>2</sub> H <sub>5</sub>	oil	60-61	110	235	
C <sub>6</sub> H <sub>13</sub>	oil	43		97	140

Of the hexyl-substituted oligomers, DHB and HHT were isolated as oils, and DHQ and THS as white powders. The DSC plot of DHQ (Figure 53) shows a broad transition around 85 °C upon heating which we attributed to melting and confirmed by optical microscopy. The reason that this value is different from the one in the Table is probably because that value was taken using a melting point apparatus at a much slower

rate. There is also a small transition at about 15 °C that could be a softening or glass-transition-like event. Since we did not do any microscopy below room temperature, we could not confirm this transition. Upon cooling, this compound shows a transition at about 32 °C which is probably due to crystallization. THS, however, displays a DSC plot that is similar to that of OEQ, in that there are no discernable transitions.

Mechanical measurements can be sensitive indicators of weak thermal transitions and relaxation phenomena in polymers. In many cases, these transitions are too weak to be detected by DSC. In Dynamical Mechanical Analysis (DMA) measurements, an oscillatory load is applied to the sample, and the in phase and out of phase components of the response are measured. The mechanical response of glassy materials is primarily in phase with the applied stress (elastic) while that of rubbery materials is generally out of phase with the load (lossy). Typically, the data are reported in terms of E' and E", the dynamic elastic and loss moduli. Carrying out DMA measurements on polymers as a function of temperature maps thermally activated transitions such as molecular rotations and glass transition temperatures, which show up as peaks in the E" or tan  $\delta$  spectrum. The tan  $\delta$  spectrum is a plot of E"/E' versus temperature. DMA measurements of glassy OEQ (Figure 55) show transitions at 15 and 30 °C presumably due to the onset of disordering and ring rotation respectively. Neither transition is seen in the DSC scans.

OEQ also shows morphology dependent fluorescence behavior. As shown in Figure 56, freshly prepared glassy films show a distinct 2-peak fluorescence spectrum. With time, the spectrum evolves toward the solution phase results, a single peak centered near 330 nm. Inspection of the aged film shows it is crystalline, and thus the shift in the fluorescence spectrum must be associated with changes in the conformation of OEQ on

crystallization. Variable temperature measurements on glassy films also point to structure-dependent fluorescence. As shown in Figures 57 and 58, the fluorescence peak intensity decreases with temperature, with an abrupt change in slope near 30 °C. We believe these data confirm our assignment of the 30 °C transition to ring librations, or a change in the arrangement of the molecules, since changes in fluorescence for the oligomers should be associated with changes the planarity of adjacent rings.

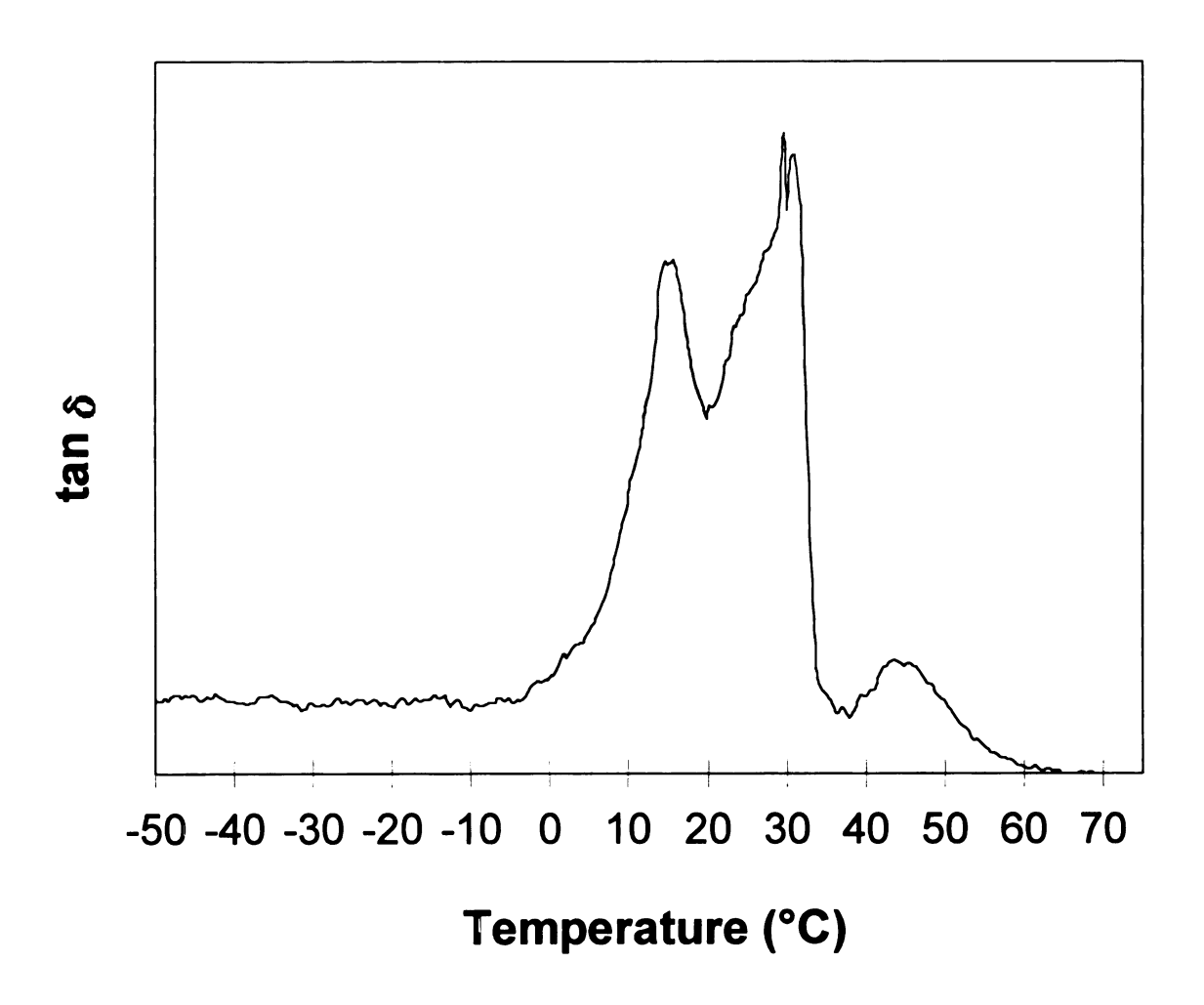


Figure 55: DMA plot of OEQ

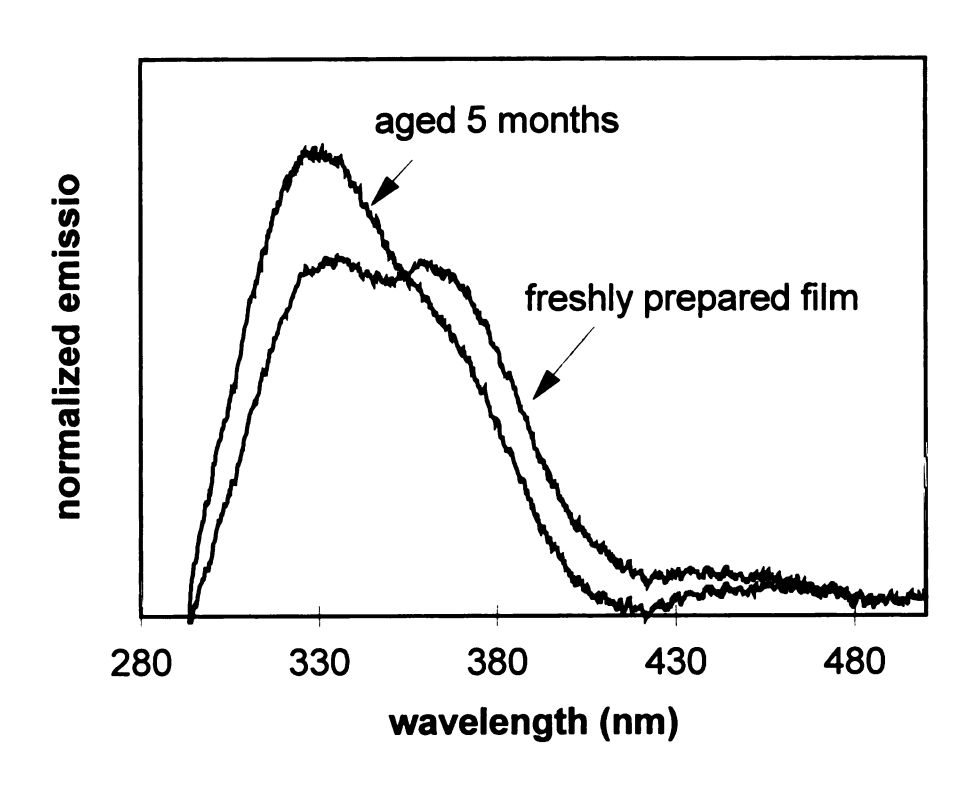


Figure 56: Solid state fluorescence of OEQ

A final experiment in this vein is again related to the aged solid state fluorescence sample. When observing this sample under the microscope after aging, it appeared crystalline with spherulite-like regions. By doing a more careful study, we see that the sample begins to show crystallinity after one day, forming a solid phase reminiscent of a nematic liquid crystal. We are attempting to monitor this crystallization by optical microscopy by using a silicon photodiode detector in the camera mount. This detector is read by a Hewlett-Packard multimeter, which is interfaced with a computer. The program Instrument Basic can be used to record voltage measurements from the multimeter at timed intervals. The voltage recorded reflects the amount of light passing through the sample. We will analyze these results more thoroughly in the discussion section.

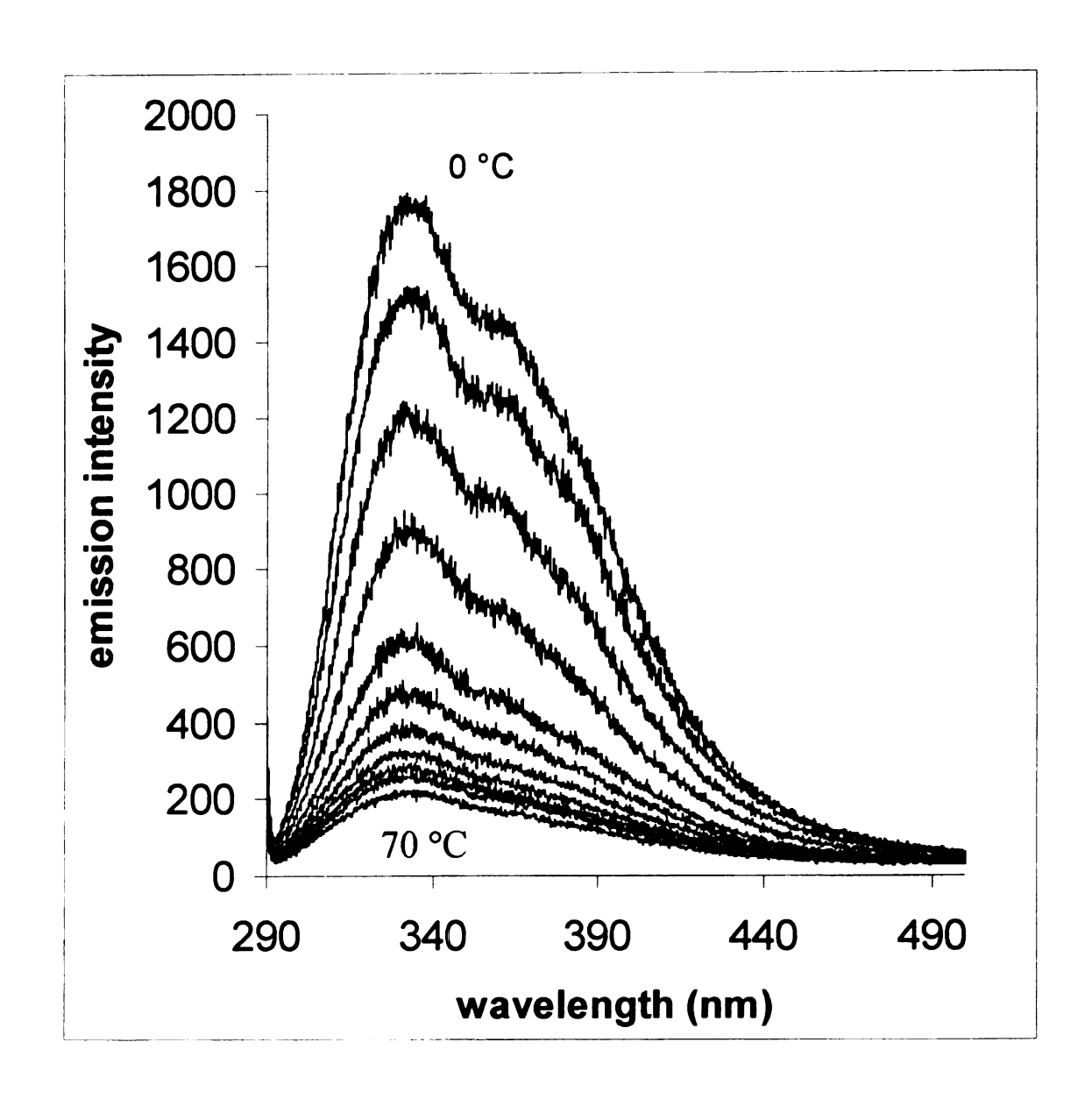


Figure 57: Variable temperature fluorescence spectra of OEQ

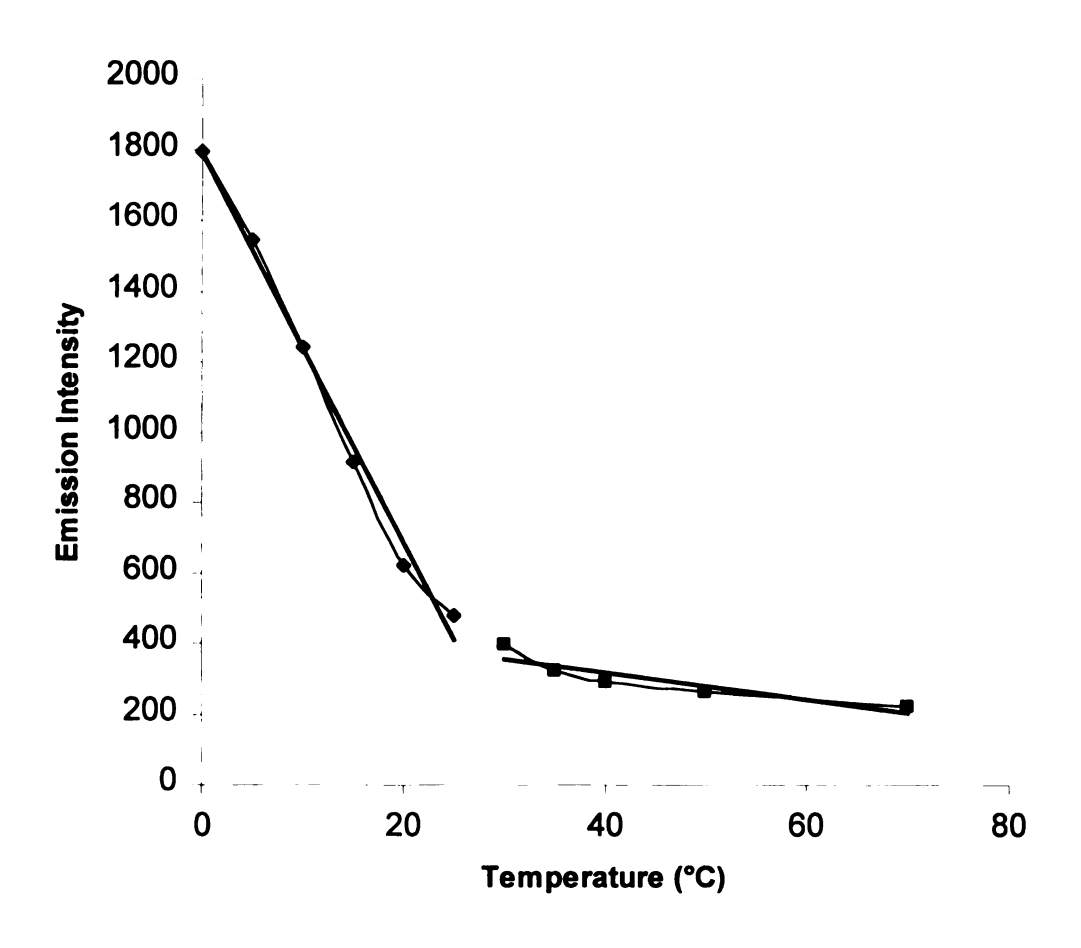
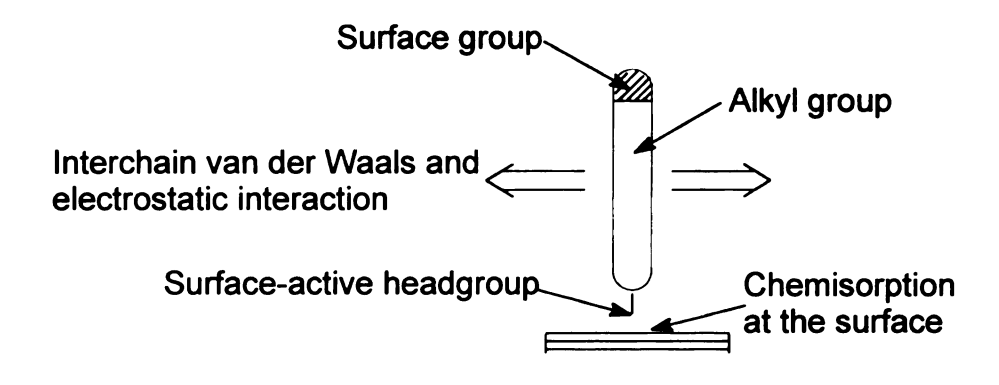


Figure 58: Plot of emission intensity vs. temperature for VT fluorescence of OEQ

### E. Self-assembled monolayers

This section presents the preliminary results obtained while exploring PPP oligomers for use as self-assembled monolayers (SAMs). This project was approached from two angles: 1) The ability of PPP oligomers to form a SAM, and 2) The use of PPPs in a SAM as a non-linear optical device. We wished to study monolayers on a silicon surface, which has a native oxide coating of about 20 Å. The hydroxyl groups on the oxide surface can be coupled to triethoxysilyl terminated PPP oligomers. 109,110 (Figure 59) To utilize this chemistry, we synthesized PPP oligomers that were functionalized with a bromine atom at one end of the oligomer. This bromide was converted to a triethoxysilyl group by the Barbier-Grignard reaction. 111 (Figure 60)

We developed synthetic routes to functionalized PPP oligomers for thermally stable SAMs, and nonlinear optical (NLO) devices. The synthetic schemes for the NLO chromophore will be presented in the Discussion section, since they are more appropriately classified as "future work". We first attempted to characterize monolayers on Si wafers by ellipsometry and reflectance Fourier transform infrared spectroscopy (FT-IR). Neither technique gave satisfactory results, probably because the monolayers we are examining are estimated to be on the order of 3-9 Å thick, while those commonly studied by these methods in the literature are at least ~20 Å thick. The ellipsometry measurements were not reproducible from sample to sample, and the thicknesses did not increase in a linear fashion as would be expected for increasing oligomer length. There



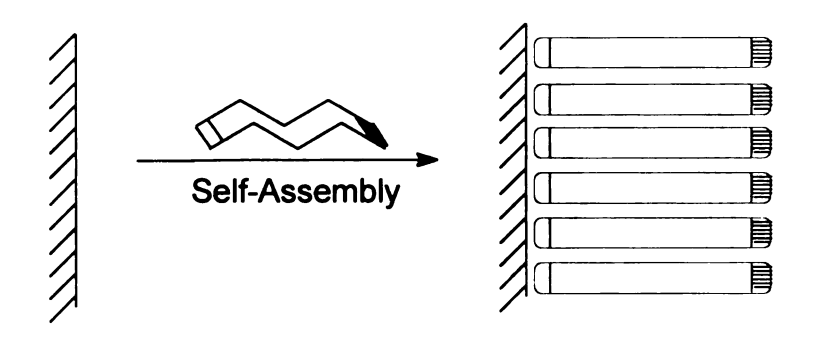


Figure 59: Structure of a self-assembled monolayer

Figure 60: Synthetic scheme for SAMs

are three possible explanations for this result. One possibility is that the monolayers were not stable and desorbed before the measurements were taken. The second possibility is that the oligomers are not all oriented perpendicular to the silicon surface but some or all of them are lying parallel to the surface. It is also possible that the surface attachment was inefficient, resulting in a low surface density of organic molecules. Some suggested improvements to this experiment will be explored in the Discussion section.

The reflectance FT-IR experiments were also unsuccessful. We determined that this method of examining the monolayers, while an excellent tool for long alkyl SAMs, 109,112-115 is not appropriate for such short oligomers. The amount of signal that arises from the alkyl groups in our monolayers is too small in comparison to the extraneous hydrocarbons in the instrument to be detected.

Perhaps a more appropriate method of conducting preliminary studies on these monolayers is to form them on substrates with much larger surface area, such as fumed silica. Fumed silica contains 2 mmol of hydroxyl groups per gram, so that even if a small percentage of the hydroxyl groups react, there will still be a perceptible amount of monolayer present. We did not attempt to measure the amount of monolayer on the silica. By following the method of Hou<sup>116</sup>, we attached benzene and the methyl substituted benzene, biphenyl and terphenyl oligomers to fumed silica. FTIR spectra of pressed pellets of the functionalized silica gel are shown in Figure 61. As the oligomers increase in length, the intensities of the alkyl peaks in the spectrum increase relative to the peaks arising from the silica.

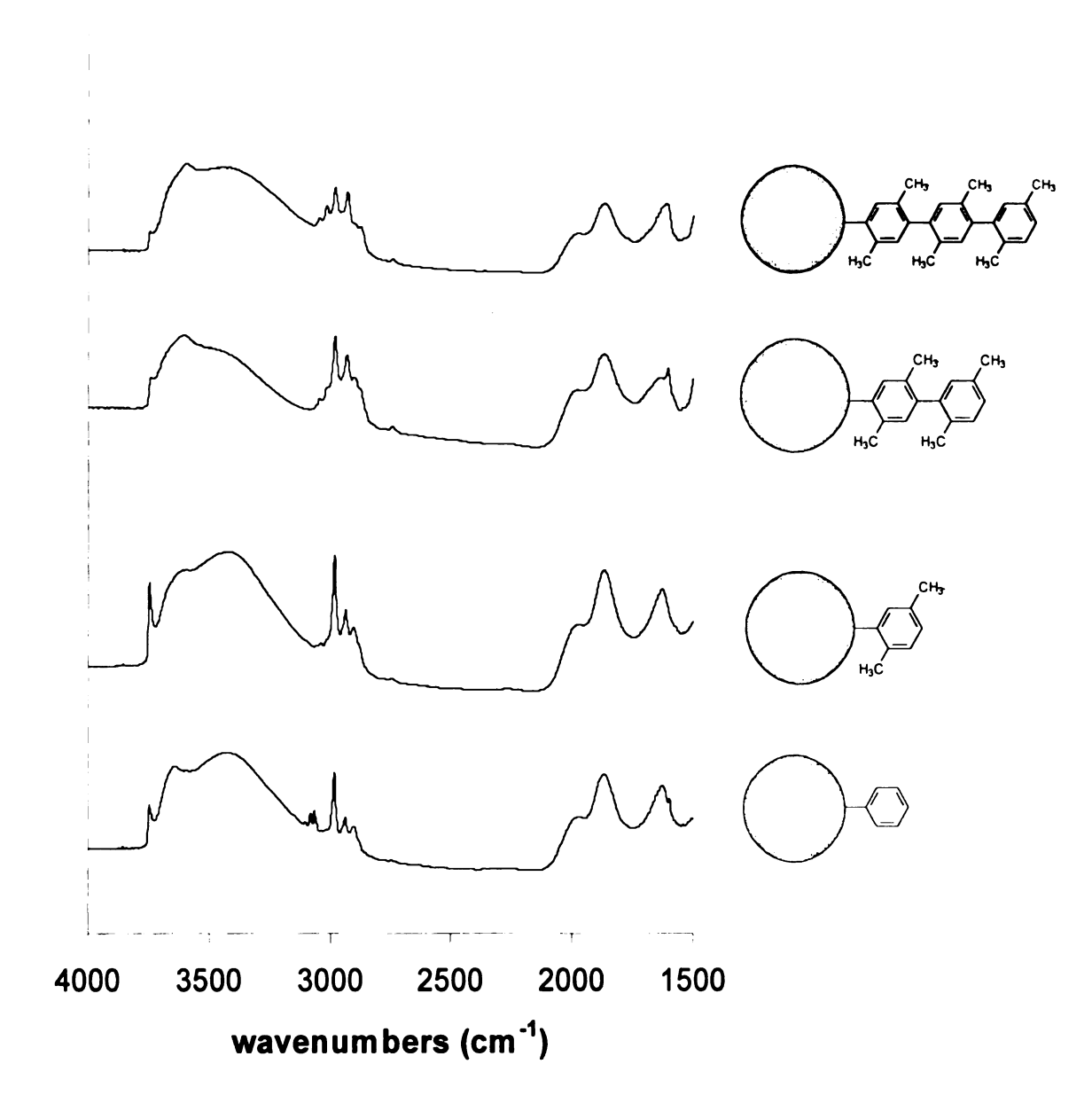


Figure 61: FT-IR spectra of SAMs on A200 fumed silica

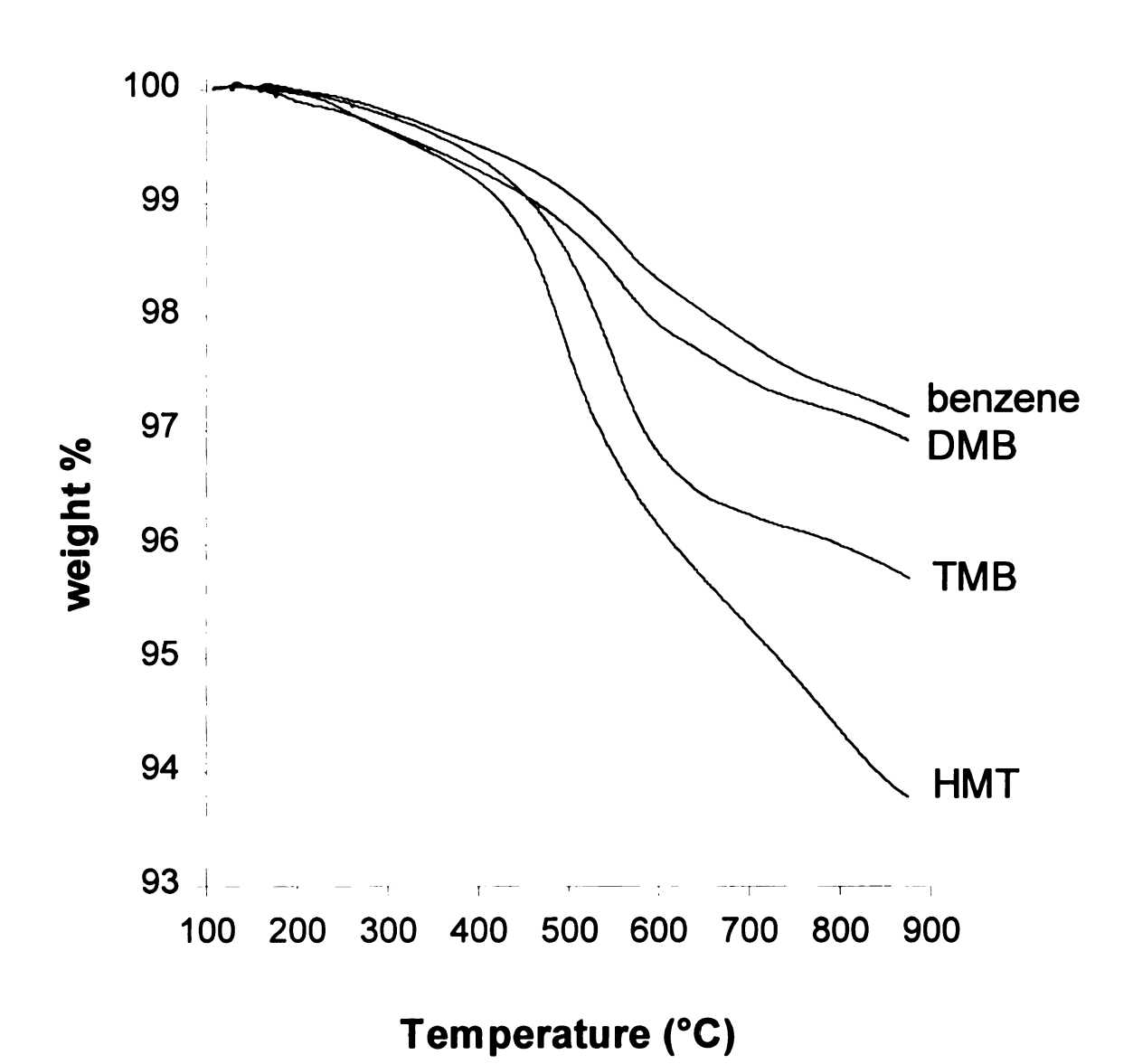


Figure 62: TGA plots of SAMs on silica

Figure 62 shows the thermogravimetric analysis (TGA) plots of the monolayers on furned silica. The samples were dried at 150 °C at < 100 mtorr for at least 12 h before TGA scans were taken. Once the samples were placed in the TGA sample pan, they were heated at 110 °C under nitrogen for about 30 minutes. These plots show the expected increase in weight loss with increasing percentage of organic material. These scans were run under nitrogen, so it is possible that cross-linking reactions may have occurred. There seem to be two periods of weight loss for the oligomers, the first is a gentle slope from ~200-400 °C, and the second is the steep slope occurring after 400 °C. Alkylated and unalkylated oligomers behave similarly upon heating in the TGA analyzer. We did not conduct an analysis of the gas emitted from the burning sample. A useful experiment to help identify the source of the two weight loss periods would be to remove the sample from the pan and examine the FTIR spectrum after each period.

### III. DISCUSSION

From the data presented in the Results section, we learned that PPP oligomers are reasonable models for PPP. For substituted oligomers, the conjugation lengths are relatively short, so by examining a series of oligomers we can draw conclusions about the effects of these substituents on a polymer. The important issues to be addressed are the solubility and processibility of the polymers and the band gap, both of which are important for application of PPPs in devices.

# A. Electronic Properties of PPPs

PPPs are commonly explored for use in LEDs, so it is important that a polymer or oligomer should emit light at the desired wavelength, and be processible and oxidatively stable. Substituents alter the electronic properties of the oligomer or polymer by severely decreasing the conjugation between phenyl rings because of the increased twist angle between the rings. The decreased conjugation can be observed as an increase in the band gap (E<sub>g</sub>) of the molecule, which results in a blue shift in the absorbance and emission spectra. There is also evidence for some inductive effect, especially for strongly electron-donating or electron-withdrawing groups, but in dialkyl-substituted PPPs and oligomers, the twist angle dominates the band gap. We can determine which effect

dominates by examining the plot of E vs. 1/n (Figure 44). The trendlines for all the substituted oligomers are nearly parallel, indicating that the effect of adding another ring is equivalent for an oligomer with any alkyl substituent.

### B. Band Gap Engineering

Adding substituents to a PPP can also be used to "tune" a molecule to absorb or emit light at a given wavelength. The solution UV absorbance spectra show a blue shift of about 40 nm when two alkyl substituents are added to each ring of a terphenyl. For devices such as light emitting diodes which must emit light in the visible range of the spectrum, this is a disadvantage, but there are reports 117-119 of PPPs substituted with alkoxy groups which decrease the band gap and allow a blue-violet emission from a solid film.

The effective conjugation length is often defined as the polymer length at which the optical properties converge to their limiting value, but we assume from the plot of E vs. 1/n that E continues to decrease with increasing chain length and does not actually reach a limiting value. However, for our purposes, we define effective conjugation length to be the oligomer length at which the band gap does not increase enough by adding another phenyl ring to observe a change in properties (i.e. for use in a light emitting diode if the luminescence of a polymer asymptotically approaches 430 nm and the luminescence of a decamer is 420 nm, we can say that the effective conjugation length of the polymer is 10 units, because the human eye cannot distinguish between 420 nm and 430 nm wavelength light). The effective conjugation length of an unsubstituted PPP has been estimated to be  $\sim$ 20 rings  $^{106}$ , by extrapolating from the  $\lambda_{max}$  values in the

UV absorbance spectra. However, since it is unknown if a film of PPP has a degree of polymerization higher than 20, this number may not be valid. The longest oligomer measured, p-sexiphenyl, showed a longest wavelength absorption at 308 nm in solution and 345 nm in the solid state. We estimate the effective conjugation length in a dialkylsubstituted PPP to be 6-7 rings, increasing the band gap of the polymer, so there is an obvious decrease in the desirable electronic properties found in unsubstituted PPP. It seems that the solubility and low band gaps are inversely related, but a number of investigators have devised means to retain conjugation while increasing the solubility and processibility of a polymer. One method is to place substituents on selected rings instead of every ring, thus imparting less solubility but retaining more conjugation. In an early study, Wirth 120 examined a series of quaterphenyls and quinquephenyls with varying side chains on only the terminal rings. A table from this paper is reproduced here (Table 10). We can see that the addition of only one ring has a huge effect on the solubility in toluene and melting points of these oligomers, but these oligomers are much more processible than the unsubstituted oligomers and their optical properties remain virtually unchanged. This study also showed that an increase in length of a linear side chain has an optimum value, *n*-butyl in this case. To further increase the solubility of the quinquephenyl derivative, the authors used long branched alkyl groups to obtain solubilities of over 500 g/L with a 9-heptadecyl substituent. This strategy is similar to that employed by Gorman, Ginsburg and Grubbs<sup>121</sup> in their synthesis of soluble polyacetylenes (Figure 63)

Table 10: Solubilities and melting points for substituted PPP oligomers

R	Solubility		Melting	Solubility		Melting
	[g/L]	[mMol/L]	point (°C)	[g/L]	[mMol/L]	point (°C)
Н	0.12	0.39	320	< 0.005	<0.013	395
Methyl	3.7	11.1	213	0.01	0.24	313
Ethyl	7.5	20.7	194	0.18	0.41	291
n-Butyl	43	103	165	0.48	0.97	268
n-Hexyl	46	97	157	0.52	0.94	259
n-Octyl	48	90	150	0.55	0.91	253

(PAs). The polymers are synthesized by ring opening metathesis polymerization of cyclooctatetraene (COT) with one substituent on the COT ring. By altering that substituent, the authors were able to tune the properties of the polymer, eventually obtaining a soluble PA with electronic properties very similar to the unsubstituted PA.

Figure 63: Grubbs's synthesis of soluble polyacetylene

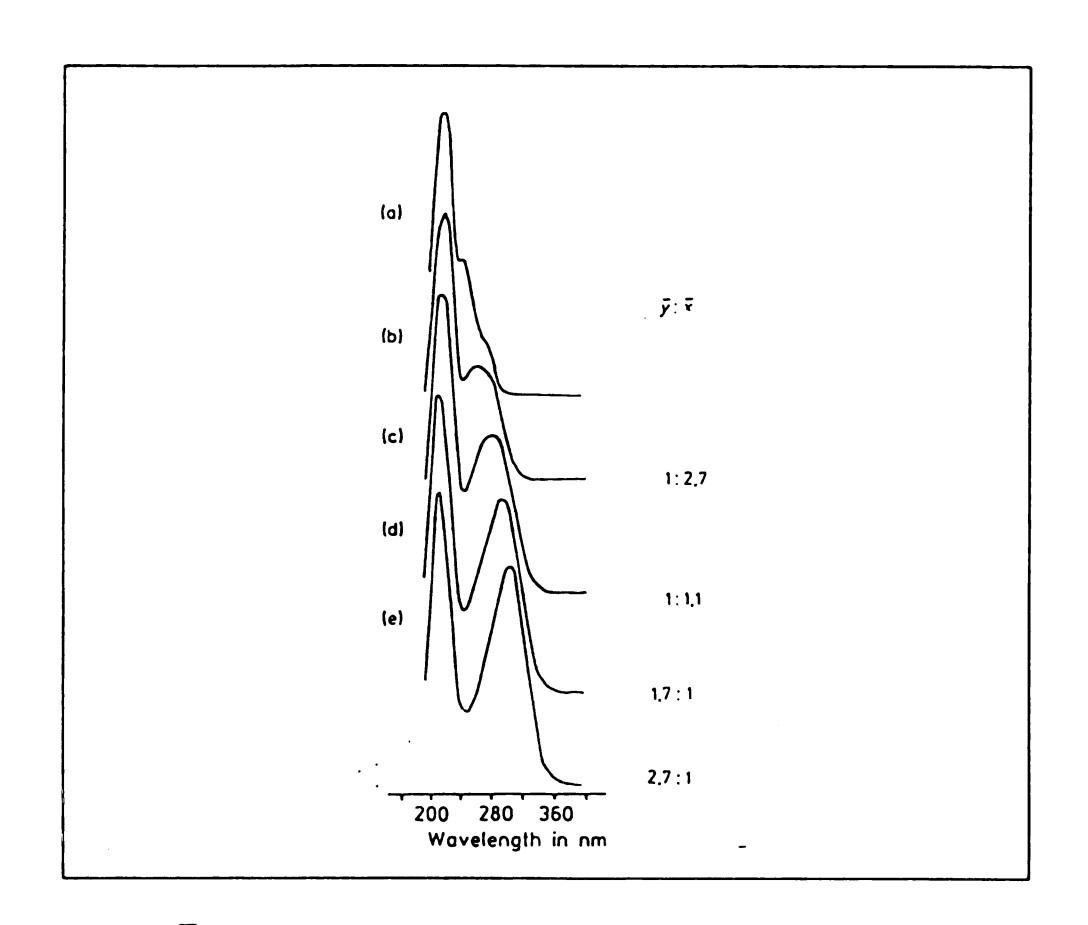


Figure 63: UV absorbance spectra of Rehahn's copolymers. The feed ratios are listed on the right.

Using a similar idea, Rehahn, et al. 77 synthesized PPPs by introducing varying ratios of monomers with and without side chains. They saw an expected increase in the wavelength of the lowest energy band with an increasing fraction of unsubstituted monomers in the feed. (Figure 64)

Several groups have synthesized PPPs with planarizing moieties connecting adjacent phenyl rings and forcing them into a planar conformation. These polymers, nicknamed "ladder polymers" (Figure 65) such as Grimme, *et al.*'s<sup>106</sup> substituted fluorene-based polymer, can be solubilized by placing alkyl groups on either the phenyl rings or the planarizing groups. These polymers retain the conjugation present in an unsubstituted PPP, but they are soluble, processible and can be characterized by NMR and gel permeation chromatography (GPC). In fact, Lamba and Tour<sup>122</sup> calculated the twist angle between phenyl rings for their imine-bridged ladder polymer to be less than 1°.

$$\begin{array}{c|c} R & R' \\ \hline R' & R' \\ \hline R' & R' \\ \hline \end{array}$$

Figure 65: Soluble ladder polymers

To summarize, if a certain conjugation length is desired, there are several options for tuning the band gap of PPPs and similar rigid rod polymers. A substitution on every ring provides the most processibility, but causes the greatest decrease in conjugation. By

synthesizing a molecule with a solubilizing group on only some rings, we can increase the conjugation but retain solubility. Placing alkyl groups on only the ends of molecules also increases solubility but with retention of the optical properties of an unsubstituted PPP. However, this strategy is only feasible for oligomers of less than 5 or 6 phenyl rings. Finally, substituted ladder polymers offer the most conjugation, some even higher than unsubstituted PPP, while retaining processibility.

Thermal stability is important in electronic applications such as coatings for integrated circuit devices because these devices often run at high temperatures. PPP is stable up to ~660-675 °C in nitrogen and about 400 °C in air. 10 When substituents are placed on the rings, the stability decreases somewhat because of the reactivity of the alkyl groups. Oligomers are not suitable for these applications since they tend to sublime at fairly low temperatures even though the molecular structure is still intact. Their volatility is however useful for preparing LEDs and organic transistors. Common thermally induced side reactions include cross-linking and bond cleavage.

### C. Solubility And Crystallinity

To completely understand how side chains impart solubility to PPPs, we must first understand why unsubstituted PPPs are insoluble. Polyphenylene is insoluble due to its high heat of fusion, rigid-rod geometry, large aspect ratio, and contributions from  $\pi$ - $\pi$  interactions. The rigid rod geometry of PPP means that there are fewer conformations available to the polymer chains, thus the molecules can easily pack together. Once the rods are aligned, the energy to "pry" them apart is much greater than for flexible

polymers, since the rigid rod structure requires all the monomers to be separated at once, rather than sequentially. The  $\pi$ - $\pi$  intermolecular attraction and strong polarizability of PPP rods also increases the energy needed to separate the polymer chains. This concept can be illustrated by comparing polyphenylene to polystyrene. (Figure 66) Atactic polystyrene is more soluble than isotactic polystyrene because of its random coil structure. Isotactic polystyrene, a poorly soluble polymer, has a more regular structure and readily crystallizes. By studying how those properties that make polyphenylene insoluble can be disrupted, we can understand what makes a hexyl-substituted polyphenylene soluble. Several types of disruptions are possible: 1) twisting between rings, 2) varying the barrier to rotation around bonds connecting rings, 3) increasing the

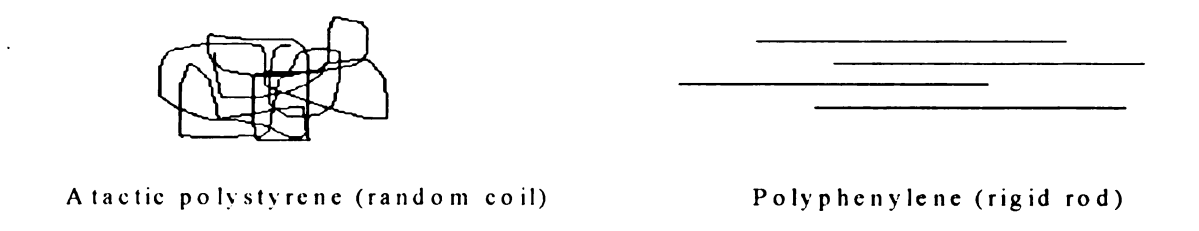


Figure 66: Comparison of a random coil polymer with a rigid-rod polymer

entropy by introducing functionality on the rings, or 4) simply sterically blocking interactions between the polymer chains by the side groups. In each case, we assume that factors that lead to inefficient packing also lead to increased solubility.

## 1. Increased ring twist

The increased twisting between rings induced by *ortho* interactions of the alkyl chains causes polymer chains to be less planar, making it more difficult for the individual

polymer molecules to pack in geometries that have appreciable  $\pi$ -overlap with adjacent chains. (Figure 67) According to literature<sup>4</sup> and our *HyperChem* calculations, an unsubstituted PPP has a dihedral angle of ~23° in the gaseous (and solution) state and ~10° in the solid state. A dialkyl substituted PPP has a dihedral angle of ~45° in the gaseous/solution state. It is fairly certain that this increase in ring twist causes some degree of increased solubility in the polymers, especially since the ring rotation is entirely random. Each ring may twist in either of two directions with respect to the previous ring creating many different diastereomeric polymers, analogous to the polystyrene example. In Figure 67, the picture on the left represents an alkyl-substituted PPP, the straight lines indicating a side view of a planar benzene ring, and the picture on the right represents an unsubstituted PPP, having a dihedral angle of 23°. The substituted PPP, having the larger dihedral angle, has increasingly poor  $\pi$ - $\pi$  overlap between each polymer chain than the PPP with a smaller dihedral angle. However, this phenomenon alone does not account for the increase in solubility between the three types of substituted oligomers synthesized in this research and the unsubstituted PPP and its oligomers (Table 11).

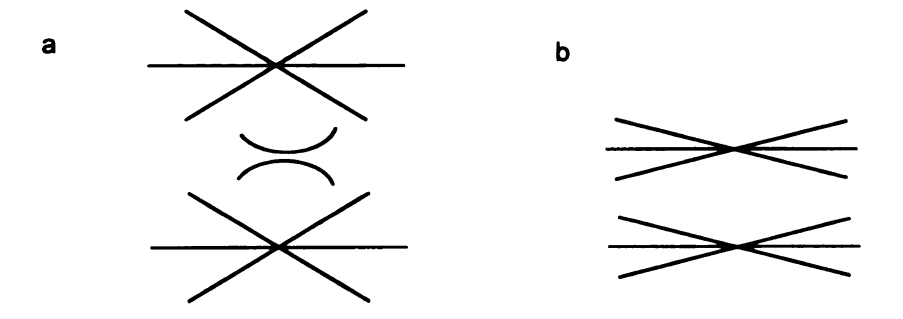


Figure 67: Side view of PPPs with different dihedral angles a. 45° b. 23°

Table 11: Solubility in toluene of substituted quinquephenyls

Oligomer	Solubility (g/L)	Solubility (mol/L)	
Quinquephenyl	0.005	1.6 x 10 <sup>-5</sup>	
DMQ	0.240	0.0005	
DEQ	66	0.10	
DHQ	116	0.09	

#### 2. Rotational Barriers

Rotational barriers have the possibility of offering insight to the mechanism of crystallization. (Figure 68) Since molecules in the same conformation pack together and crystallize more easily, it is possible that the barrier to rotation around the phenyl-phenyl bond can be a limiting step to crystallization and an important factor in determining the solubility of a PPP. The larger the barrier, the lower the likelihood that the molecules can adopt the same conformation and crystallize. However, our measurements of the actual barriers showed that there was a significant difference between the methyl-substituted oligomer and the ethyl-substituted oligomers, but a negligible difference between the ethyl- and hexyl-substituted oligomers. Remembering that an ethyl-substituted PPP is insoluble while a hexyl-substituted PPP is completely soluble in hot toluene, the magnitude of the barrier cannot alone explain solubility. It may, however, be responsible for the slow crystallization rates of many oligomers.

As implied above, the oligomers with longer side chains are less crystalline than those with short or no side chains. While it is probably accurate to generalize that oligomers disubstituted with short side chains are more crystalline than oligomers

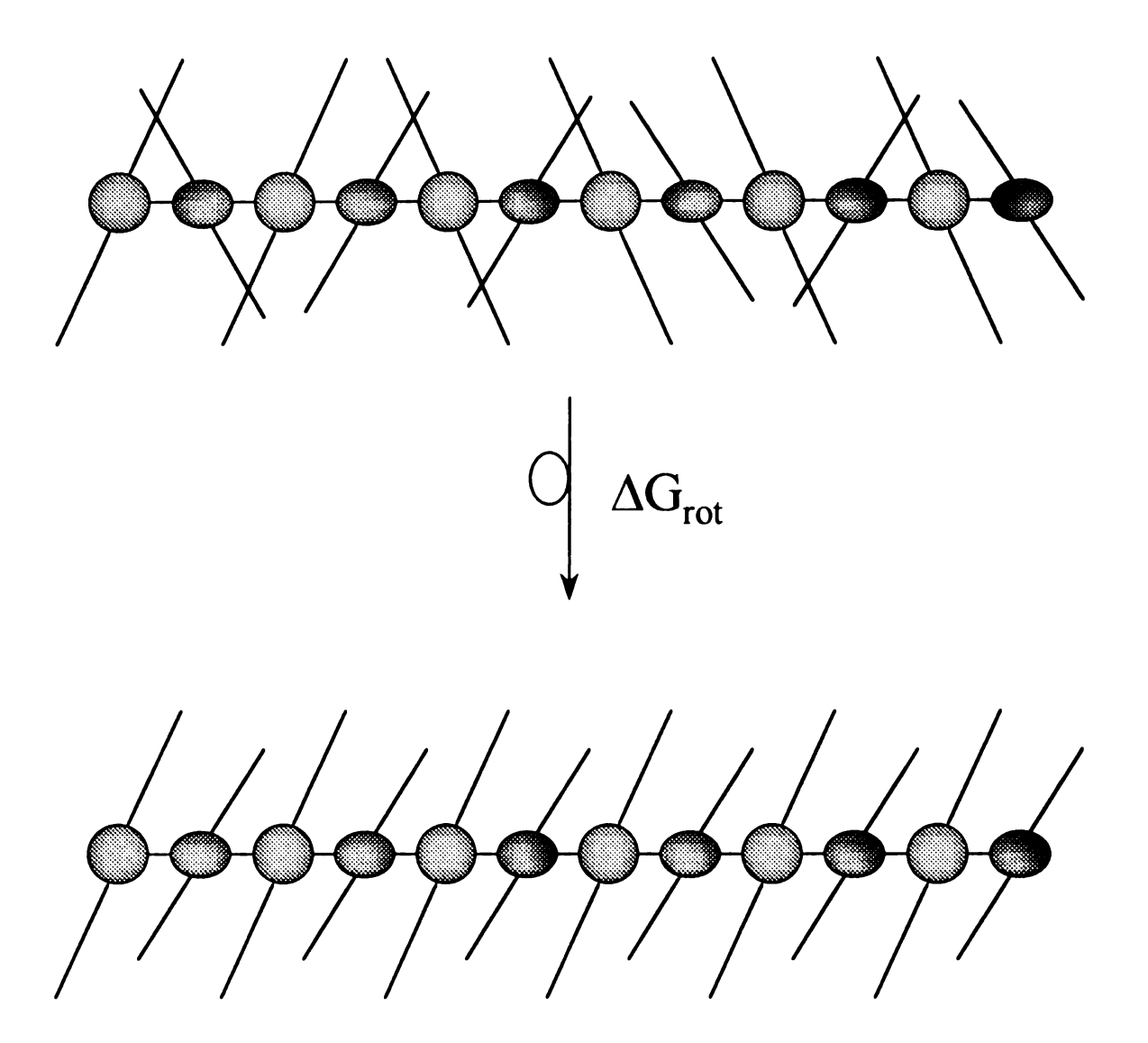


Figure 68: Rotational barriers of substituted PPPs

disubstituted with longer side chains, we believe that there are other factors that contribute to crystallinity. First, by examining the DSC scans of THS and DHQ, we can see that DHQ shows apparent melting and crystallization peaks, while THS does not, displaying a plot very similar to that of OEQ. As noted earlier OEQ typically forms a glass at room temperature and crystallizes very slowly. To measure the rate of crystallization of OEQ, we equipped a microscope with a silicon photodiode detector and a hot stage to detect crystal formation. With the sample under crossed polarizers, crystallization causes a greater fraction of the viewable area to become birefringent, and more light is allowed through to the detector. Figure 69 shows the results from two trials of the crystallization of OEQ. By examining the plot, we see that it takes approximately two days for the entire viewable area to become crystalline. For HMT, the viewable area

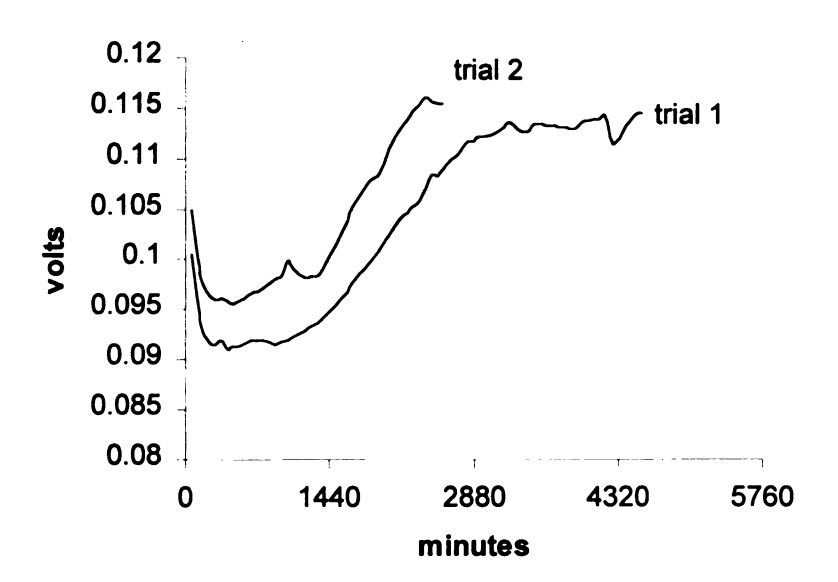


Figure 69: Measurement of crystallization rate of OEQ

becomes crystalline in a matter of minutes or seconds, depending on the crystallization temperature. The increase in birefringence is consistent with a model of constant linear growth from a nucleation site. Since one must know the number of sites and the optical constants for the crystals, we did not attempt to fit the data. HMT crystallized as spherulites (Figure 70), while OEQ crystallizes with a nematic-like structure. (Figure 71)

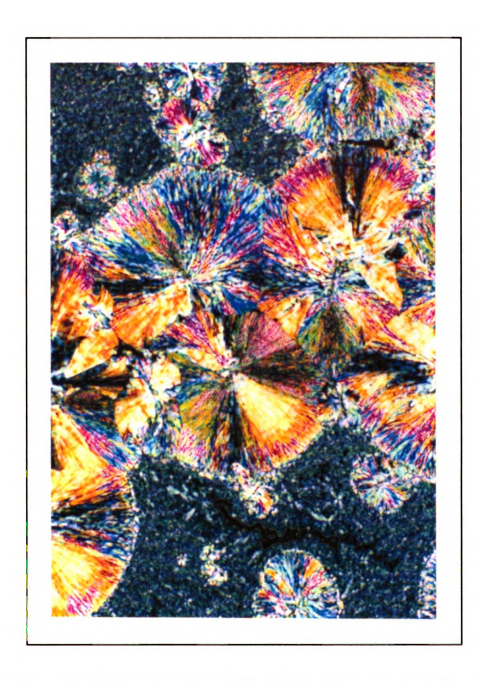


Figure 70: Photograph of crystalline HET under crossed polarizers

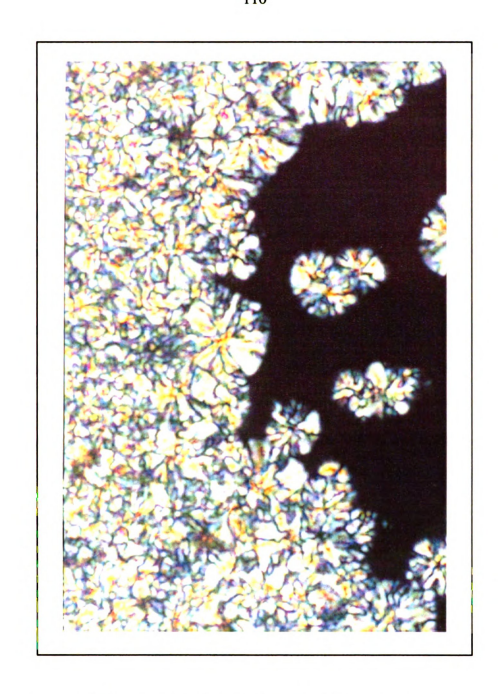


Figure 71: Photograph of crystalline OEQ under crossed polarizers

## 3. Increased entropy of oligomers

In agreement with Goldfinger, et al.  $^{123}$ , it is possible that the increase in entropy caused by the addition of longer side chains is the driving force for solubilization. Figure 72 illustrates the possible fates of a crystal. By measuring  $\Delta H_{fus}$ , we can calculate  $\Delta S$  for the transition from the equation  $\Delta G = \Delta H - T\Delta S$ . If  $\Delta S$  is small, indicating that the average geometry of the crystal is similar to the average geometry of the solvated molecule, then  $\Delta H_{fus}$  is also small. The overall energy of dissolution can be reduced to  $\Delta G_{mix}$  when  $\Delta H_{fus}$  is zero. The reduction in  $\pi$ - $\pi$  interactions between polymer chains that is induced by long side chains allows the polymers to adopt geometries similar to their solution geometries. This is shown by the data presented in Rehahn's paper. This paper demonstrates that by increasing the side chain length on polymers of the same molecular weight, the first thermal transition, attributed to side chain melting, decreases by only 20 °C while the second transition, attributed to the transition into the isotropic melt, decreases by 120 °C with increasing side chain length. (Figure 73)

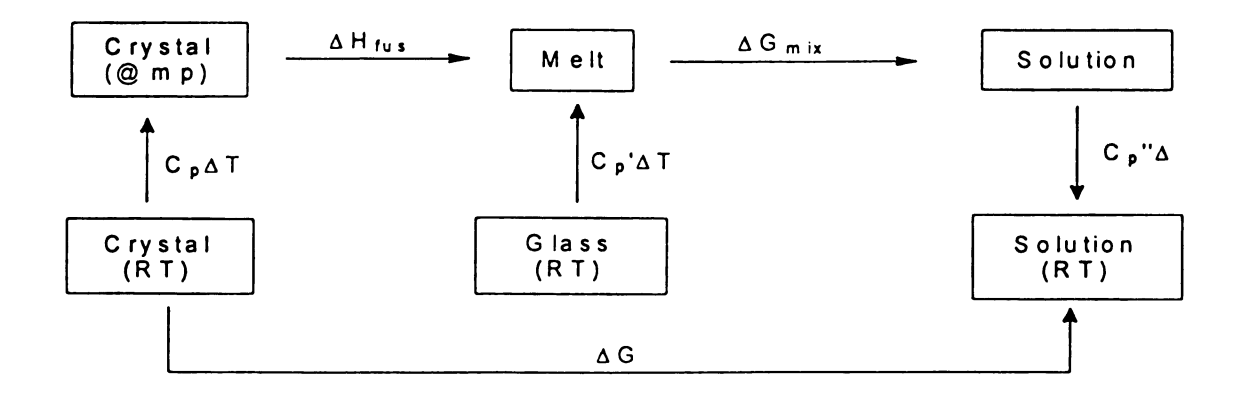


Figure 71: Schematic energy diagram for dissolution of PPPs

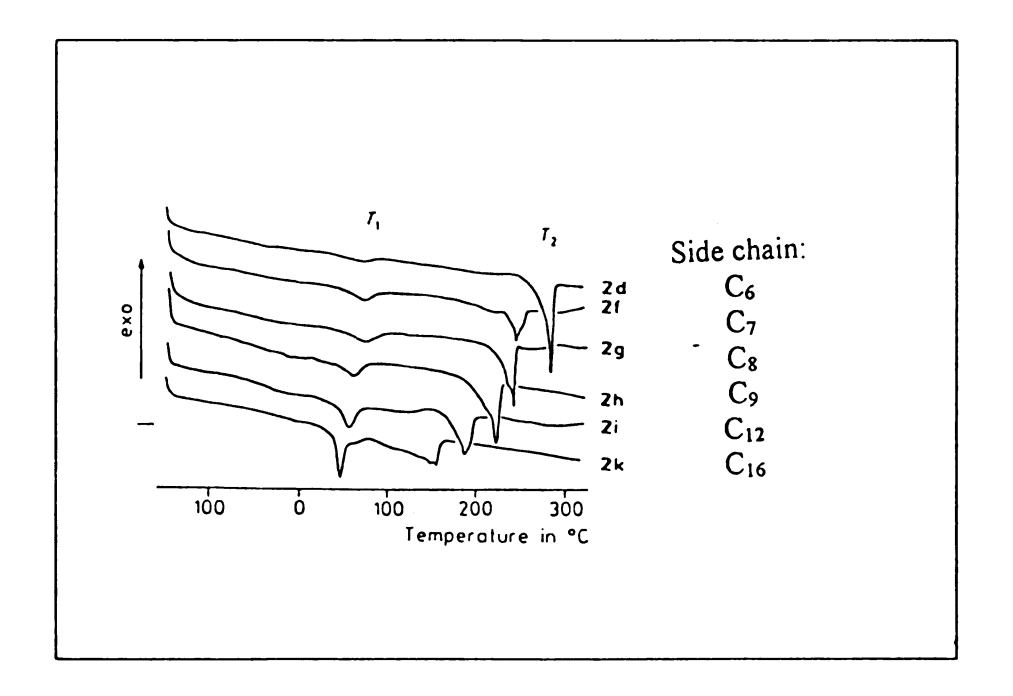


Figure 72: DSC curves of substituted PPP derivatives

# 4. Steric blocking

Finally, the increase in solubility could be due to a simple steric interaction or blocking between the main chains of the polymer. This is probably the case in soluble polyacetylenes which have  $\alpha$ ,  $\omega$  *tert*-butyl groups. (Figure 74) This type of steric blocking is unlikely to play a role in substituted PPPs.

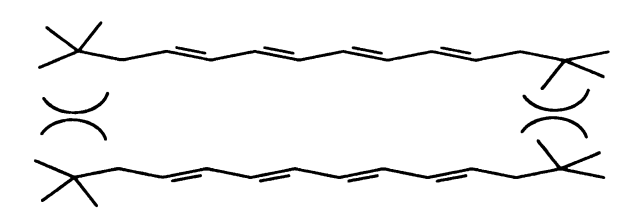


Figure 74: Polyacetylenes solubilized by terminal t-butyl groups

Actually, the increase in solubility is probably due to a combination of all of these theories. The solubility of a molecule or polymer can be related to its crystallinity within a series. The dissolution of a solid in a solvent is equal to the energy of melting followed by the energy of mixing for the two liquids, 124 so assuming the  $\Delta G_{mix}$  values are similar, the solubility of these oligomers can be directly related to their melting points. The melting points of the oligomers we synthesized decrease with increasing side chain length, and increase with increasing main chain length and their solubilities increase accordingly, in agreement with the thermodynamic arguments presented in the previous section.

It is our belief that a combination of the factors listed above contribute to the increased solubility of the PPPs substituted with longer chains. The chains often "get in the way" of packing by moving around and not allowing the main chains to come close

enough together to crystallize. The longer side chains also increase the entropy of the polymer while decreasing its heat of fusion per gram. The increase in twist angle between rings and the increase in rotational barrier prevents the main chains from being in a common configuration, thus impeding crystallization.

### D. Effect of side chains on morphology

McCarthy, et al. 99 examined the morphology of polymer films prepared from the liquid crystalline melt or by solution casting, and found that regardless of preparation method, all the films of the high molecular weight 2,5-didodecyl-substituted PPP showed some level of orientation as determined by X-ray diffraction. They showed that there is a

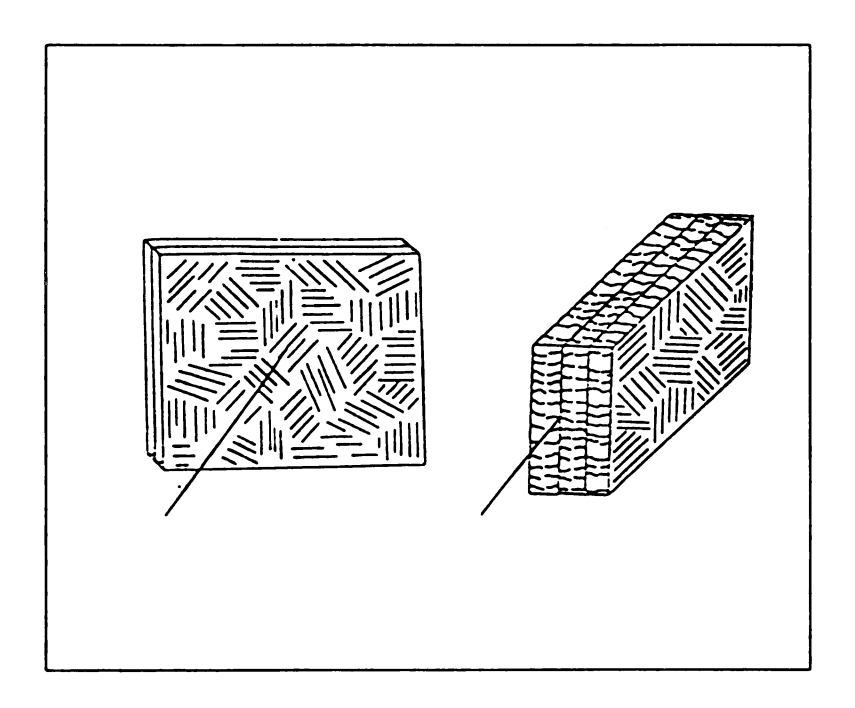


Figure 75: Sandwich type morphology of 2,5-didodecyl PPP (reproduced from McCarthy, et al. 99)

strong tendency for the side chains to segregate from the main chains, forming a sandwich type structure. (Figure 75) The layer spacing showed a linear decrease with increasing temperature, probably due to ordering of the side chains. At lower temperatures there are defects present in the side chain packing as seen by the weak, diffuse reflections seen in the diffraction pattern.

From these results, we can propose a crystalline structure for the ethyl-substituted PPP oligomers that accounts for the solution-like fluorescence of the films and the slow crystallization. Based on space-filling models, there are two likely packing arrangements for 2,5-dialkyl substituted PPPs. The first, a raft-like arrangement, is analogous to that proposed by McCarthy. The second (Figure 76) stacks molecules in a staggered arrangement. The second arrangement would be more favorable for PPPs with short side chains. In both cases the rings are nearly orthogonal to each other. If McCarthy's structure were also true for our oligomers, then we would have observed a red shift in the solid film fluorescence spectra, but instead the fluorescence results point to a twist angle between the rings of 50-60°, similar to the solution conformation. The solid state spectra of OEQ support this theory, since as the molecule crystallizes, the fluorescence  $\lambda_{max}$  undergoes a blue shift. The raft-like arrangement allows for easy solution of the oligomers and may be the main source of solubility.

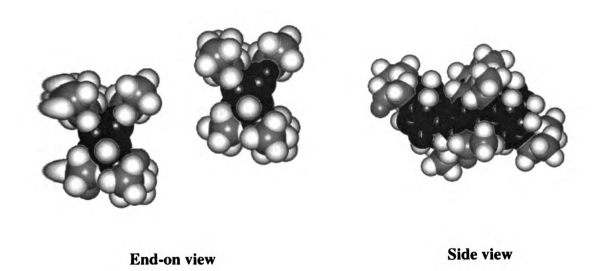


Figure 76: HyperChem depiction of proposed packing structure for OEQ

### E. Design Rules

By examining what we have learned about the effects of substituents on PPP oligomers and how they may apply in general to rigid-rod or disc-like molecules, we can describe a set of "design rules" to help predict the properties of PPPs. The rules are based on the conjugation length desired, how the side chains will affect the properties of the molecule, and what role the aspect ratio plays. These "design rules" will enable us to design molecules for a specific purpose, and they are derived from a combination of our results and those found in the literature.

The side chains on a rigid rod molecule affect more than just the solubility, as they can also impart other properties to the molecules such as liquid crystallinity and chirality and they can determine the degree of crystallinity in a molecule. In examining our oligophenylenes by optical microscopy, we observed great differences in the degree of crystallinity and the rate of crystallization in oligomers that were the same length but had differing side chains. We have not yet identified a liquid crystalline phase in any of our oligomers, which is reasonable since McCarthy *et al.* <sup>99</sup> reported that the minimum axial ratio (length:width) for a main chain liquid crystalline polymer is about 6, while we calculated the axial ratios for our oligomers to be around 2. Witteler, *et al.* <sup>78</sup> also noted that disubstituted PPPs showed liquid crystalline behavior only above a certain molecular weight (about 40,000). For methyl substituted oligomers, a chain length of 8 rings is necessary for liquid crystal formation. <sup>98</sup>

The conjugation length of an oligomer or polymer can be controlled by properly spacing solubilizing groups along the backbone of the molecule. Our results show that while the solubility and processibility of a substituted PPP oligomer can be greatly

increased by the addition of side chains, the electronic properties do not vary significantly in response to PPP length or side chain length. Therefore the band gap can only be adjusted by changing the number of contiguous unsubstituted phenyl rings in the backbone, or by placing electron-donating or withdrawing groups on the phenyl rings.

To obtain a polymer or oligomer with properties appropriate for some application or study, these "design rules" can help predetermine a starting point for optimization of the desired property. A combination of the right molecular weight (or chain length), conjugation length and side chains can provide a large range of molecules that are suitable for study or application.

## F. Suggestions for Future Work

## 1. Synthetic Methodology

An important topic that we did not explore in this research was why some of the coupling reactions were successful and others were not. Determining the reason for this apparent discrepancy would be a valuable contribution to the scientific literature. It is possible that these reactions can indeed be completed, but for some reason, such as an impurity in one of the starting materials, they did not work through our attempts. The synthesis of OMQ is particularly puzzling since we could only synthesize this compound through Novak's accelerated Suzuki coupling and not through the traditional Suzuki coupling. The steric constraints are the same for both OMQ and TMB and the electronic effects of the side groups should be similar for both reactions.

If experimental errors such as impurities in the starting materials can be ruled out, then the difference in reactivity can probably be attributed to the differences in reaction between a dibromobenzene and a dibromobiphenyl. A simple mechanistic study could help determine the cause for this difference. The first approach should be to determine all products formed in the reaction of the purified starting materials. As stated in the results section, the major product isolated in this study was 4-bromohexamethylterphenyl, so perhaps there is an electronic reason for the inability of the Pd catalyst to perform the oxidative addition step twice. It is also possible that the reaction simply proceeds at a much slower rate than for dibromobenzenes. This hypothesis can be tested by simply taking samples from a refluxing solution of the dibromobiphenyl and Pd(PPh<sub>3</sub>)<sub>4</sub> to monitor the progress of the oxidative addition by <sup>1</sup>H NMR.

It seems likely that this experiment will provide an answer to the problem of synthesizing OMQ, since it has been reported 125 that the rate determining step for the Pd(PPh<sub>3</sub>)<sub>4</sub> coupling of an aryl bromide is the oxidative addition step, while for an aryl iodide it is the transmetallation step. This study also noted that differences in boronic acids synthesized in different batches, containing different amounts of trace impurities, showed an effect on the rate. In this research, we also noted that the greater the steric hindrance in the boronic acid, the more carefully it needed to be purified in order for the reaction to work. Thus a scheme in which the boronic acid is rigorously purified should be adapted for all compounds to ensure consistent results.

### 2. Self-Assembled Monolayers

The results section outlined the progress to date on the study of PPP oligomers as self-assembled monolayers (SAMs). One problem in the characterization of these monolayers on Si wafers was obtaining reproducible ellipsometry data, which could be

linked to the way they were prepared. Since we proved that the monolayers formed on fumed silica, monolayers on Si wafers could be prepared in the same manner, using a small amount of triethyl amine to initiate the reaction. After the reaction is complete, the monolayer should be rinsed thoroughly with an organic solvent to remove any excess triethoxysilane, and then heated under vacuum to promote polymerization of the siloxanes. This procedure should ensure a more stable monolayer that will provide reproducible ellipsometry results

$$N(CH_3)_2$$
 $O_2N$ 
 $Si(OR)_3$ 

Figure 77: Proposed NLO chromophore

One particularly interesting application of these monolayers is their use in a nonlinear optical (NLO) device. For a molecule to exhibit second order NLO activity, it must be noncentrosymmetric and have a permanent dipole, so a nitroaniline derivative was selected. (Figure 77) The synthesis of this chromophore is quite challenging since it requires incorporation of three functional groups, and all the molecules must be identical, i.e. the nitro group and the amino group cannot be interchanged. We attempted two synthetic schemes that were unsuccessful before devising a final scheme that is likely to succeed. (Figure 78) 2-Amino-4-bromo-5-nitrobenzoic acid is a known compound, so the first five steps in the synthesis are not likely to introduce any major problems in this synthetic route. The methylation of the amine in the presence of a carboxylic acid has

Figure 78: Proposed synthetic route to NLO chromophore

Figure 79: PPP oligomer functionalized with a cross-linking group

also been cited in the literature, and the following Suzuki coupling should also not pose any problems since the reaction is tolerant to a number of functional groups. The conversion of a benzoic acid to an aryl bromide is a questionable reaction, but we tested this reaction on a model compound and the amount of product detected in the reaction mixture was appreciable (< 50%), and the product should be easily separated from the solvent and side products by distillation. Unfortunately, the most worrisome step is the final Stille coupling reaction. We have not had much success with the Stille coupling in our lab, but by testing various reaction conditions on model compounds, the reaction should be optimized and yield the desired NLO chromophore.

Another application of SAMs of PPP oligomers is as a thermally stable monolayer coating. This can be accomplished by simply incorporating a cross-linkable unit into the oligomer structure. An example of such a molecule is shown in Figure 79. This molecule contains a reactive *o*-quinodimethane functionality that will rapidly react with an adjacent unfunctionalized oligomer to link the two together by a six-membered ring.

(Figure 80) This cross-linking will thermally stabilize the monolayer, preventing desorption and breakdown of the oligomer structure. This particular monomer is terminated with a thiol as opposed to a siloxane, since this monolayer is designed to form on gold instead of silicon, but the scheme is still valid for the silicon monolayers. An alternative cross-linking scheme is to synthesize monolayers functionalized with methoxymethyl groups, which when treated with acid, lose methanol and form a benzylic

Figure 80: Thermal cross-linking of PPP oligomers

Figure 81: Chemical cross-linking of PPP oligomers

cation which can add to a neighboring oligomer via electrophilic aromatic substitution. (Figure 81) This cross-linking scheme is likely to be "messier", but the oligomers will be easier to synthesize.

#### 3. Crystallinity and Thermal Transitions

We began some interesting work on the relationship between the oligomer length. identity of the side chains and the crystallinity and thermal transitions of these oligomers. Completing this study will help round out the design rules discussed above, and provide a valuable contribution to the scientific literature on this topic. The first project that should be completed is to determine the identity of the two transitions in the DMA scan of OEQ. It would also be useful to examine DMA plots of some other oligomers to look for similarities and differences in the plots such as THS, which shows a similar DSC plot to OEQ, and also oligomers such as HMT which have well defined and characterized crystallization schemes. Assuming that the two transitions are due to the main chain and the side chains respectively, there are two experiments that can confirm or deny this hypothesis. First, transitions in the main chain should be evident in the optical spectrum either as a shift of  $\lambda_{max}$  or as a change in intensity, so continuing variable temperature fluorescence experiments similar to those described in the Results section will help us determine if one of the transitions is due to movement of the main chain. Second, solid state NMR experiments may be able to tell us something about the side chain movement. Preliminary results showed that the ethyl group have a strong signal in the CP/MAS NMR spectrum, and side chain movement should be manifested as either a change in the line shape or intensity, or in the T<sub>1</sub> spin lattice relaxation time of either the protons or the carbons in the ethyl groups of OEQ. We have attempted these experiments, but we have not yet been able to find a definite, reproducible result yet. Some experiments with model compounds may be helpful in determining the correct procedures for these tests. It is reported that oligophenyls have unusually long relaxation times (biphenyl is reported to have a T<sub>1</sub> value of 910 s! 126), so it is possible that some of the difficulties encountered in this experiment were due to this unusual characteristic. Substituted oligophenyls have a much shorter T<sub>1</sub> time, because the relatively efficient motions of an amorphous or less crystalline compound shorten the relaxation time.

#### E. Summary

This thesis describes the synthesis and characterization of a series of exact-length dialkyl substituted PPP oligomers. We synthesized the oligomers through an iterative approach using a combination of traditional and accelerated Suzuki coupling reactions. By determining the barrier to rotation around the single bonds connecting phenyl rings, we realized that twist angles between rings and rotational barriers are not the sole causes for an observed increase in solubility. We theorize that the increase in solubility is due to a combination of the twist angle, rotational barrier, increase in entropy from the longer side chains, and the more amorphous state of functionalized oligomers.

We also examined the optical properties of these oligomers to determine if they have any usefulness in devices and how the side chains affect the optical and electronic properties of the oligomers and related polymers. We estimate the effective conjugation length to be about 5-6 rings, which is much shorter than that reported for unsubstituted

PPPs. There is very little difference between oligomers of the same length with different side chains (except H).

By analyzing these results, we can propose a set of "design rules" that can be used to design appropriate molecules with desired properties. The main considerations are chain length (or molecular weight), conjugation length, and the nature of the side chains, if any. Once the crystallization data is complete, one will be able to define the molecular properties even more specifically.

Although the oligomers synthesized in this study are not suitable for use in organic LEDs, they have a number of potential applications aside from being models for a polymer. We began the investigation of PPP oligomers as self-assembled monolayers and propose their use in a nonlinear optical device or as a thermally stable coating on silicon.

## IV. EXPERIMENTAL

General: Toluene, tetrahydrofuran (THF), methanol and carbon tetrachloride were purchased from Mallinckrodt; dichloromethane was purchased from EM Science and diethylether was purchased from CCI, Inc. All solvents were used as received except THF and toluene, which were dried and deoxegenated by distillation first from CaH<sub>2</sub> then from sodium benzophenone ketyl. Deionized water was deoxygenated by bubbling nitrogen through it for at least 2 h. Magnesium, stannous chloride, acetyl chloride, mossy zinc and mercuric chloride were purchased from Mallinckrodt and used as received excepted acetyl chloride, which was distilled under nitrogen before each use. Palladium acetate, tetrakis(triphenylphosphine) palladium, triisopropyl borate, trimethyl borate, nbutyllithium, trimethylsilyl chloride, ethylbenzene, 2,5-dibromo-p-xylene, silver tetrafluoroborate, and iodine monochloride were purchased from Aldrich Chemical Company and used as received. Bromine was purchased from Fisher Scientific. Aluminum chloride and concentrated hydrochloric acid were purchased from EM Science. p-Xylene and sodium bicarbonate were purchased from Baker. Magnesium sulfate and sodium carbonate were purchased from CCI, Inc. Reactions requiring inert conditions were conducted under argon or nitrogen. Preparatory thin layer chromatography (TLC) plates were 1000 µm thick silica gel with fluorescent indicator

(silica gel GF) purchased from Analtech, Inc. All reactions were stirred magnetically unless otherwise indicated. UV absorption spectra were taken using a Unicam Spectrophotometer and fluorescence emission spectra were taken using a Hitachi F-4500 Fluorimeter. The solutions were 1x10<sup>-4</sup> M in spectrophotometric grade cyclohexane (Spectrum Chemical) for the fluorescence experiments and 1 x 10<sup>-5</sup> M in spectrophotometric grade cyclohexane for the UV absorption experiments. Fluorescence emission spectra were taken by exciting the solution at 274 nm and recording the emission spectrum from 275 to 500 nm. Routine <sup>1</sup>H and <sup>13</sup>C spectra were taken at 300 MHz and 75.43 MHz respectively, using either a Varian VXR-300 NMR Spectrometer or a Varian-Gemini NMR Spectrometer. NMR data are reported in parts per million (ppm). <sup>1</sup>H and <sup>13</sup>C spectra taken in CDCl<sub>3</sub> (Isotec, Inc.) are referenced to residual CHCl<sub>3</sub> at 7.24 or 77.0 ppm, respectively. The reported melting points are uncorrected, and were determined by either optical microscopy (by observing the point at which the sample is no longer birefringent under crossed polarizers) or using an Electrothermal Melting point Melting points for boronic acids were not taken because they are apparatus. irreproducible due to dehydration reactions that occur during heating.

Dynamic NMR Experiments: Dynamic <sup>1</sup>H NMR experiments were conducted at 500 MHz using a Varian (VXR-500) NMR Spectrometer with the temperature controlled using an FTS Systems air-jet. VTNMR experiments for ethyl and hexyl- substituted oligomers were conducted in o-dichlorobenzene- $d_4$  (Aldrich) from 20 to 140 °C and experiments for methyl-substituted oligomers were taken in toluene- $d_8$  (Cambridge Isotope Laboratories) from 20 to 80 °C. The methyl groups on the ethyl- and hexyl-

substituted oligomers were decoupled during the variable temperature experiments. The barriers to rotation were calculated by observing spectra at various temperatures to determine the coalescence temperature and then applying the Gutowsky-Holm approximation. 80,81

Optical Microscopy: All optical microscopy was conducted on a Nikon microscope equipped with crossed-polarizers and a photomicrographic attachment. The sample temperature was controlled by a Mettler FP82HT hot stage which was controlled by a Mettler FP90 central processor.

Solid State Fluorescence Experiments: Solid state fluorescence spectra were obtained from films of oligomers on 2 cm by 1 cm quartz slides. The films were created by two methods. In the first method, a small amount of powdered oligomer was placed between two slides and the compound was heated to 20 degrees above the melting point. After holding at that temperature for one minute, the films were flash cooled by placing the slide into a dewar filled with liquid nitrogen. Flash cooling prevented crystallization of the compounds and minimized light scattering from the sample. Compounds that decomposed at their melting points were spin cast from a concentrated toluene solution. The slides were placed in the fluorimeter at approximately 45° to the incident beam.

For the variable temperature fluorescence experiments, the samples were prepared in the same manner and stored in liquid nitrogen until the measurements were taken. The temperature was varied using a home-built sample holder. The copper holder had a window sized for the sample, and was equipped with a heater and thermocouple. The

sample was cooled by running dry nitrogen gas through a copper heat exchanger, and then into the sample holder through a tunnel in the holder. The gas was vented into the sample chamber to purge the chamber of air and to prevent condensation on the sample. Each sample was allowed to equilibrate at each temperature for 10 minutes before a spectrum was taken.

Solid State UV Absorbance Experiments: For solution spectra, the samples were prepared as described above. For solid state spectra, the samples were prepared as for the fluorescence experiments. The spectra were taken by scanning air as the background, then scanning a blank quartz slide, then scanning the sample. The quartz absorbance was manually subtracted from the sample spectrum. The samples were placed in the cuvette holder at a 45° angle to the incident beam.

4-Ethylacetophenone(1). Compound 1 was prepared according to literature procedures <sup>127</sup> from 20.0 g (0.149 mol) of ethylbenzene, 15.7 g (0.118 mol) of AlCl<sub>3</sub>, and 8.15 g (0.104 mol) of acetyl chloride. The product was purified by vacuum distillation (bp 70-78 °C @ 360 mtorr) (lit. <sup>128</sup> bp 116-117 °C @ 130 mtorr) to yield 13.8 g (99%) as a clear, colorless oil.

<sup>1</sup>H NMR: δ 7.90 (d, 2H), 7.30 (d, 2H), 2.70 (quartet, 2H), 2.60 (s, 3H), 1.25 (t, 3H).

1,4-Diethylbenzene (2b). The synthesis of 2b was adapted from Read and Wood<sup>129</sup> using 5.00 g (0.034 mol) of 1 and the following workup. The reaction mixture was held at reflux temperature and was stirred with a mechanical stirrer for 24 h. After cooling to

room temperature, the reaction mixture was poured into a separatory funnel, diethyl ether was added and the layers were separated. The aqueous layer was extracted with diethyl ether (3x25 mL) and the combined organic layers were washed with saturated NaHCO<sub>3</sub> until the washings were neutral to litmus paper. The organic layers were dried (MgSO<sub>4</sub>), filtered and concentrated. The yellow oil was purified by vacuum distillation (34 °C @ 640 mtorr) (lit. 130 bp 181-182 °C) to yield 3.20 g (71%) as a clear colorless oil.

<sup>1</sup>H NMR: δ 7.10 (s, 4H), 2.60 (quartet, 4H), 1.20 (t, 6H).

p-Di-n-hexylbenzene (2c). This compound was synthesized according to the literature procedure 105 bp 117 °C @ 146 mtorr (lit. 105 bp 134 °C @ 99 mtorr)

<sup>1</sup>H NMR: δ 7.08 (s, 4H), 2.55 (t, 4H), 1.60 (m, 4H), 1.30 (m, 12H), 0.78 (t, 6H).

2,5-Dibromo-1,4-diethylbenzene (4b). The synthesis of compound 4b was adapted from Rehahn, et al. 105 To a 500 mL three-necked round-bottomed flask equipped with an addition funnel and an outlet to a KOH<sub>(aq)</sub> trap were added 20.0 g (0.149 mol) of 2b and 50 mL of methylene chloride. The apparatus was rigorously shielded from light and cooled to 0 °C. In the dark, 52.5 g (0.328 mol) of bromine in 50 mL of methylene chloride were added to the addition funnel. The bromine solution was added dropwise to the reaction mixture over 20 minutes and allowed to warm slowly to room temperature. After 36 h, an additional 23.0 g of Br<sub>2</sub> in 25 mL of methylene chloride were added and the mixture was allowed to stir for an additional day. With the reaction still protected from light, 100 mL of an aqueous KOH (20% w/w) solution were added and the reaction was stirred until no orange color remained. The light yellow solution was poured into a

separatory funnel and the layers were separated. The aqueous layer was extracted with CH<sub>2</sub>Cl<sub>2</sub> (3x40 mL) and the combined organic layers were washed once with water, dried (MgSO<sub>4</sub>), filtered and concentrated to yield a yellow oil which crystallized from a small amount of absolute ethanol to yield 21.2 g (49%) as colorless needles. mp 30-32 °C. (lit.<sup>131</sup> mp 33-35 °C)

<sup>1</sup>H NMR: δ 7.35 (s, 2H), 2.70 (quartet, 4H), 1.20 (t, 6H)

**2,5-Dibromo-1,4-di-n-hexylbenzene** (4c). Compound 4c was synthesized from 20.0 g (0.081 mol) of 2c and 52.0 g (0.325 mol) of bromine in the same manner as 4b. The crude product was recrystallized from ethanol to yield 29.1 g (89%) as a white powder. mp 42-43 °C (lit. 105 mp 33 °C)

<sup>1</sup>H NMR: δ 7.34 (s, 2H), 2.62 (t, 4H), 1.60 (m, 4H), 1.30 (m, 14H), 0.90 (m, 6H)

<sup>13</sup>C NMR: δ 144.3, 133.7, 123.1, 35.5, 31.6, 29.8, 29.0, 22.6, 14.1.

2-Bromo-1,4-diethylbenzene (3b). The synthesis of compound 8b from 11.1 g (82.9 mmol) of diethylbenzene is identical to that of 4b, except that only 1.2 equivalents of bromine were used. More bromine (12.3 g) was added after 36 h to compensate for evaporation of bromine through the outlet to the KOH trap. The product was purified by vacuum distillation (bp 90-100 °C @ 384 mtorr) to afford 16.1 g (91%) as a clear colorless liquid.

<sup>1</sup>H NMR: δ 7.35 (s, 1H), 7.15 (d, 1H), 7.05 (d, 1H), 2.7 (quartet, 2H), 2.6 (quartet, 2H), 1.2 (t, 6H).

<sup>13</sup>C NMR: δ 143.6, 133.0, 131.9, 129.3, 127.0, 124.1, 28.9, 28.0, 15.4, 14.3.

**HRMS:** calc. for  $C_{10}H_{13}Br$  212.0201, found 212.0201

Alternate Synthesis for Monobromination of Aromatics: <sup>132</sup> a) 2-Bromo-1,4-diethylbenzene (3b): An ice-chilled solution of bromine (4.78 g, 29.9 mmol) in 5 mL of DMF, prepared by adding the bromine dropwise to DMF in a jacketed pressure-equalizing addition funnel, was added dropwise to a light-protected ice-chilled solution of diethylbenzene (1.00 g, 7.26 mmol) in 10 mL of DMF. After the addition was complete, the reaction mixture was allowed to stir for an additional 2 h. The mixture was quickly poured into an iced solution of Na<sub>2</sub>SO<sub>3</sub> (19g/L) and extracted with pentane. The combined organic layers were dried over MgSO<sub>4</sub>, filtered and concentrated to yield 1.23 g (80.4%) of a yellow oil. The product can be vacuum distilled as above.

b) 2-Bromo-1,4-di-n-hexylbenzene (3c): This compound was synthesized from 10.00 g (41.0 mmol) of di-n-hexylbenzene and 26.0 g (163 mmol) of bromine. The reaction was monitored by <sup>1</sup>H NMR and was stirred overnight at room temperature. The product was distilled under vacuum (bp 128 °C @ 83 mtorr, lit. <sup>7</sup>bp 158-161 °C @ 10 mtorr) to yield 12.5 g (94%) as a colorless oil.

<sup>1</sup>**H NMR:** δ 7.34 (s, 1 H), 7.10 (d, 1H), 7.00 (d, 1H), 2.65 (t, 2H), 2.50 (t, 2H), 1.60 (m, 4H), 1.30 (m, 12H), 0.90 (m, 6H).

**2-Bromo-p-xylene** (3a). The synthesis of compound 3a from 100 g (0.943 mol) of p-xylene and 62.4 g (0.391 mol) of bromine is identical to that of 3b except that p-xylene

was used as the solvent. The crude product was purified by distillation (bp 195-201 °C) (lit. 133bp 203-204 °C) to yield 49.9 g (69%) as a colorless liquid.

<sup>1</sup>**H NMR:** δ 7.40 (s, 1H), 7.12 (d, 1H), 7.00 (d, 1H), 2.38 (s, 3H), 2.30 (s, 3H).

**2,5-Diiodo-1,4-diethylbenzene** (5b). Compound **5b** was synthesized according to the literature procedure[Suzuki, 1971 #111] from 10.0 g (74.6 mmol) of **2b**, 6.80 g (29.9 mmol) of H<sub>5</sub>IO<sub>6</sub> and 15.2 g (59.7 mmol) of iodine. The crude product was purified by two recrystallizations from acetone to yield 18.6 g (64%) as white needles. mp 70-71 °C.

<sup>1</sup>H NMR: δ 7.60 (s, 2H), 2.60 (quartet, 4H), 1.15 (t, 6H)

<sup>13</sup>C NMR: δ 145.8, 138.6, 100.3, 33.1, 14.4.

**2,5-Diiodo-1,4-di-n-hexylbenzene** (5c). Compound **5c** was synthesized from 5.00 g (20.3 mmol) of **2c**, 1.85 g (8.13 mmol) of  $H_5IO_6$ , and 4.10 g (16.2 mmol) of iodine to yield 3.12 g (31%) as white needles. mp 53-54 °C

<sup>1</sup>H NMR δ 7.60 (s,2H), 2.60 (t, 4H), 1.50 (m, 4H), 1.30 (m, 12H), 0.90 (t, 6H)

<sup>13</sup>C NMR δ 144.7, 139.2, 100.4, 39.8, 31.6, 30.1, 29.0, 22.6, 14.1.

General Procedure for 2-bromo-1,4-dialkyl-5(trimethylsilyl)benzene: a) 2-Bromo-5-(trimethylsilyl)-p-xylene (6a). To a 500 mL round bottomed flask fitted with a Schlenk vacuum adapter were added 30.0 g (0.114 mol) of 2,5-dibromo-p-xylene (4a). The flask was placed under an argon atmosphere and 80 mL of tetrahydrofuran were added. After cooling the solution in a dry ice/acetone bath, 107 mL (1.60 M, 0.171 mol) of n-BuLi were added dropwise via a syringe. After stirring for 4 h, 24.7 g (0.227 mol) of

trimethylsilyl chloride were added dropwise via a syringe and the mixture was allowed to warm to room temperature. A white precipitate formed (probably LiCl) which dissolved when 75 mL of water were added to the reaction. The layers were separated and the aqueous layer was extracted with diethylether (3 x 50 mL). The combined organic layers were dried over MgSO<sub>4</sub>, filtered and concentrated to yield a yellow oil. The oil was distilled (bp 95-105 °C @ 520 mtorr) to afford 27.9 g (95%) as a clear colorless oil.

<sup>1</sup>H NMR: δ 7.32 (s, 1H), 7.24 (s, 1H), 2.37 (s, 3H), 2.34 (s, 3H), 0.30 (s, 9H)

<sup>13</sup>C NMR: δ 142.6, 137.5, 136.6, 133.9, 133.3, 126.1, 22.3, 22.0, -0.3.

HRMS calc. for C<sub>11</sub>H<sub>17</sub>BrSi 258.0283, found 258.0259

2-Bromo-1,4-diethyl-5-(trimethylsilyl)benzene (6b). The synthesis of this compound from 10.0 g (34.2 mmol) of 4b is as described for 6a. The crude product was purified by vacuum distillation (bp 90 °C @ 335 mtorr) to yield 7.71 g (79%) as a clear colorless oil.

<sup>1</sup>**H NMR:** δ 7.35 (s, 1H), 7.25 (s, 1H), 2.70 (m, 4H), 1.20 (m, 6H), 0.30 (s, 9H)

<sup>13</sup>C NMR: δ 149.2, 137.2, 135.5, 134.0, 132.0, 125.9, 29.0, 28.2, 16.2, 14.5, 0.3.

HRMS calc. for C<sub>13</sub>H<sub>21</sub>BrSi 284.0598, found 284.0600

2-Bromo-1,4-di-n-hexyl-5-(trimethylsilyl)benzene (6c). Compound 6c was synthesized from 10.0 g (24.8 mmol) of 4c. The crude product was purified by vacuum distillation (bp 175 °C @ 60 mtorr) to yield 9.30 g (94%) as a clear colorless viscous oil.

<sup>1</sup>H NMR: δ 7.35 (s, 1H), 7.23 (s, 1H), 2.65 (m, 4H), 1.60 (m, 4H), 1.37 (m, 12H), 0.90 (t, 6H), 0.30 (s, 9H)

<sup>13</sup>C NMR: δ 148.0, 138.3, 137.1, 136.2, 132.5, 125.9, 35.8, 35.6, 32.4, 31.8, 31.7, 30.1, 29.6, 29.2, 22.7, 22.6, 14.1, 0.4

HRMS: calc. for C<sub>21</sub>H<sub>37</sub>BrSi 398.1830, found 398.1830

General Procedure for replacing trimethylsilyl (TMS) group with bromine a) 4-Bromo-2,2',5,5'-tetramethylbiphenyl (19a): Compound 19a was synthesized from 10.0 g (35.4 mmol) of 4-TMS-2,2',5,5'-tetramethylbiphenyl and 6.80 g (42.5 mmol) of bromine using a procedure was adapted from Walker, et. al. 102 which uses methanol as the solvent. We used a mixture of dichloromethane/methanol to increase the solubility of the starting material. The TMS-terminated compound was dissolved in the minimum amount of dichloromethane at 0°C and then the required amount of methanol was added. Compound 19a was isolated as a light yellow oil which crystallized from ethanol to yield 8.00 g (78%) as white needles. mp 34-34.5 °C

<sup>1</sup>**H NMR:** δ 7.40 (s, 1H), 7.15 (d, 1H), 7.05 (d, 1H), 6.95 (s, 1H), 6.86 (s, 1H), 2.37 (s, 3H), 2.31 (s, 3H), 2.00 (s, 6H)

<sup>13</sup>C NMR: δ 141.0, 140.3, 135.3, 135.0, 134.7, 133.2, 132.5, 131.5, 129.8, 129.7, 128.0, 123.1, 22.3, 20.9, 19.3, 19.0.

HRMS: calc. for C<sub>16</sub>H<sub>17</sub>Br 290.0495, found 290.0488

b) 4-Bromo-2,2',5,5'-tetrahexylbiphenyl (19c): This compound was synthesized from 2.50 g (4.45 mmol) of 18c and 0.850 g (5.34 mmol) of bromine to yield 2.52 g (100%) of the product as a light yellow oil. This product was used directly without further purification.

<sup>1</sup>H NMR: δ 7.40 (s, 1H), 7.15 (d, 1H), 7.08 (dd, 1H), 6.93 (s, 1H), 6.86 (d, 1H), 2.60 (m, 4H), 2.25 (m, 4H), 1.60 (m, 4H), 1.20 (m, 28H), 0.80 (m, 12H)

<sup>13</sup>C NMR: δ 140.5, 140.2, 139.7, 139.6, 138.5, 137.7, 132.5, 131.6, 129.7, 128.7, 127.4, 122.8, 35.6, 35.4, 32.7, 32.6, 31.7, 31.6, 31.5, 31.4, 31.0, 30.7, 30.0, 29.2, 29.1, 29.0, 22.6, 22.5, 14.1, 14.0

**HRMS:** calc. for C<sub>36</sub>H<sub>57</sub>Br 570.3630, found 570.3622

c) 4-Bromo-2,2',2",5,5',5"-hexamethylterphenyl (22a): This compound was synthesized from 5.00 g (12.9 mmol) of 21a to yield 4.21 g (83%) as a white powder. mp 182.5-183.5 °C

<sup>1</sup>**H NMR:** δ7.45, s, 1H; δ7.15, d, 1H; δ7.05, m, 2H; δ6.95, m, 3H; δ2.39, s, 3H; δ2.35, s, 3H; δ2.03, m, 12H

<sup>13</sup>C NMR: δ141.8, 141.2, 139.1, 135.4, 134.8, 133.2, 132.6, 132.5, 131.8, 131.7, 130.7, 130.4, 130.1, 130.0, 129.6, 121.8, 123.1, 22.3, 22.2, 20.9, 19.4, 19.3, 19.2, 19.0

General procedure for replacing TMS with iodine: a) 4,4'-Diiodo-2,2',5,5'tetramethylbiphenyl (13a). This procedure was adapted from Jacob, et al. 103 with the
following modifications: To a 100 mL round-bottomed flask were added 0.210 g (0.565
mmol) of 11a, 0.144 g (0.739 mmol) of AgBF<sub>4</sub>, 50 mL of methanol and 20 mL of
methylene chloride. The solution was cooled to 0°C and a solution of ICl (0.101 g, 0.622
mmol) in methanol (0.54 mL) was prepared and added dropwise to the reaction mixture.
This solution was allowed to warm to room temperature and stirring was continued
overnight. The reaction was quenched using 30 mL of a solution (20% w/w) of SnCl<sub>2</sub> in

methanol and stirred for 2 h. The reaction mixture was then partitioned between CH<sub>2</sub>Cl<sub>2</sub> and water. The layers were separated and the aqueous layer was extracted with CH<sub>2</sub>Cl<sub>2</sub> (3 x 30 mL). The combined organic layers were washed with aqueous KOH (20% w/w) and then dried (MgSO<sub>4</sub>), filtered and concentrated. The crude product was purified by recrystallization from ethanol to yield 0.210 g (76%) as white needles. mp 94-95 °C A small portion was further purified by preparatory TLC (silica, hexane) to obtain pure white needles. mp 102-103 °C (lit. 15 mp 110 °C)

<sup>1</sup>**H NMR:** δ 7.70 (s, 2H), 6.90 (s, 2H), 2.35 (s, 6H), 1.95 (s, 6H)

b)4,4"-Diiodo-2,2',2",5,5',5"-hexamethylterphenyl (14a). Compound 14a was synthesized from 1.00 g (2.18 mmol) of 12a. The crude product was recrystallized twice from benzene/ligroin to obtain 0.560 g (46%) of the pure product. mp 254-255 °C (lit.15mp 254-255 °C)

<sup>1</sup>**H NMR:** δ 7.7 (s, 2H), 7.0 (d, 2H), 6.9 (d, 2H), 2.4 (s, 6H), 2.0 (s, 6H)

c)4,4'-Diiodo-2,2',5,5'-tetraethylbiphenyl (13b): Compound 13b was synthesized from 0.50 g (1.22 mmol) of 11b. The crude product was isolated as a colorless oil to yield 0.450 g (72%) and was used without further purification.

<sup>1</sup>H NMR: δ 7.7 (s, 2H), 6.9 (s, 2H), 2.68 (quartet, 4H), 2.25 (m, 4H), 1.2 (t, 6H), 1.0 (t, 6H)

<sup>13</sup>C NMR: δ 143.4, 141.4, 140.2, 138.9, 129.4, 99.4, 33.5, 28.4, 15.0, 14.6.

HRMS: calc. for C<sub>20</sub>H<sub>24</sub>I<sub>2</sub> 517.9968, found 517.9963

d)4,4"-Diiodo-2,2',2",5,5',5"-hexaethylterphenyl (14b). Compound 14b was synthesized from 0.500 g (0.920 mmol) of 12b. The crude product was isolated as a white powder and was used without further purification to yield 0.540 g (90%)

<sup>1</sup>H NMR: δ 7.7 (s, 2H), 7.0 (s, 2H), 6.95 (d, 2H), 2.7 (quartet, 4H), 2.3 (m, 8H), 1.2 (t, 6H), 1.0 (m, 12H)

<sup>13</sup>C NMR: δ 143.3, 141.8, 141.7, 141.3, 141.2, 139.0, 138.9, 138.8, 138.7, 138.6, 138.5, 129.9, 129.8, 129.2, 99.1, 99.0, 33.6, 25.7, 25.5, 25.4, 15.3, 15.2, 14.9, 14.8, 14.6 HRMS: calc. for C<sub>30</sub>H<sub>36</sub>I<sub>2</sub> 650.0907, found 650.0933

e)4,4"-Diiodo-2,2',2",5,5',5"-hexahexylterphenyl (14c). Compound 14c was synthesized from 1.50 g (1.71 mmol) of 12c. The crude product was recrystallized from ethanol to yield 1.40 g (83%) as a white powder. mp 61.5-63 °C

<sup>1</sup>**H NMR:** δ 7.6 (s, 2H), 6.9 (d, 2H), 6.9 (d, 2H), 2.6 (m, 4H), 2.2 (m, 8H), 1.1-1.6 (m, 48H), 0.8 (m, 18H)

<sup>13</sup>C NMR: δ 142.0, 141.3, 141.1, 140.6, 140.5, 139.4, 139.3, 138.9, 137.2, 137.1, 130.8, 130.6, 130.0, 99.0, 40.3, 32.6, 32.4, 31.7, 31.6, 31.5, 31.0, 30.9, 30.8, 30.7, 30.5, 30.3, 29.3, 29.2, 29.1, 29.0, 22.6, 22.5, 14.1

HRMS: calc. for C<sub>54</sub>H<sub>84</sub>I<sub>2</sub> 986.4662, found 986.4667

General procedure for Pd(OAc)<sub>2</sub> coupling: a) 2,2',2",5',5",5"'-Octamethylquaterphenyl (15a). This coupling procedure was adapted from Wallow and Novak.<sup>50</sup> To a 50 mL Schlenk flask were added 0.200 g (0.433 mmol) of 13a, 0.220 g (0.991 mmol) of 7a and 0.114 g (1.08 mmol) of Na<sub>2</sub>CO<sub>3</sub>. The flask was placed under an

Ar atmosphere by 3 pump-fill cycles. Pd(OAc)<sub>2</sub> (0.001g) was placed in a Schlenk tube under an Ar atmosphere. THF (30 mL) was added to the catalyst and the catalyst solution was transferred to the reaction flask via a cannula. Water (10 mL) was added to the reaction flask via syringe and the reaction mixture was stirred at reflux for 2 h. Upon cooling to room temperature, the mixture was poured into a separatory funnel and the layers were separated. The aqueous layer was extracted with CH<sub>2</sub>Cl<sub>2</sub> (3x30 mL) and the combined organic layers were dried over MgSO<sub>4</sub>. The solution was heated before filtering to ensure complete dissolution of the product and was concentrated to yield 0.122 g as an off-white powder. A small portion was purified by preparatory TLC (silica/hexane). mp 260-261 °C (lit.<sup>15</sup> mp 264-266 °C)

<sup>1</sup>H NMR: δ 7.15 (d, 2H), 7.05 (m, 4H), 6.98 (m, 4H), 2.34 (s, 6H), 2.08 (2 singlets, 12H), 2.03 (s, 6H).

<sup>13</sup>C NMR: δ141.5, 140.3, 134.8, 132.8, 132.6, 130.7, 130.6, 130.1, 129.6, 127.7, 20.9, 19.4, 19.3.

b)2,2',2"',2"'',5,5',5",5"',5"''-Decamethylquinquephenyl (16a). Compound 16a was synthesized from 0.200 g (0.354 mmol) of 14 to yield 0.185 g as a white powder. A small portion was purified by preparatory TLC (silica/hexane). mp 315 °C (lit. 15 mp 307-309 °C)

<sup>1</sup>H NMR: δ 7.15 (d, 2H), 7.06 (m, 6H), 7.0 (m, 4H), 2.34 (s, 6H), 2.08 (m, 18H), 2.04 (s, 6H).

<sup>13</sup>C NMR: δ141.6, 140.3, 134.8, 132.8, 130.7, 130.6, 130.5, 130.2, 130.1, 129.6, 127.7, 21.0, 19.5, 19.3.

c) 4,4"-Bis(trimethylsilyl)-2,2',2",5,5',5"-hexaethylterphenyl (12b). This compound was synthesized from 1.00 g (2.59 mmol) of 5 and 1.46 g (5.70 mmol) of 8b. The crude product was recrystallized from ethanol to yield 0.79 g (56%) as a white fluffy powder. mp 139-141 °C

<sup>1</sup>H NMR: δ 7.35 (d, 2H), 7.05 (d, 2H), 7.03 (s, 1H), 7.0 (s, 1H), 2.74 (quartet, 4H), 2.36 (m, 8H), 1.21 (2 triplets, 6H), 1.02 (m, 12H), 0.35 (s, 18H).

<sup>13</sup>C NMR: δ 146.7, 142.0, 141.9, 139.7, 139.6, 138.4, 138.3, 138.2, 138.1, 136.2, 136.1, 134.4, 134.3, 129.6, 129.4, 129.2, 129.1, 28.5, 26.0, 25.9, 25.7, 16.5, 16.4, 15.6, 15.4, 15.3, 15.2, 0.6.

HRMS: calc. for C<sub>36</sub>H<sub>54</sub>Si<sub>2</sub> 542.3764, found 542.3762

d) 2,2',2",5,5',5",5"'-Octaethylquaterphenyl (15b). Compound 15b was synthesized from 0.200 g (0.390 mmol) of 13b and 0.151 g (0.850 mmol) of 7b. The crude product was recrystallized from ethanol to yield 0.050 g (24%) as a white powder. mp 110-112 °C

<sup>1</sup>H NMR: δ 7.00-7.23 (m, 10H), 2.65 (quartet, 14H), 2.40 (m, 12H), 1.24 (2 triplets, 6H), 1.04 (m, 18H)

<sup>13</sup>C NMR: 8 141.1, 140.9, 139.8, 139.7, 139.3, 138.7, 138.6, 138.5, 138.4, 129.5, 129.3, 128.0, 127.9, 126.7, 126.6, 28.4, 25.9, 25.8, 15.6, 15.5, 15.4, 15.2, 15.0

**HRMS:** calc for  $C_{40}H_{50}$  530.3912, found 530.3920

e) 2,2',2"',2"'',5,5',5",5"',5"''-Decaethylquinquephenyl (16b). Compound 16b was synthesized from 0.200 g (0.308 mmol) of 14b to yield 0.215 g of a white powder. A small portion was recrystallized from ethanol. mp 235-237 °C (dec.)

<sup>1</sup>H NMR: δ 7.00-7.30 (m, 12H), 2.70 (quartet, 4H), 2.40 (m, 16H), 1.25 (t, 6H), 1.10 (m, 24H)

<sup>13</sup>C NMR: δ 140.9, 139.7, 139.3, 138.7, 138.5, 129.6, 129.5, 129.4, 128.0, 127.9, 126.7, 28.4, 25.9, 15.6, 15.5, 15.4, 15.3

HRMS: calc. for C<sub>50</sub>H<sub>62</sub> 662.4852, found 662.4852

f) 4,4"-Bis(trimethylsilyl)-2,2',2",5,5',5"-hexahexylterphenyl (12c). Compound 12c was synthesized from 1.52 g (3.00 mmol) of 5c and 2.32 g (6.40 mmol) of 8c. The reaction was monitored by <sup>1</sup>H NMR and was allowed to reflux for 29 h. The crude product was crystallized from ethanol to yield 1.67 g (64%) as a white powder. mp 67-68.5 °C.

<sup>1</sup>**H NMR:** δ 7.30 (s, 2H), 7.03 (d, 2H), 6.97 (d, 2H), 2,70 (t, 4H), 2.30 (m, 8H), 1.05-1.65 (m, 48H), 0.85 (m, 18H), 0.35 (s, 18H)

<sup>13</sup>C NMR: δ 145.3, 142.0, 141.8, 139.6, 137.0, 136.9, 136.0, 135.1, 130.3, 130.0, 36.0, 35.9, 33.1, 33.0, 32.8, 32.7, 32.5, 31.9, 31.7, 31.6, 31.3, 31.2, 30.8, 29.6, 29.5, 29.3, 29.2, 29.1, 22.7, 22.5, 14.1, 0.70

HRMS: calc. for C<sub>60</sub>H<sub>102</sub>Si<sub>2</sub> 878.7520, found 878.7515

g) 2,2',2'',2''',5,5',5'',5''',5''''-Decahexylquinquephenyl (16c). Compound 16c was synthesized from 0.424 g (0.852 mmol) of 5c and 1.00 g (1.87 mmol) of 20c. The crude product was recrystallized from isopropyl alcohol to yield 0.650 g (65%) as a white powder. mp 95-97 °C

<sup>1</sup>H NMR: δ 7.00-7.20 (m, 12H), 2.60 (m, 4H), 2.36 (m, 16H), 1.00-1.70 (m, 80H), 0.80 (m, 30H)

<sup>13</sup>C NMR: δ 141.1, 140.9, 139.6, 139.5, 138.0, 137.3, 137.1, 130.1, 130.0, 128.7, 128.5, 127.0, 35.5, 33.1, 33.0, 32.9, 31.7, 31.5, 31.2, 30.9, 30.7, 29.4, 29.2, 29.1, 29.0, 22.6, 22.5, 14.1, 14.0

**HRMS:** calc for  $C_{90}H_{142}$  1223.1110, found 1223.1110.

(17c). Compound 17c was synthesized from 0.840 g (0.852 mmol) of 14c and 1.00 g (1.87 mmol) of 20c. The crude product was recrystallized from ligroin and run through a column of silica gel (cyclohexane) to yield 0.300 g (21%) as a shiny white solid. mp

h)2,2',2'',2''',2'''',2''''',5,5',5'',5''',5'''',5'''''-Tetradecahexylseptaphenyl

<sup>1</sup>H NMR: δ 7.00-7.20 (m, 16H), 2.60 (m, 4H), 2.30 (m, 24H), 1.00-1.70 (m, 120H), 0.80 (m, 34H)

<sup>13</sup>C NMR: NMR δ 140.9, 139.7, 138.1, 137.4, 130.2, 128.6, 127.0, 35.5, 32.9, 31.7, 31.5, 31.2, 30.9, 29.5, 29.3, 29.0, 22.6, 14.1, 14.0

HRMS: calc. for C<sub>126</sub>H<sub>198</sub> 1712.5530, found 1712.5557

138-140 °C

2,2',2",5,5',5"-Hexaethylterphenyl (10b): This compound was synthesized from 12b according to Bennetau, et al. 104 mp 60-61 °C

<sup>1</sup>H NMR: δ 7.22 (dd, 2H), 7.14 (dd, 2H), 7.04 (d, 2H), 7.01 (d, 2H), 2.70 (quartet, 4H), 2.35 (m, 8H), 1.25 (t, 6H), 1.05 (m, 12H).

<sup>13</sup>C NMR: δ 141.0, 140.9, 140.9, 139.7, 139.3, 139.2, 138.4, 138.4, 129.4, 129.3, 129.2, 128.0, 127.9, 126.7, 126.6, 28.4, 25.9, 25.8, 25.7, 15.6, 15.5, 15.4, 15.2, 15.2, 15.1.

HRMS: calc. for C<sub>30</sub>H<sub>38</sub> 398.2974, found 398.2973

2,2',5,5'-Tetraethylbiphenyl (9b). Compound 9b was synthesized analogously to 10b from 0.310 g (0.760 mmol) of 11b.

<sup>1</sup>H NMR: δ 7.20 (d, 2H), 7.13 (d, 2H), 6.94 (s, 2H), 2.60 (quartet, 4H), 2.31 (m, 4H), 1.22 (t, 6H), 1.00 (t, 6H)

<sup>13</sup>C NMR: δ 140.9, 139.0, 129.2, 127.9, 126.7, 28.3, 25.8, 15.5, 15.2

HRMS: calc for C<sub>20</sub>H<sub>26</sub> 266.2035, found 266.2011

General procedure for boronic acid synthesis:<sup>40</sup> a) 1,4-Diethyl-2-phenylboronic acid (7b). To a dry 50 mL Schlenk flask containing 0.860 g (35.0 mmol) of dry magnesium metal turnings were added 5.00 g (23.5 mmol) 3b in ~15 mL of THF. This reaction was stirred at reflux for 1 h and then cooled to room temperature. A second flask was prepared containing 8.83 g (46.9 mmol) of triisopropylborate in 60 mL of THF. This solution was cooled in a dry ice/acetone bath and the Grignard reagent was added dropwise to the solution via a cannula. The mixture was allowed to warm to room temperature. After stirring for an additional 2 h, 60 mL of 2N HCl were added and

stirring was continued for 1 h. The mixture was poured into a separatory funnel and the layers were separated. The aqueous layer was extracted with diethylether (3x40 mL), and the combined organic layers were dried over MgSO<sub>4</sub>, filtered and concentrated to afford a white solid suspended in a light yellow oil. This mixture was then dried under vacuum to yield 3.75 g (90%) as a white powder. All boronic acid products were used directly for coupling reactions unless otherwise indicated.

<sup>1</sup>H NMR: δ 8.10 (s, 1H), 7.30 (s, 1H), 7.20 (s, 1H), 3.20 (quartet, 2H), 2.70 (quartet, 2H), 1.30 (t, 3H), 1.20 (t, 3H).

<sup>13</sup>C NMR: δ 143.7, 138.6, 128.3, 100.4, 33.6, 27.8, 15.4, 14.7.

b)1,4-Diethyl-5-(trimethylsilyl)-2-phenylboronic acid (8b). Compound 8b was synthesized from 4.00 g (14.0 mmol) of 6b to yield 3.10 g (88%) as an oily white solid.

<sup>1</sup>H NMR: δ 8.10 (s, 1H), 7.40 (s, 1H), 3.20 (quartet, 2H), 2.80 (quartet, 2H), 1.35 (t, 3H), 1.30 (t, 3H), 0.35 (s, 9H).

<sup>13</sup>C NMR: δ 148.8, 146.4, 143.0, 136.7, 135.4, 129.3, 28.6, 28.5, 17.8, 16.3, 0.3.

c)1,4-Dimethyl-2-phenylboronic acid (7a). Compound 7a was synthesized from 5.00 g (27.0 mmol) of 6a to yield 3.85 g (95%) as a white powder.

<sup>1</sup>H NMR (CD<sub>3</sub>OD): δ 7.05 (m, 3H), 2.25 (d, 6H).

<sup>13</sup>C NMR (CD<sub>3</sub>OD): δ 132.9, 130.6, 130.3, 21.8, 22.0.

d)1,4-Dimethyl-5-(trimethylsilyl)-2-phenylboronic acid (8a). Compound 8a was synthesized from 10.0 g (38.9 mmol) of 6a to yield 8.37 g (97%) as an off-white powder.

<sup>1</sup>**H NMR:** δ 7.95 (s, 1H), 7.37 (s, 1H), 2.75 (s, 3H), 2.50 (s, 3H), 0.30 (s, 9H).

<sup>13</sup>C NMR: δ 143.3, 141.9, 139.8, 138.0, 136.5, 22.6, 22.5, -0.3.

e) 1,4-Dihexyl-5-(trimethylsilyl)-2-phenylboronic acid (8c). Compound 8c was synthesized from 5.62 g (14.2 mmol) of 6c, 0.520 g (21.0 mmol) of magnesium and 12.0 g (56.6 mmol) of trimethylborate. The Grignard reaction was monitored by <sup>1</sup>H NMR and was allowed to reflux for 3 h. After work-up, the crude product was purified by column chromatography (silica gel) using toluene as the solvent to remove side products and then switching to diethyl ether to elute the boronic acid. This reaction yielded 3.40 g (66%) of a colorless oil which solidified upon standing.

<sup>1</sup>H NMR: δ 8.00 (s, 1H), 7.35 (s, 1H), 3.15 (t, 2H), 2.70 (t, 2H), 2.65 (m, 4H), 1.20 – 1.45 (m, 12H), 0.95 (t, 3H), 0.80 (t, 3H), 0.35 (s, 9H)

<sup>13</sup>C NMR: δ 146.9, 145.1, 142.4, 137.1, 136.0, 36.1, 35.2, 33.3, 32.9, 31.9, 29.8, 29.3, 22.7, 14.1, 14.0, 0.4

f) 2,2',5,5'-Tetrahexyl-4-biphenylboronic acid (20c). This compound was synthesized from 7.00 g (12.0 mmol) of 19c. It was purified analogously to 8c to yield 2.26 g (34%).

<sup>1</sup>H NMR: δ 8.20 (s, 1H), 7.00-7.20 (m, 3H), 6.90 (s, 1H), 3.40 (m, 1H), 3.15 (m, 1H), 2.60 (t, 2H), 2.40 (m, 4H), 1.00-1.80 (m, 32H), 0.80 (m, 12H).

General procedure for Pd(PPh<sub>3</sub>)<sub>4</sub>-catalyzed coupling of aryl halides and aryl boronic acids: a) 2,2',2",5,5',5"-Hexamethylterphenyl (10a). This procedure was adapted from Miyaura, et al.<sup>38</sup> To a 50 mL Schlenk flask fitted with a reflux condenser were added

0.500 g (1.89 mmol) of 4a, 0.600 g (4.00 mmol) of 7a, and 1.06 g (10.0 mmol) of Na<sub>2</sub>CO<sub>3</sub>. The flask was purged with argon, and 15 mL of water were added to the flask containing the starting materials. To a second Schlenk flask was added 0.050 g of Pd(PPh<sub>3</sub>)<sub>4</sub> and 30 mL of toluene. The catalyst solution was transferred to the reaction flask via a cannula and the heterogeneous reaction mixture was stirred vigorously at reflux for 24 h. The reaction mixture was cooled to room temperature and transferred to a separatory funnel and the layers were separated. The aqueous layer was extracted with low boiling petroleum ether (3x25mL) and the combined organic layers were dried (MgSO<sub>4</sub>), filtered through a short pad of silica gel/Celite and concentrated to yield an off-white powder. The crude product was recrystallized from ethanol to yield 0.420 g (78%) of a white powder. mp 183-185 °C (lit, 15 mp 182-183 °C)

<sup>1</sup>**H NMR:** δ 7.15 (d ,2H), 7.05 (dd, 2H), 6.98 (d, 2H), 6.95 (d, 2H), 2.33 (s, 6H), 2.06 (s, 3H), 2.05 (s, 3H), 2.01 (s, 6H)

<sup>13</sup>C NMR: δ 141.5, 140.4, 134.8, 132.8, 130.5, 130.1, 129.6, 127.7, 21.0, 19.3

b)2,2',5,5'-Tetramethylbiphenyl (9a). This product was synthesized from 0.700 g (4.70 mmol) of 7a and 0.800 g (4.30 mmol) of 3a. The crude product was isolated as a yellow oil which was crystallized from ethanol to yield 0.340 g (35%) as colorless needles. mp 50.0-50.5 °C (lit.15mp 53-54 °C)

<sup>1</sup>H NMR: δ 7.14 (d, 2H), 7.05 (d, 2H), 6.90 (s, 2H), 2.30 (s, 6H), 2.00 (s, 6H).

<sup>13</sup>C NMR: δ 141.6, 134.8, 132.6, 129.9, 129.6, 127.7, 20.9, 19.3.

c) 4,4'-Bis(trimethylsilyl)-2,2',5,5'-tetramethylbiphenyl (11a). Compound 11a was synthesized from 2.00 g (7.78 mmol) of 6a and 1.90 g (8.56 mmol) of 8a. The crude product was recrystallized from ethanol to yield 2.01 g (66%) as white needles. mp 185-185.5 °C

<sup>1</sup>H NMR: δ 7.30 (s, 2H), 6.90 (s, 2H), 2.40 (s, 6H), 2.00 (s, 6H), 0.35 (s, 18H).

<sup>13</sup>C NMR: δ 142.3, 140.4, 136.7, 135.9, 131.7, 130.6, 22.4, 19.4, 0.0.

HRMS: calc. for C<sub>22</sub>H<sub>34</sub>Si<sub>2</sub> 354.2199, found 354.2195

d) 4,4"-Bis(trimethylsilyl)-2,2',2",5,5',5"-hexamethylterphenyl (12a). Compound 12a was synthesized from 5.55 g (25.0 mmol) of 8a and 3.00 g (11.4 mmol) of 4a. The crude product was purified by washing with ethanol until the washings were colorless to yield 1.95 g (38%) as a white powder. mp 241-243 °C

<sup>1</sup>**H NMR:** δ 7.35 (s, 2H), 6.90 (s, 4H), 2.40 (s, 6H), 2.10 (d, 6H), 2.00 (s, 6H), 0.35 (s, 18H).

<sup>13</sup>C NMR: δ 142.2, 140.4, 140.2, 136.6, 135.9, 132.6, 131.9, 130.9, 130.8, 130.5, 22.4, 19.4, 19.3, 0.0.

**HRMS:** calc. for  $C_{30}H_{42}Si_2$  458.2825, found 458.2792

e) 4-(Trimethylsilyl)-2,2',5,5'-tetramethylbiphenyl: The crude product was synthesized from 10.9 g (42.5 mmol) of 6a and 7.00 g (46.7 mmol) 7a. The product was recrystallized from absolute ethanol to yield 10.9 g (91%) as a white flaky solid. mp 60-61 °C

<sup>1</sup>**H NMR:** δ 7.31 (s, 1H), 7.15 (d, 1H), 7.05 (d, 1H), 6.92 (s, 1H), 6.90 (s, 1H), 2.42 (s, 3H), 2.32 (s, 3H), 2.03 (s, 6H), 0.35 (s, 9H).

<sup>13</sup>C NMR: δ 142.4, 141.4, 140.4, 136.7, 135.8. 134.8, 132.5, 131.8, 130.7, 129.9, 129.6, 127.7, 22.4, 20.9, 19.4, 19.3, 0.0.

HRMS: calc. for C<sub>15</sub>H<sub>26</sub>Si 282.1804, found 282.1804

from 3.00 g (8.52 mmol) of 4c and 3.39 g (9.38 mmol) of 8c. The crude product was run through a short column of silica gel (hexane) to remove traces of catalyst and then distilled under vacuum (bp 249-250 °C @ 610 mtorr) to yield 2.71 g (57%) of a viscous colorless oil.

<sup>1</sup>H NMR: δ 7.29 (s, 1H), 7.15 (d, 1H), 7.03 (d, 1H), 6.92 (broad s, 2H), 2.65 (t, 2H), 2.55 (t, 2H), 2.28 (m, 4H), 0.90-1.60 (m, 44H), 0.34 (s, 9H)

<sup>13</sup>C NMR: δ 145.2, 142.0, 140.9, 139.4, 137.7, 136.7, 136.0, 135.0, 130.1, 129.8, 128.6, 127.1, 35.9, 35.5, 32.9, 32.8, 32.6, 31.9, 31.8, 31.6, 31.5, 31.1, 29.7, 29.3, 29.2, 29.0, 22.7, 22.6, 22.5, 14.1, 0.7

HRMS: calc. for C<sub>39</sub>H<sub>66</sub>Si 562.4934, found 562.4930

g) 4-(Trimethylsilyl)-2,2',2",5,5',5"-hexamethylterphenyl (21a): This compound was synthesized from 5.00 g (17.3 mmol) of 19a and 4.91 g (19.0 mmol) of 8a. The crude product was recrystallized from absolute ethanol to yield 6.41 g (96%) as a white powder. A small portion was recrystallized for analysis. mp. 180-180.5 °C.

<sup>1</sup>H NMR: δ 7.35 (s, 1H), 7.17 (d, 1H), 7.09 (d, 1H), 7.00 (m, 4H), 2.45 (s, 3H), 2.35 (s, 3H), 2.05 (m, 12H), 0.39 (s, 9H)

<sup>13</sup>C NMR: δ 140.4, 135.9, 132.6, 132.5, 130.8, 130.5, 130.1, 130.0, 129.6, 127.7, 22.4, 20.9, 19.4, 19.3, 0.0

HRMS: calc. for C<sub>27</sub>H<sub>34</sub>Si 386.2430, found 386.2445

h) 4-(Trimethylsilyl)-2,2',2",5,5',5"-hexahexylterphenyl (21c). Compound 21c was synthesized from 1.00 g (1.76 mmol) of 19c and 0.70 g (1.93 mmol) of 8c. The crude product was purified by first running it through a short column of silica gel/hexane and then recrystallizing from ethanol to yield 0.56 g (39%).

<sup>1</sup>H NMR: δ 7.30 (s, 1H), 7.18 (d, 1H), 7.09 (d, 1H), 7.00 (m, 4H), 2.70 (t, 2H), 2.60 (t, 2H), 2.35 (m, 8H), 1.00 – 1.50 (m, 48H), 0.80 (m, 18H), 0.35 (s, 9H)

<sup>13</sup>C NMR: δ 145.3, 142.0, 141.8, 141.1, 140.9, 139.8, 139.6, 139.5, 138.0, 137.1, 137.0, 136.9, 136.0, 135.9, 135.1, 135.0, 130.3, 130.1, 130.0, 128.6, 128.5, 127.0, 36.0, 35.9, 35.6, 35.5, 33.2, 33.0, 32.8, 32.7, 32.6, 32.5, 31.9, 31.8, 31.7, 31.6, 31.4, 31.3, 31.2, 31.1, 31.0, 30.8, 30.7, 29.8, 29.7, 29.5, 29.4, 29.3, 29.2, 29.1, 22.6, 15.3, 14.1, 14.0, 0.7

HRMS: calc. for C<sub>57</sub>H<sub>94</sub>Si 806.7125, found 806.7131

2,2',2",5,5',5"-Hexahexylterphenyl (10c): This compound was synthesized according to Rehahn, et al. 7,8 mp 42-43 °C (lit. 7 mp 47 °C)

<sup>1</sup>H NMR: δ 6.90-7.20 (complex aromatics, 8H), 2.60 (2 triplets, 4H), 2.30 (m, 8H), 1.60 (quartet, 4H), 1.00-1.50 (m, 44H), 0.80 (m, 18H).

General procedure for triethoxysilyl-terminated oligomers: 111 a)2-(triethoxysilyl)-1.4dimethylbenzene (23a). To a 250 mL three-necked round bottom flask fitted with a condenser and an addition funnel was added 1.97 g (81.1 mmol) of magnesium, 56.3 g (270 mmol) of tetraethylorthosilane (TEOS) and 75 mL of THF. A small iodine crystal was added and the reaction mixture was heated to just below reflux temperature. The reaction was cooled slightly and 10.00 g (54.05 mmol) of 2-bromo-p-xylene in 25 mL of THF was added dropwise. Upon completion of the addition the reaction was heated at reflux for 1 h, and then cooled to room temperature. The condenser and addition funnel were removed and a distillation apparatus was attached. The THF was distilled under argon from the reaction mixture at atmospheric pressure. To the remaining residue were added 100 mL of freshly distilled hexanes (from CaH<sub>2</sub>) to precipitate magnesium salts. This slurry was filtered under argon through a glass frit. The hexane was evaporated in vacuo and the remaining liquid was fractionally distilled under vacuum. The product was collected at 156°C @ 33 torr to yield 10.34 g (71%) as a clear colorless oil and was stored in a dessicator.

<sup>1</sup>H NMR: δ 7.51 (s, 1H), 7.15 (d, 1H), 7.07 (d, 1H), 3.85 (quartet, 6H), 2.45 (s, 3H), 2.30 (s, 3H), 1.25 (t, 9H)

<sup>13</sup>C NMR: δ 141.3, 137.0, 133.7, 131.2, 129.6, 129.4, 58.4, 21.8, 20.9, 18.1

<sup>29</sup>Si NMR: δ -56.4

b) 4-(triethoxysilyl)-2,2'-5,5'-tetramethylbiphenyl (24a). Compound 24a was synthesized from 2.00 g (6.92 mmol) of 19a. The product was distilled (153-154 °C @ 220 mtorr) to yield 1.89 g (74%) as a clear colorless oil.

<sup>1</sup>H NMR: δ 7.62 (s, 1H), 7.18 (d, 1H), 7.10 (d, 1H), 6.95 (s, 2H), 3.95 (quartet, 6H), 2.52 (s, 3H), 2.38 (s, 3H), 2.07 (2 singlets, 6H), 1.32 (t, 9H)

<sup>13</sup>C NMR: δ 143.8, 141.3, 137.8, 134.7, 132.4, 131.7, 130.6, 129.9, 129.6, 127.7, 58.5, 21.8, 20.8, 19.2, 18.2

<sup>29</sup>Si NMR: δ -56.37

c) 4-(triethoxysilyl)-2,2'2",-5,5',5"-hexamethylterphenyl (25a). Compound 25a was synthesized from 1.00 g (2.54 mmol) of 22a. The product was distilled (165-170 °C @ 200 mtorr) to yield 0.64 g (52%) as a white solid.

<sup>1</sup>H NMR: δ 7.60 (s, 1H), 7.15 (d, 2H), 7.08 (d, 2H), 7.00 (m, 1H), 3.95 (quartet, 6H), 2.50 (s, 3H), 2.35 (s, 6H), 2.10 (m, 9H), 1.30 (t, 9H)

<sup>13</sup>C NMR: δ 143.8, 141.5, 141.4, 140.5, 140.4, 140.3, 140.2, 137.9, 134.8, 132.8, 132.7, 132.5, 132.4, 131.9, 130.9, 130.8, 130.6, 130.3, 130.5, 130.1, 129.6, 127.7 58.6, 21.9, 20.9, 19.4, 19.3, 18.2.

APPENDIX I: <sup>1</sup>H NMR spectra of selected compounds

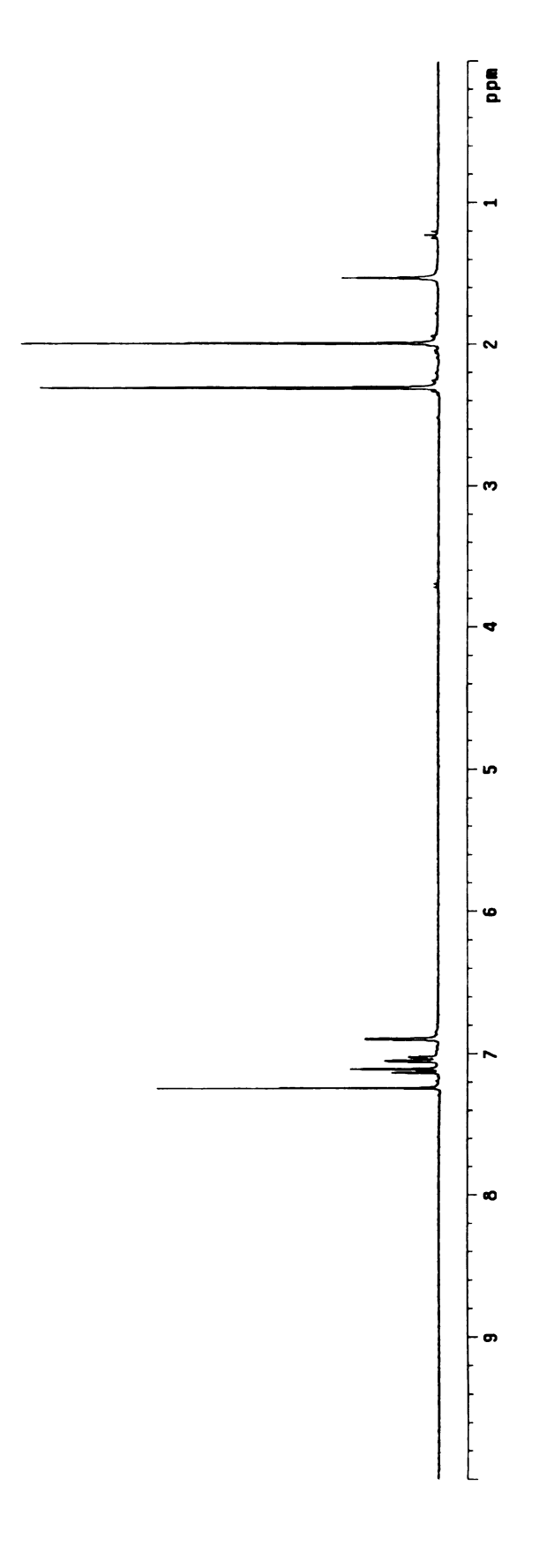


Figure 82: <sup>1</sup>H NMR spectrum of TMB

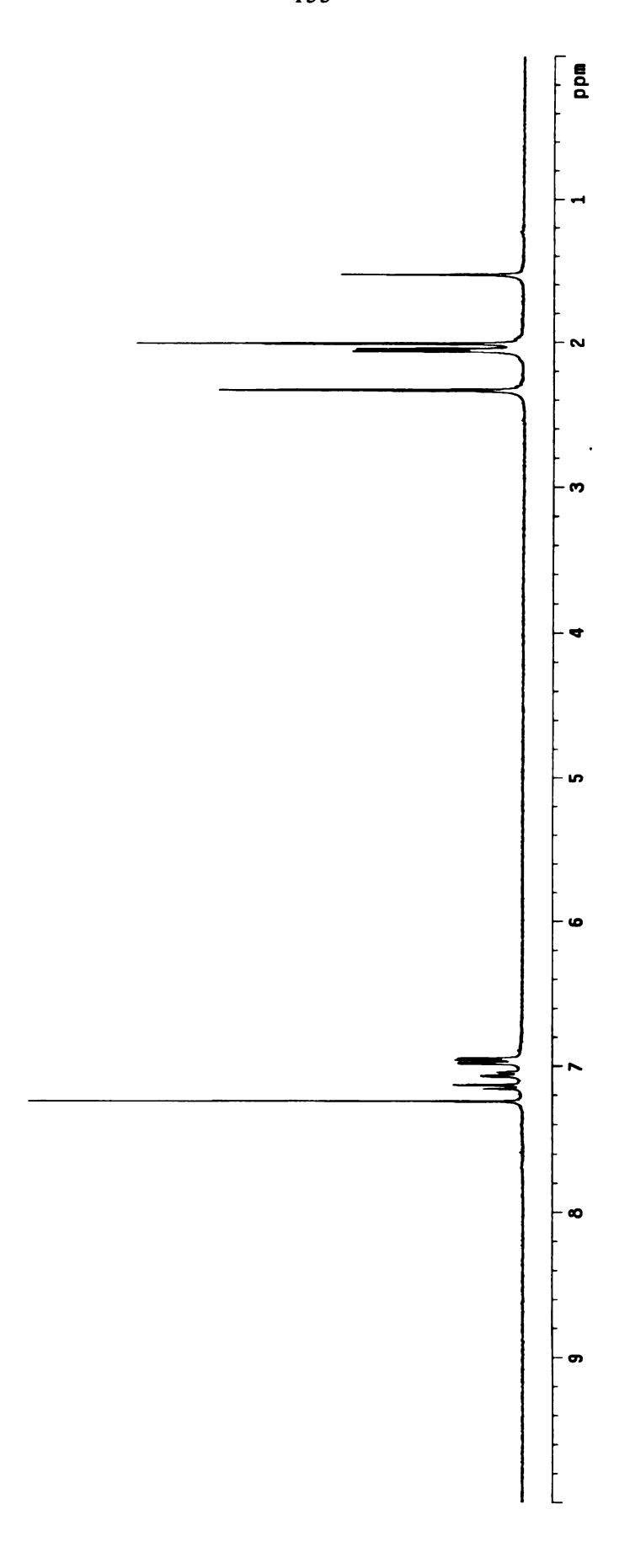


Figure 83: <sup>1</sup>H NMR spectrum of HMT

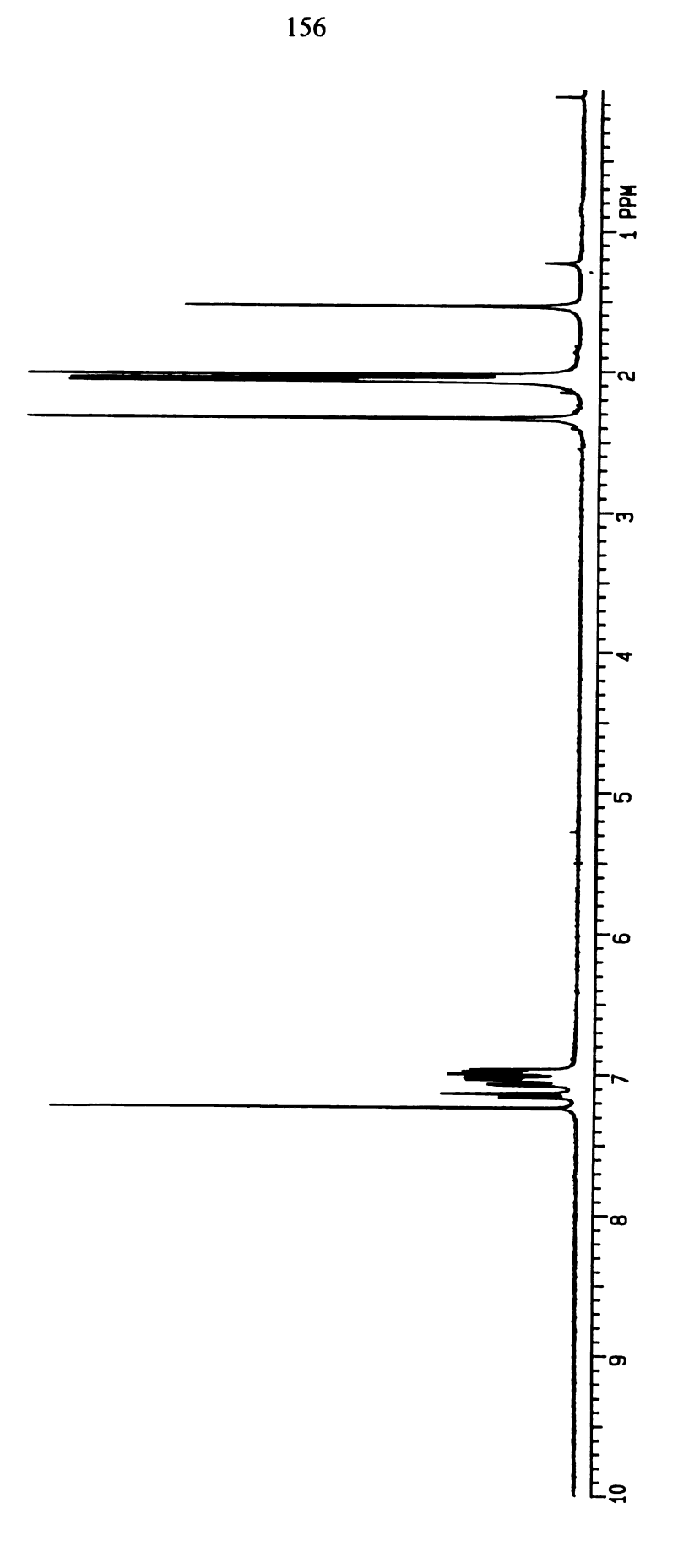


Figure 84: <sup>1</sup>H NMR spectrum of OMQ

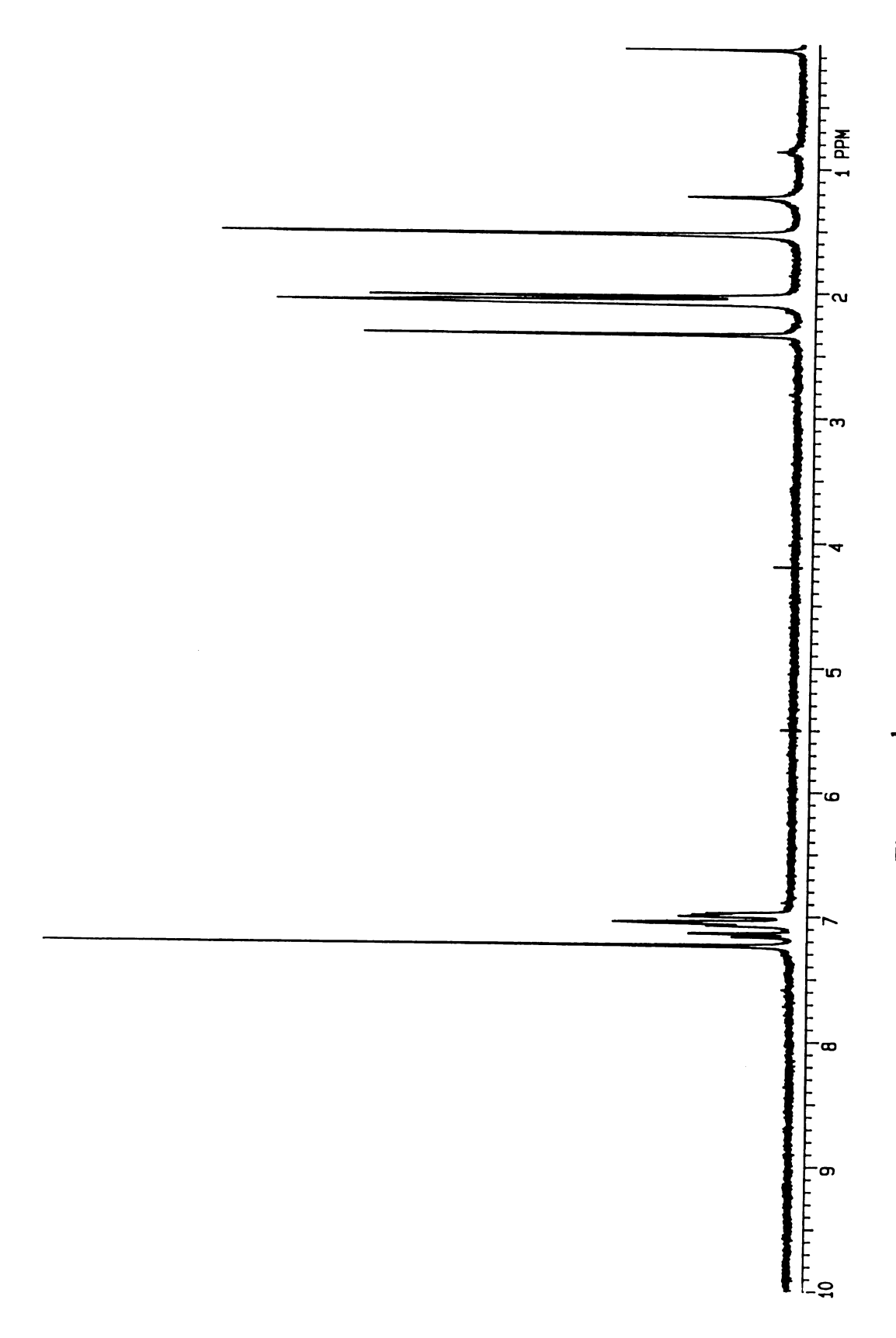


Figure 85: <sup>1</sup>H NMR spectrum of DMQ

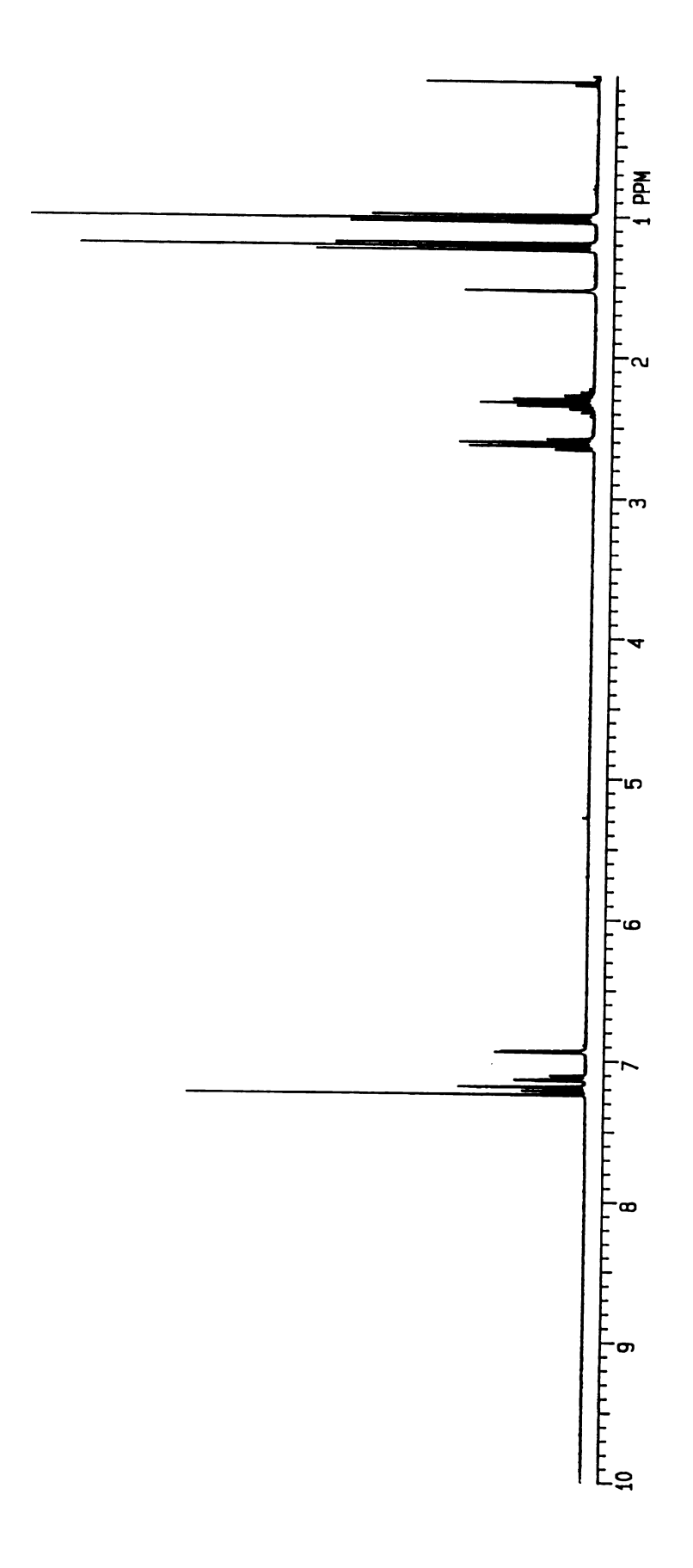


Figure 86: <sup>1</sup>H NMR spectrum of TEB

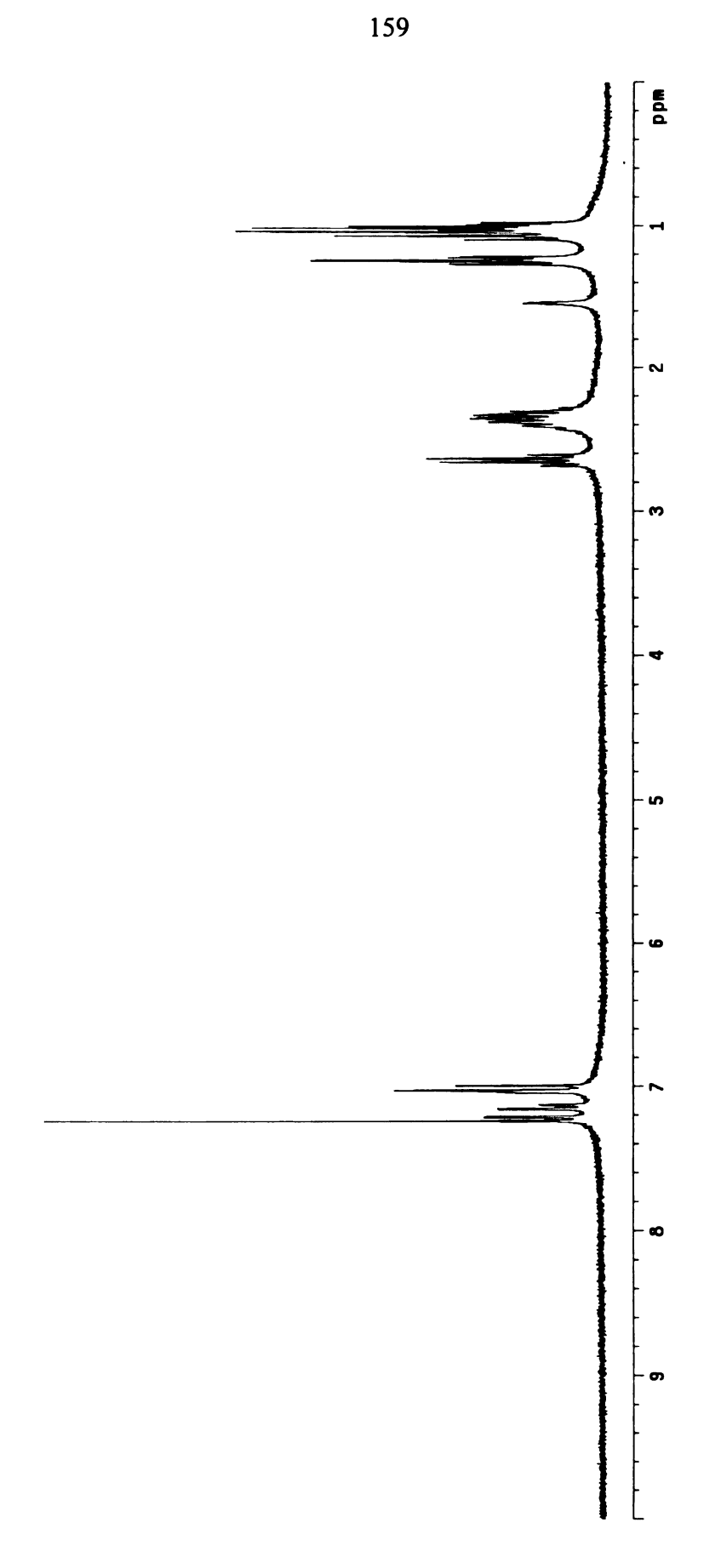


Figure 87: <sup>1</sup>H NMR spectrum of HET

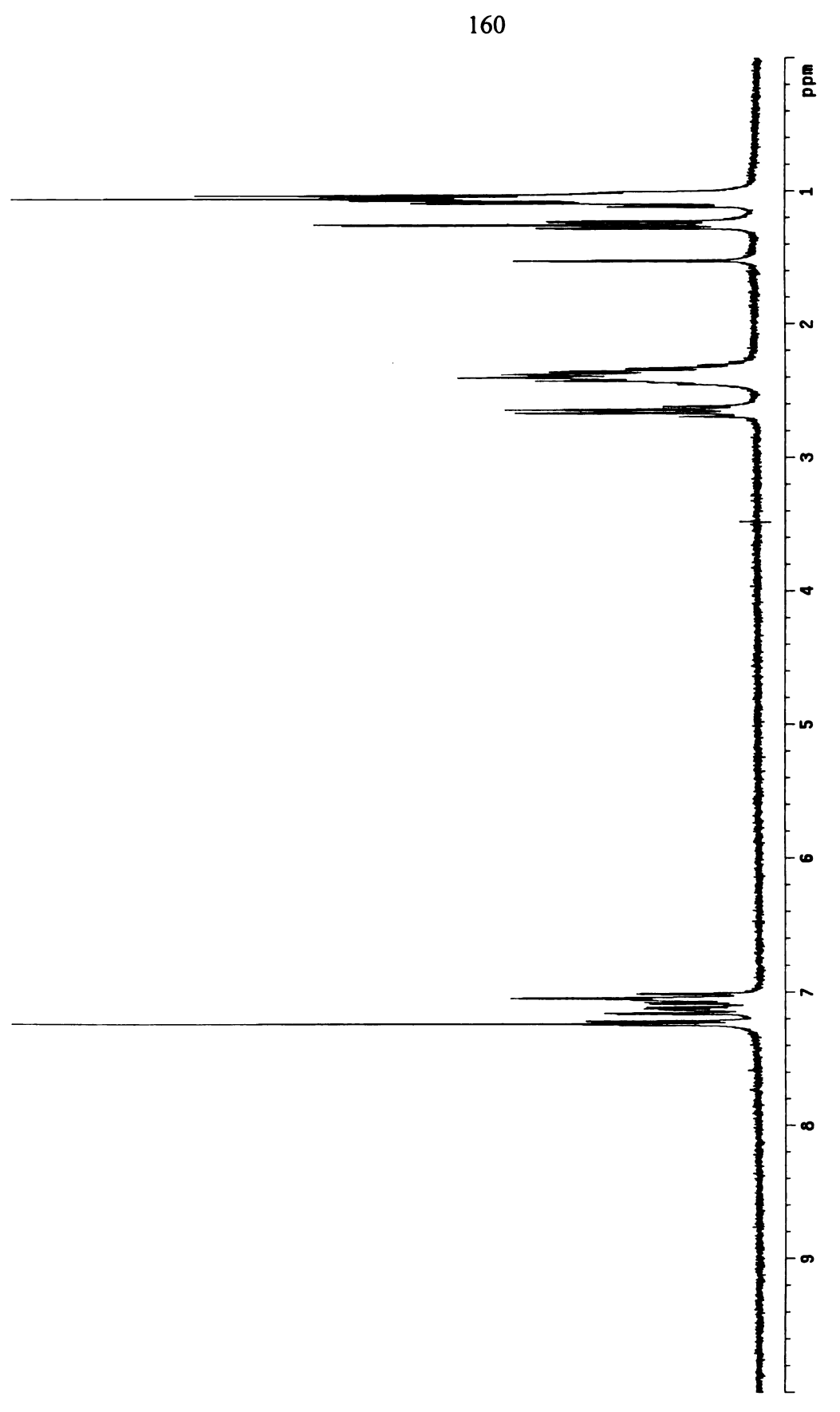


Figure 88: <sup>1</sup>H NMR spectrum of OEQ

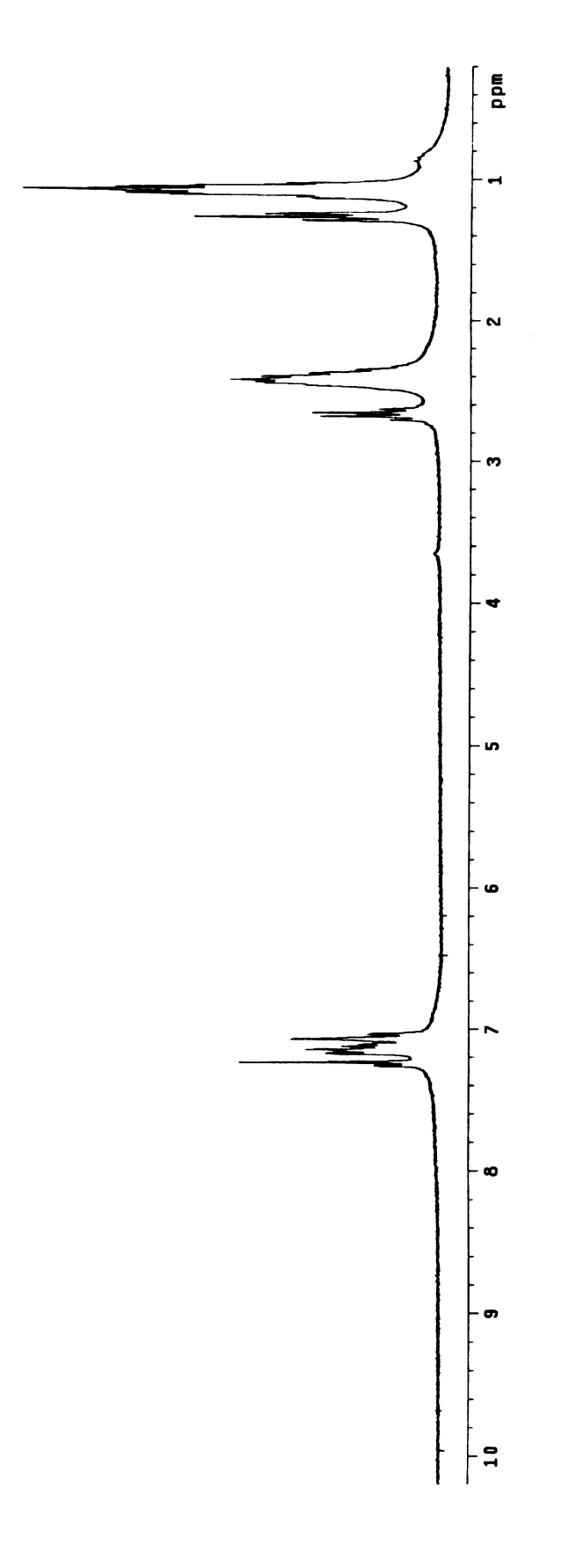


Figure 89: <sup>1</sup>H NMR spectrum of DEQ

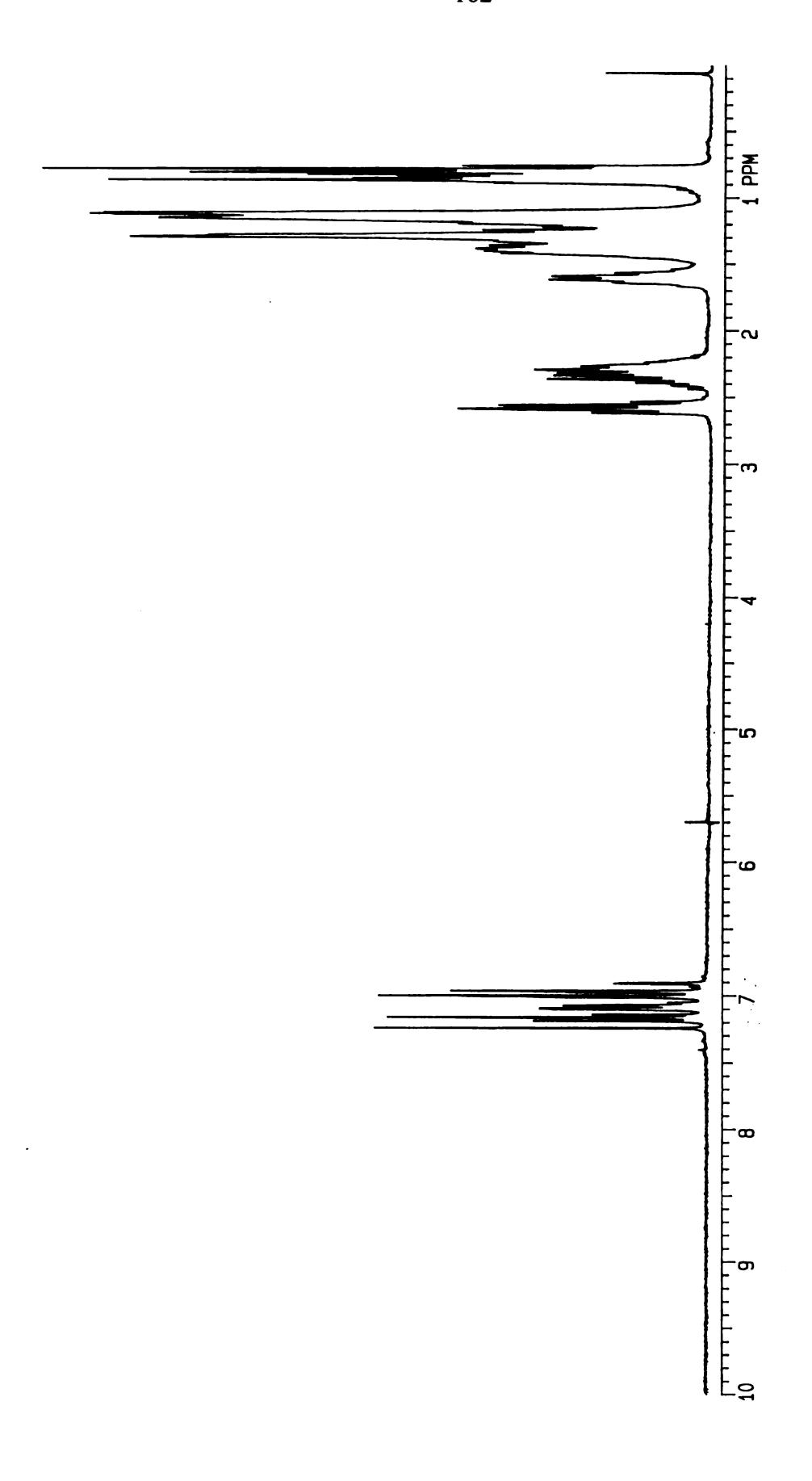
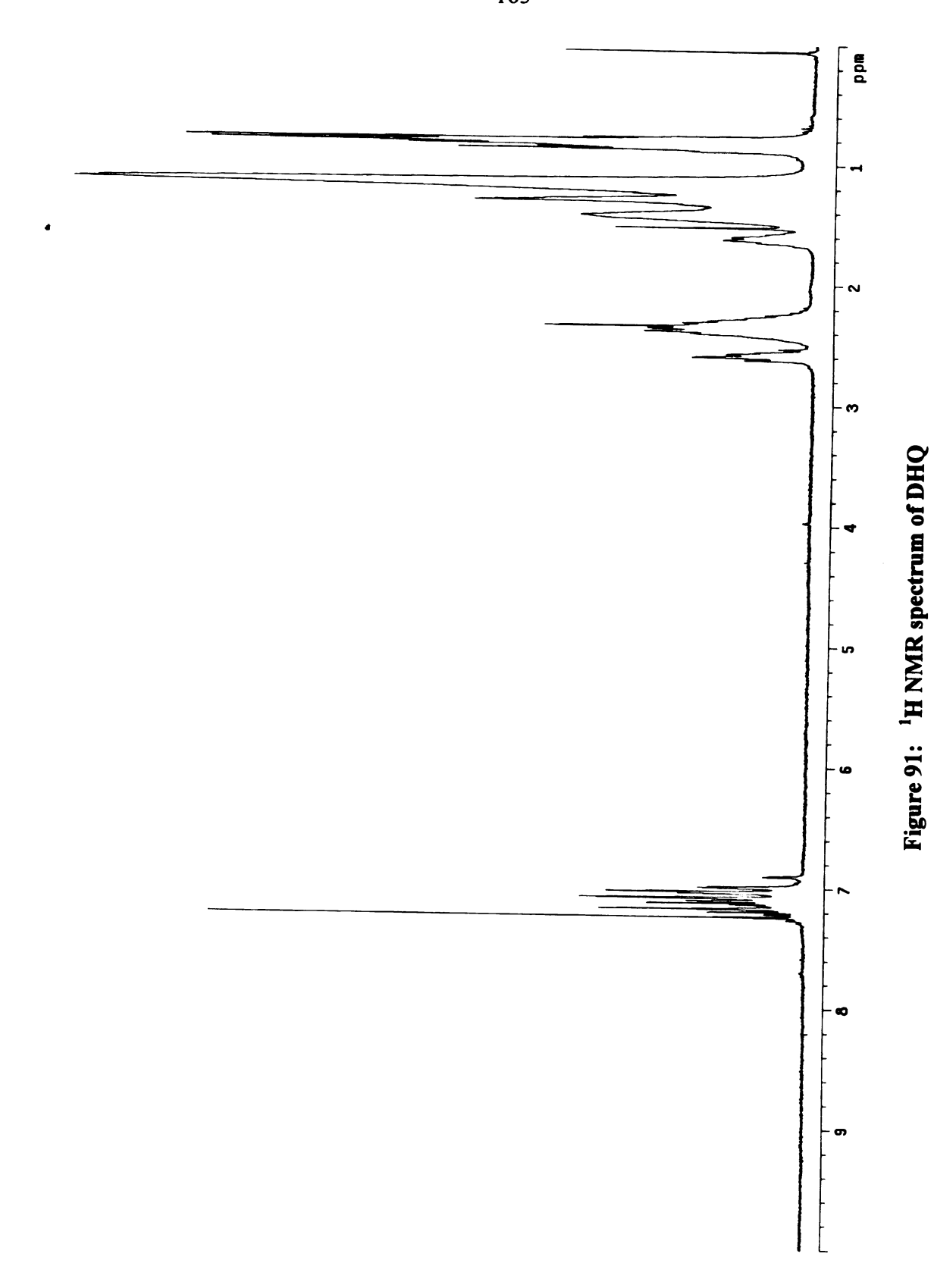


Figure 90: <sup>1</sup>H NMR spectrum of HHT



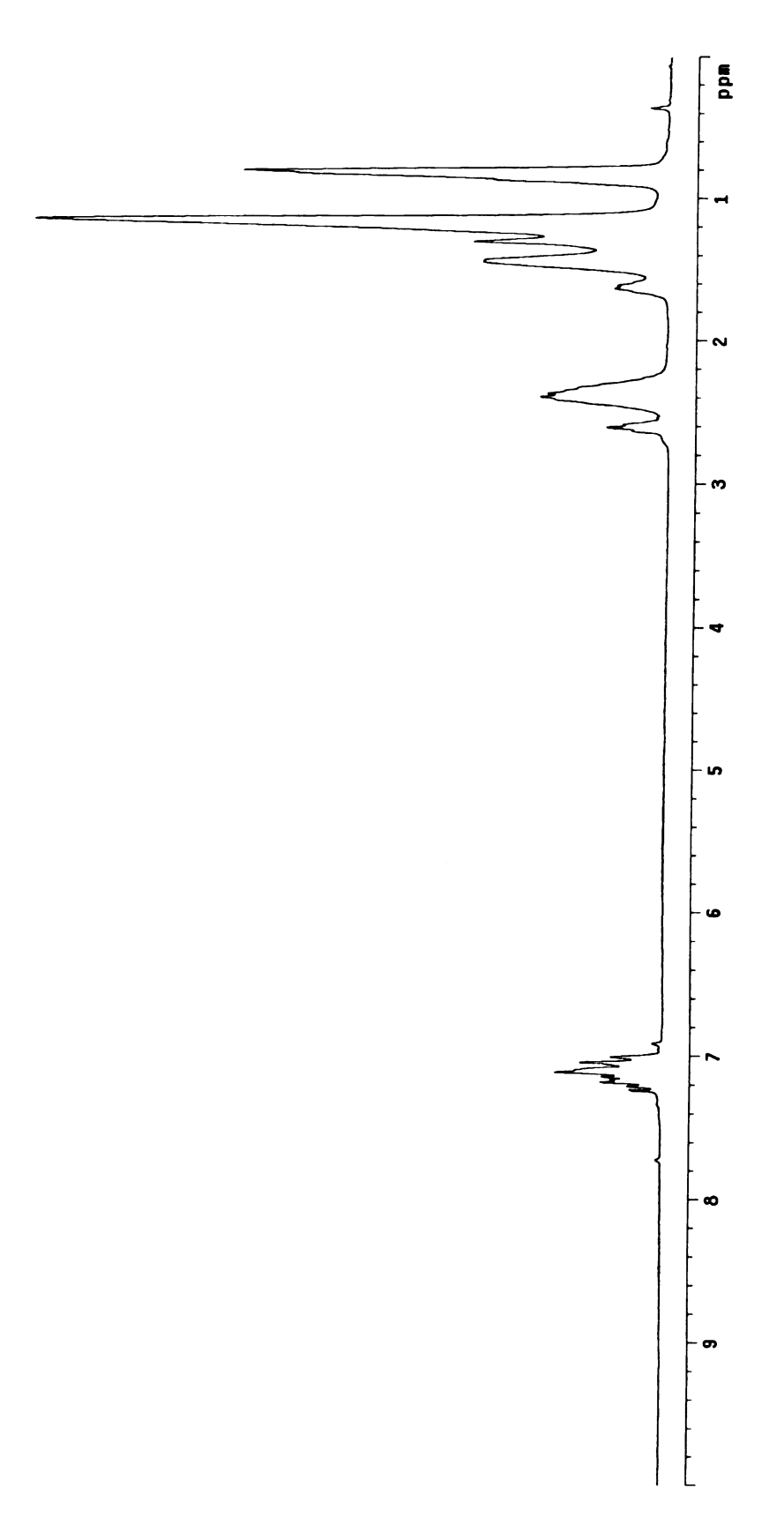


Figure 92: <sup>1</sup>H NMR spectrum of THS

APPENDIX II: Numbering of compounds

1

 $R = CH_3$ 2  $R = CH_2CH_3$ 

 $R = CH_3$ 3a  $R = CH_2CH_3$ 3b

4a 4b

 $\mathbf{R} = \mathbf{C_6}\mathbf{H_{13}}$ 

**3c** 

 $\mathbf{R} = \mathbf{C_6}\mathbf{H_{13}}$ 

4c

Si(CH<sub>3</sub>)<sub>3</sub> Br

B(OH)<sub>2</sub>

 $R = CH_2CH_3$ 5b

 $R = CH_3$ 

6a

 $R = CH_3$ 

7a 7b

 $\mathbf{R} = \mathbf{C_6}\mathbf{H_{13}}$ **5c**   $R = CH_2CH_3$  $\mathbf{R} = \mathbf{C_6}\mathbf{H_{13}}$ 

6b 6c

 $R = CH_2CH_3$  $R = C_6 H_{13}$ 7c

 $R = CH_3$ 

8a 8b  $R = CH_3$  $R = CH_2CH_3$  9a 9b

 $R = CH_3$  $R = CH_2CH_3$  10a

 $R = CH_2CH_3$  $\mathbf{R} = \mathbf{C_6}\mathbf{H_{13}}$ 

8c

10b  $\mathbf{R} = \mathbf{C_6}\mathbf{H_{13}}$ 10c

$$- \left\{ \begin{array}{c} R \\ A \end{array} \right\}_{4}$$

$$- \left\{ \right\}_{5}$$

 $R = CH_3$ 

15a

 $R = CH_3$  $R = CH_2CH_3$ 

16a 16b  $R = C_6 H_{13}$ 

17c

 $R = CH_2CH_3$ 15b  $\mathbf{R} = \mathbf{C_6}\mathbf{H_{13}}$ 15c

 $\mathbf{R} = \mathbf{C_6}\mathbf{H_{13}}$ 

16c

$$(CH_3)_3Si$$
 $R$ 
 $R$ 
 $Si(CH_3)_3$ 

$$R = CH_3$$
 11a  
 $R = CH_2CH_3$  11b

$R = CH_3$	12a
$R = CH_2CH_3$	12b
$\mathbf{R} = \mathbf{C_6}\mathbf{H_{13}}$	12c

$R = CH_{3}, X = Si(CH_{3})_{3}$	18a
$R = C_6H_{13}, X = Si(CH_3)_3$	18c
$R = CH_3$ , $X = Si(OCH_2CH_3)_3$	24a
$R = CH_3$ , $X = Br$	19a
$R = C_6H_{13}, X = Br$	19c
$R = C_6H_{13}, X = B(OH)_2$	<b>20c</b>

 $X = Si(CH_3)_3$  21a  $X = Si(OCH_2CH_3)_3$  25a X = Br 22a

23a

## **BIBLIOGRAPHY**

- 1)Gale, D. M. J. Appl. Polym. Sci. 1978, 22, 1971-1976.
- 2) Elsenbaumer, R. L.; Jen, K. Y.; Oboodi, R. Synth. Met. 1986, 15, 169-174.
- 3) Speight, J. G.; Kovacic, P.; Koch, F. W. J. Macromol. Sci. Revs. Macromol. Chem. 1971, C5, 295-386.
- 4)Tour, J. M. Adv. Mater. 1994, 6, 190-198.
- 5)Gin, D. L.; Conticello, V. P.; Grubbs, R. H. J. Am. Chem. Soc. 1994, 116, 10507-10519.
- 6) Chaturvedi, V.; Tanaka, S.; Kaeriyama, K. Macromolecules 1993, 26, 2607-2611.
- 7) Rehahn, M.; Schluter, A.-D.; Wegner, G.; Feast, W. J. Polymer 1989, 30, 1054-1059.
- 8) Rehahn, M.; Schluter, A.-D.; Wegner, G.; Feast, W. J. Polymer 1989, 30, 1060-1062.
- 9) Noren, G. K.; Stille, J. K. Macromol. Rev. 1971, 5, 385-430.
- 10)Kovacic, P.; Jones, M. B. Chem. Rev. 1987, 87, 357-379.
- 11)Bringmann, G.; Walter, R.; Weirich, R. Agnew. Chem., Int. Ed. Engl. 1990, 29, 977-991.
- 12) Fanta, P. E. Synthesis 1974, 9-21.
- 13) Sainsbury, M. Tetrahedron 1980, 36, 3327-3359.

- 14) Takahashi, M.; Koruda, T.; Ogibu, T.; Ohmizu, H.; Kondo, K.; Iwasaki, T.
- Tetrahedron Lett. 1991, 32, 6919-6922.
- 15) Wirth, H. O.; Herrmann, F. U.; Hern, W. Makromol. Chem. 1964, 80, 120-140.
- 16) Tour, J. M.; Stephens, E. B. J. Am. Chem. Soc. 1991, 113, 2309-2311.
- 17) Tour, J. M.; Stephens, E. B.; Davis, J. F. Macromolecules 1992, 25, 499-500.
- 18) Stephens, E. B.; Kinsey, K. E.; Davis, J. F.; Tour, J. M. *Macromolecules* 1993, 26, 3519-3532.
- 19)Semmelhack, M. F.; Helquist, P. M.; Jones, L. D. J. Am. Chem. Soc. 1971, 93, 5908-5910.
- 20) Yamamoto, T. H., Y.; Yamamoto, A. Bull. Chem. Soc. Jpn. 1978, 51, 2091-2097.
- 21) Zhu, L.; Wehmeyer, R. M.; Rieke, R. D. J. Org. Chem. 1991, 56, 1445-1453.
- 22) Chen, T.-A.; O'Brien, R. A.; Rieke, R. D. Macromolecules 1993, 26, 3462-3463.
- 23) Jutand, A.; Mosleh, A. J. Org. Chem. 1997, 62, 261-274.
- 24)Iyoda, M.; Otuska, H.; Sato, K.; Nisato, N.; Oda, M. Bull. Chem. Soc. Jpn. 1990, 63, 80-87.
- 25)Stille, J. K. Agnew. Chem. Int. Ed. Engl. 1986, 25, 508-524.
- 26) Bumagin, N. A.; Bumagina, I. G.; Beletskaya, I. P. Dokl. Chem. 1984, 274, 39-42.
- 27) Scott, W. J.; Stille, J. K. J. Am. Chem. Soc. 1986, 108, 3033-3040.
- 28) Echavarren, A. M.; Stille, J. K. J. Am. Chem. Soc. 1987, 109, 5478-5486.
- 29)Saa, J. M.; Martorell, G. J. Org. Chem. 1993, 58, 1963-1966.
- 30)Qian, X.; Pena, M. Macromolecules 1995, 28, 4415-4420.
- 31)Bao, Z.; Chan, W. K.; Yu, L. J. Am. Chem. Soc. 1995, 117, 12426-12435.
- 32) Mitchell, T. N. Synthesis 1992, 803-815.

- 33)Larhed, M.; Hoshino, M.; Hadida, S.; Curran, D. P.; Hallberg, A. J. Org. Chem. 1997, 62, 5583-5587.
- 34) Forman, F. W.; Sucholeiki, I. J. Org. Chem. 1995, 60, 523-528.
- 35) Miyaura, N.; Yamada, K.; Suginome, H.; Suzuki, A. J. Am. Chem. Soc. 1985, 107, 972-980.
- 36) Miyaura, N.; Suzuki, A. Chem. Rev. 1995, 95, 2457-2483.
- 37) Martin, A. R.; Yang, Y. Acta Chem. Scand. 1993, 47, 221-230.
- 38) Miyaura, N.; Yanagi, T.; Suzuki, A. Syn. Comm. 1981, 11, 513-519.
- 39) Watanabe, T.; Miyaura, N.; Suzuki, A. Synlett 1992, 207-210.
- 40) Thompson, W. J.; Gaudino, J. J. Org. Chem. 1984, 49, 5237-5243.
- 41) Moreno-Manas, M.; Perez, M.; Pleixats, R. J. Org. Chem. 1996, 61, 2346-2351.
- 42) Nielsen, D. R.; McEwen, W. E. J. Am. Chem. Soc. 1957, 79, 3081-3084.
- 43) Wakefield, B. J. Organomet. Chem. Rev. 1966, 1, 131-156.
- 44) Washburn, R. M.; Levens, E.; Albright, C. F.; Billig, F. A.; Cernak, E. S. Adv. Chem. Ser. 1959, 23, 102-128.
- 45) Coutts, I. G. C.; Goldschmid, H. R.; Musgrave, O. C. J. Chem. Soc. C 1970, 488-493.
- 46) Suzuki, A. Acc. Chem. Res. 1982, 15, 178-184.
- 47) Heaney, H. Organomet. Chem. Rev. 1966, 1, 27-42.
- 48) Gronowitz, S.; Bobosik, V.; Lawitz, K. Chem. Scripta 1984, 23, 120.
- 49) Gronowitz, S.; Honfeldt, A.-B.; Yang, Y. Chem. Scripta 1988, 28, 281-283.
- 50) Wallow, T. I.; Novak, B. M. J. Org. Chem. 1994, 59, 5034-5037.
- 51) Tour, J. M. Chem. Rev. 1996, 96, 537-553.

- 52) Wautelet, P.; Moroni, M.; Oswald, L.; Le Moigne, J.; Pham, A.; Bigot, J.-Y.; Luzzati,
- S. Macromolecules 1996, 29, 446-455.
- 53) Belletete, M.; Mazerolle, L.; Derosiers, N.; Leclerc, M.; Durocher, G.

Macromolecules 1995, 28, 8587-8597.

- 54)Schumm, J. S.; Jones, L.; Pearson, D. L.; Hara, R.; Tour, J. M. *Polym. Prepr.* 1994, 35, 687-688.
- 55)Schumm, J. S.; Pearson, D. L.; Tour, J. M. Agnew. Chem. Int. Ed. Engl. 1994, 33, 1360-1363.
- 56)Bredas, J. L.; Heeger, A. J. Chem. Phys. Lett. 1994, 217, 507-512.
- 57) Grem, G.; Leditzky, G.; Ullrich, B.; Leising, G. Adv. Mater. 1992, 4, 36-37.
- 58) Bumm, L. A.; Arnole, J. J.; Cygan, M. T.; Dunbar, T. D.; Burgin, T. P.; Jones II, L.;
- Allara, D. L.; Tour, J. M.; Weiss, P. S. Science 1996, 271, 1705-1707.
- 59) Dodabalapur, A.; Torsi, L.; Katz, H. E. Science 1995, 269, 1560-1562.
- 60) Andersson, M. R.; Berggren, M.; Inganas, O.; Gustafsson, G.; Gustafsson-Carlberg, J.
- C.; Selse, D.; Hjertberg, T.; Wennerstrom, O. Macromolecules 1995, 28, 7525-7529.
- 61) Meerholz, K.; Gregorius, H.; Mullen, K.; Heinze, J. Adv. Mater. 1994, 6, 671-674.
- 62) Nakayama, J.; Konishi, T.; Hoshino, M. Heterocycles 1988, 27, 1731-1754.
- 63) Fichou, D.; Horowitz, G.; Nishikitani, Y.; Garnier, F. Chemtronics 1988, 3, 176.
- 64) Garnier, F.; Horowitz, G.; Fichou, D. Synth. Met. 1989, 28, C705-C714.
- 65)Bauerle, P. Adv. Mater. 1993, 5, 879-886.
- 66)Becker, R. S. Theory and Interpretation of Fluorescence and Phosphorescence; Wiley Interscience: New York, 1969.

- 67) Harris, D. C.; Bertolucci, M. D. Symmetry and Spectroscopy: An Introduction to Vibrational and Electronic Spectroscopy; Dover Publications, Inc.: Mineola, N. Y., 1989.
- 68) Leising, G.; Pilcher, K.; Stelzer, F. Electronic Properties of Conjugated Polymers III; Springer: Heidelberg, 1989.
- 69) Nijegorodov, N. I.; Downey, W. S. J. Phys. Chem. 1994, 98, 5639-5643.
- 70) Furukawa, Y. J. Phys. Chem. 1996, 100, 15644-15653.
- 71)Bredas, J. L.; Silbey, R.; Boudreaux, D. S.; Chance, R. R. J. Am. Chem. Soc. 1983, 105, 6555-6559.
- 72) Ambrosch-Draxl, C.; Majewski, J. A.; Vogl, P.; Leising, G. *Phys. Rev. B* 1995, 51, 9668-9675.
- 73) Ehrendorfer, C.; Karpfen, A. J. Phys. Chem. 1995, 99, 10196-10200.
- 74) Silverstein, R. M.; Bassler, G. C.; Morrill, T. C. Spectrometric Identification of Organic Compounds; 5th ed.; John Wiley & Sons, Inc.: New York, 1991.
- 75)Gillam, A. E.; Hey, D. H. J. Chem. Soc. 1939, 1170-1177.
- 76)Grem, G.; Leising, G. Synth. Met. 1993, 55-57, 4105-4110.
- 77) Rehahn, M.; Schluer, A.-D.; Wegner, G. Makromol. Chem. 1990, 191, 1991-2003.
- 78) Witteler, H.; Leiser, G.; Wegner, G.; Schulze, M. *Makromol. Chem., Rapid Commun.* 1993, 14, 471-480.
- 79) Tieke, B.; Bubeck, C.; Leiser, G. Makromol. Chem., Rapid Commun. 1982, 3, 261.
- 80)Gutowsky, H. S.; Holm, C. H. J. Chem. Phys. 1956, 25, 1228-1234.
- 81) Sandstrom, J. Dynamic NMR Spectroscopy; Academic Press: New York, 1982.
- 82) Meyer, W. L.; Meyer, R. B. J. Am. Chem. Soc. 1963, 85, 2170-2171.
- 83)Oki, M.; Yamamoto, G. Bull. Chem. Soc. Jpn. 1971, 44, 266-270.

- 84)Bott, G.; Field, L. D.; Sternhell, S. J. Am. Chem. Soc. 1980, 102, 5618-5626.
- 85)Kankare, J.; Lukkari, J.; Pasanen, P.; Sillanpaa, R.; Laine, H.; Harmaa, K.

Macromolecules 1994, 27, 4327-4334.

- 86) Dewitt, L.; Blanchard, G. J.; LeGoff, E.; Benz, M.; Liao, J. H.; Kanatzidis, M. G. J. Am. Chem. Soc. 1993, 115, 12158-12164.
- 87) Horne, J. C.; Blanchard, G. J.; LeGoff, E. J. Am. Chem. Soc. 1995, 117, 9551-9558.
- 88) Coleman, R. S.; Grant, E. B. J. Am. Chem. Soc. 1995, 117, 10889-10904.
- 89)Belohradsky, M.; Budesinsky, M.; Gunterova, J.; Hodacova, J.; Holy, P.; Zavada, J.;

Cisarova, I.; Podlaha, J. J. Org. Chem. 1996, 61, 1205-1210.

- 90) Charlton, J. L.; Oleschuk, C. J.; Chee, G.-L. J. Org. Chem. 1996, 61, 3452-3457.
- 91) Kranz, M.; Clark, T.; Schleyer, P. v. R. J. Org. Chem. 1993, 58, 3317-3325.
- 92)Cooke, A. S.; Harris, M. M. J. Chem. Soc. C 1963, 2365-2373.
- 93) Colter, A. K.; Clemens, L. M. J. Phys. Chem. 1964, 68, 651.
- 94) Solladie, G.; Hugele, P.; Bartsch, R.; Skoulios, A. Agnew. Chem. Int. Ed. Engl. 1996, 35, 1533-1535.
- 95)Hu, Q.-S.; Vitharana, D.; Liu, G.; Jain, V.; Pu, L. *Macromolecules* 1996, 29, 5075-5082.
- 96)Hu, Q.-S.; Vitharana, D.; Liu, G.; Jain, V.; Wagaman, M. W.; Zhang, L.; Lee, T.; Pu, L. Macromolecules 1996, 29, 1082-1084.
- 97) Mallory, F. B.; Butler, K. E.; Evans, A. C.; Brondyke, E. J.; Mallory, C. W.; Yang, C.; Ellenstein, A. J. Am. Chem. Soc. 1997, 119, 2119-2124.
- 98) Heitz, W. Chem. Ztg. 1986, 110, 385-393.

- 99)McCarthy, T. F.; Witteler, H.; Pakula, T.; Wegner, G. *Macromolecules* **1995**, *28*, 8350-8362.
- 100)Liess, P.; Hensel, V.; Schluter, A.-D. Liebigs Ann. 1996, 1037-1040.
- 101) Buckles, R. E.; Wheeler, N. G. Org. Syn. Coll. 1963, 4, 256-258.
- 102) Walker, K. A.; Markoski, L. J.; Moore, J. S. Synthesis 1992, 1265-1268.
- 103) Jacob, L. A.; Chen, B.-L.; Stec, D. Synthesis 1993, 611-614.
- 104)Bennetau, B.; Krempp, M.; Dunogues, J.; Ratton, S. *Tetrahedron* 1990, 46, 8131-8142.
- 105)Rehahn, M.; Schluter, A.-D.; Feast, W. J. Synthesis 1988, 386-388.
- 106)Grimme, J.; Kreyenschmidt, M.; Uckert, F.; Mullen, K.; Scherf, U. *Adv. Mater.*1995, 7, 292-295.
- 107)Khanna, R. K.; Jiang, Y. M.; Srinivas, B.; Smithhart, C. B.; Wertz, D. L. Chem. Mater. 1993, 5, 1792-1798.
- 108) Wagner, P. J. J. Am. Chem. Soc. 1967, 89, 2820-2825.
- 109) Ulman, A. Chem. Rev. 1996, 96, 1533-1554.
- 110)Ulman, A. An Introduction to Ultrathin Organic Films; Academic Press: Boston, 1991.
- 111) Shea, K. J.; Loy, D. A.; Webster, O. J. Am. Chem. Soc. 1992, 114, 6700-6710.
- 112) Hoffman, H.; Mayer, U.; Krischanitz, A. Langmuir 1995, 11, 1304-1312.
- 113)Banga, R.; Yarwood, J.; Morgan, A. Langmuir 1995, 11, 618-622.
- 114) Ulman, A.; Eilers, J. E.; Tillman, N. Langmuir 1989, 5, 1147-1152.
- 115)Porter, M. D.; Bright, T. B.; Allara, D. L.; Chidsey, C. E. D. J. Am. Chem. Soc. 1987, 109, 3559-3568.

- 116) Hou, J.; Hou, J., Ed.; Michigan State University: East Lansing, 1997.
- 117) Yang, Y.; Pei, Q.; Heeger, A. J. Synth. Met. 1996, 78, 263-267.
- 118)Burns, S. E.; Pfeffer, N.; Gruner, J.; Remmers, M.; Javoreck, T.; Neher, D.; Friend, R. H. *Adv. Mater.* 1997, 9, 395-398.
- 119)Remmers, M.; Schulze, M.; Wegner, G. *Macromol. Rapid Commun.* **1996**, *17*, 239-252.
- 120) Wirth, H. O.; Herrmann, F. U.; Herrmann, G.; Kern, W. Mol. Cryst. 1968, 4, 321-342.
- 121)Gorman, C. B.; Ginsburg, E. J.; Grubbs, R. H. J. Am. Chem. Soc. 1993, 115, 1397-1409.
- 122)Lamba, J. J. S.; Tour, J. M. J. Am. Chem. Soc. 1994, 116, 11723-11736.
- 123)Goldfinger, M. B.; Crawford, K. B.; Swager, T. M. J. Am. Chem. Soc. 1997, 119, 4578-4593.
- 124) Grant, D. J. W.; Higuchi, T. Solubility Behavior of Organic Compounds; John Wiley & Sons: New York, 1990; Vol. XXI.
- 125)Smith, G. B.; Dezeny, G. C.; Hughes, D. L.; King, A. O.; Verhoeven, T. R. J. Org. Chem. 1994, 59, 8151-8156.
- 126) Murray, D. P.; Dechter, J. J.; Kispert, L. D. J. Polym. Sci.: Polym. Lett. Ed. 1984, 22, 519-522.
- 127) Wilcox, C. F.; Wilcox, M. F.; Wilcox, C. F.; Wilcox, M. F., Ed.; Prentice Hall: Englewood Cliffs, N.J., 1995, pp 388.
- 128) Mowry, D. T.; Renoll, M.; Huber, W. F. J. Am. Chem. Soc. 1946, 68, 1105-1109.
- 129)Read, R. R.; Wood, J. O. Org. Syn. Coll. 1955, 3, 444-446.

- 130) Allinger, N. L.; Hu, S.-E. J. Am. Chem. Soc. 1962, 84, 370-372.
- 131)DuPont; DuPont, Ed.: DE, 1972.
- 132) Miller, A. R.; Curtin, D. Y. J. Am. Chem. Soc. 1976, 98, 1860-1865.
- 133) Kajigaeshi, S.; Kakinami, T.; Moriwaki, M.; Tanaka, T.; Fujisaki, S.; Okamoto, T.

Bull. Chem. Soc. Jpn. 1989, 62, 439-443.

MICHIGAN STATE UNIV. LIBRARIES
31293017126552